OPTIMIZATION OF A MULTI BUNCH TRAIN FILLING PATTERN FOR THE SUPPRESSION OF BEAM ION INSTABILITY IN ELECTRON STORAGE RING: CASE STUDY OF INDUS-2

By

SAROJ KUMAR JENA

PHYS03201404001

Raja Ramanna Centre for Advanced Technology, Indore

A thesis submitted to the

Board of Studies in Physical Sciences

In partial fulfillment of requirements

for the Degree of

DOCTOR OF PHILOSOPHY

of

HOMI BHABHA NATIONAL INSTITUTE

November, 2019

Homi Bhabha National Institute[1]

Recommendations of the Viva Voce Committee

As members of the Viva Voce Committee, we certify that we have read the dissertation prepared by ***Saroj Kumar Jena*** entitled "***Optimization of a multi bunch train filling pattern for the suppression of beam ion instability in electron storage ring: case study of Indus-2***" and recommend that it may be accepted as fulfilling the thesis requirement for the award of Degree of Doctor of Philosophy.

Chairman - Prof. Srinivas Krishnagopal	K. S—	Date: 14/8/2020
Guide - Prof. V. K. Senecha		Date: 14-08-2020
Examiner - Prof. R. G. Pillay	Pillay	Date: 14-08-2020
Member 1- Prof. Vinit Kumar	Vinit Kumar	Date: 14·8·20
Member 2- Prof. M. P. Singh	MaR	Date: 14.8.20
Member 3- Prof. Arup Bandyopadhyay	Arup Bandyopadhyay	Date: 14/08/2020
Member 4- Prof. Anand Moorti	Anand Moorti	Date: 14/8/2020.

Final approval and acceptance of this thesis is contingent upon the candidate's submission of the final copies of the thesis to HBNI.

I hereby certify that I have read this thesis prepared under my direction and recommend that it may be accepted as fulfilling the thesis requirement.

Date: 23/09/2020

Place: Indore

Guide: ---------------------

Prof. V. K. Senecha

[1] This page is to be included only for final submission after successful completion of viva voce.

STATEMENT BY AUTHOR

This dissertation has been submitted in partial fulfillment of requirements for an advanced degree at Homi Bhabha National Institute (HBNI) and is deposited in the Library to be made available to borrowers under rules of the HBNI.

Brief quotations from this dissertation are allowable without special permission, provided that accurate acknowledgement of source is made. Requests for permission for extended quotation from or reproduction of this manuscript in whole or in part may be granted by the Competent Authority of HBNI when in his or her judgment the proposed use of the material is in the interests of scholarship. In all other instances, however, permission must be obtained from the author.

Saroj Kumar Jena

DECLARATION

I, hereby declare that the investigation presented in the thesis has been carried out by me. The work is original and has not been submitted earlier as a whole or in part for a degree / diploma at this or any other Institution / University.

Saroj Kumar Jena

List of Publications arising from the thesis

Journals

1. "Stabilization of betatron tune in Indus-2 storage ring", **Saroj Kumar Jena**, S. Yadav, R. K. Agrawal, A. D. Ghodke, Pravin Fatnani, and T. A. Puntambekar, *Chinese Physics C,* **2014**, Vol. 38, No. 6, 067002.
2. "Observation and mitigation of ion trapping in Indus-2",**Saroj Kumar Jena** and A. D. Ghodke, *Pramana – Journal of Physics,* **2015**, Vol. 85, No. 6, 1193-1205.
3. "Simulation of fast beam ion instability (FBII) in Indus-2 and its experimental observation", **Saroj Kumar Jena**, A. D. Ghodke, and V. K. Senecha, *Journal of Instrumentation,* **2017**, 12, P11004.
4. "Investigation of fast beam-ion instability (FBII) in wake function formalism for Indus-2 ring", **Saroj Kumar Jena**, A. A. Fakhri, A. D. Ghodke, and V. K. Senecha, *Nuclear Instruments and Methods in Physics Research A ,* **2019**, 919, 113–118.

Conferences

1. "Detection of trapped ions by measuring bremsstrahlung photons in Indus-2", **Saroj Kumar Jena**, T. K. Sahu, M. K. Nayak, Haridas G., A. A. Fakhri, A. D. Ghodke, and V. K. Senecha, *National symposium on radiation physics (NSRP-22),* Nov. 8-10, **2019**, New Delhi.
2. "Ion-beam interaction in electron storage ring of high brightness synchrotron radiation source", **Saroj Kumar Jena**, A. A. Fakhri, A. D. Ghodke, and V. K. Senecha, *Indian Particle accelerator conference*, Nov. 18-21, **2019**, New Delhi.

Saroj Kumar Jena

DEDICATIONS

This thesis is dedicated to everyone who provided support during its journey,

&

Especially my diligent parents

ACKNOWLEDGEMENTS

First and foremost, I would like to thank my thesis guide *Prof. V. K. Senecha* for his initiative, constant support and guidance which made this work possible. His guidance has steered me focused to the planned work and motivated me to complete the thesis work within the stipulated time. He has reviewed my each contributions thoroughly and provided guidance during the entire course of my PhD work. The results presented here were made possible by his sincere and apt guidance.

I am indebted to *Sh. A. D. Ghodke*, my technical advisor (Head, Accelerator Physics Section, RRCAT, Indore) and express my gratitude for giving me this interesting problem to work on and also for his constant support. He has been an excellent, committed and has vast knowledge of accelerator physics which has been invaluable for the academic part of the thesis. His countless ideas and stimulating conversations on this topic were instrumental in shaping this thesis.

I extend thank to the members of my Doctoral committee for their invaluable insights, guidance and support, which help me at various stages of my research.

I thank both the thesis reviewers for the valuable comments that helps in improving my thesis and also for providing guidance for future research work.

I also thank *Sh. A. C. Thakurta (*Former Director, Electron Group Board) and *Sh. T. A Puntambekar* (Director, Electron Group Board) for their constant support, encouragement and providing the facilities to perform the experiments at Indus-2. Many thanks to all shift crew member of control room for allowing the specific measurement carried out during this thesis work.

I would also like to thank Dr. Lotta Mether (CERN) for providing the FASTION code, which help me to explore and investigate the fast beam ion instability.

I express my sincere thanks to *Dr. Amalendu Sharma* for many valuable and fruitful discussions on accelerator physics. I am also equally grateful to acknowledge all my fellow colleagues in Accelerator Physics Section and special mention are due to *Sh. Pramod Radheshyam, Dr. A. A. Fakhri, Dr. P. Kumar, Dr. Riyasat Husain, Sh. Abdurrahim, Sh. P. Kant, Sh. D. K. Tyagi, Sh. V. K. Meena, Sh. Suraj Prakash and Sh. Sanjay Prajapati.*

I want to express my gratitude to the technology divisions/sections at RRCAT, namely beam diagnostics, controls, vacuum, and computer center for providing the facilities and support to complete my thesis work. Special thanks are due to *Sh. Akashdeep, Sh. P. K. Thander, Sh. S. Yadav, Sh. R. K. Agrawal, Sh. Amit Chauhan, Sh. D. P. Yadav, Sh. K.V.A.N.P.S. Kumar, and Dr. G. Haridas.*

I am thankful from the core of my heart to all my friends for their help and support. Though the ultimate goal is to complete the thesis, it has turned out to be a fantastic learning experience.

Last, but not least, I would like to thank my family for their support during the course of thesis work, and particularly my lovely kids to bring cheers in my life.

CONTENTS

SUMMARY

The electron storage rings are dedicatedly built to provide high brightness synchrotron radiations for research and development in frontline scientific fields. This however imposes stringent requirement on quality and stability of electron beam. The electron beam rapidly ionizes the residual gas molecules present in the storage ring vacuum chamber and the generated positively charged ions may get trapped in the negative potential well of the electron beam. This phenomenon is known as ion trapping. This induces transverse oscillation to the electron beam and that causes detrimental effect on beam current accumulation, betatron tune, and beam lifetime. To suppress the effect of ion trapping, bunch gap is provided in the continuously filled bunches. The ions present in the storage ring does not experience any focusing force during the bunch gaps and in several turns, the ions drift away from the beam center. However, even if a clearing gap is provided, a fast beam ion instability (FBII) may develops along the bunch train. This could cause transverse dipole motion of the electron bunches, with the amplitude increases in time and along the bunch train and that ultimately leads to deterioration in the beam quality. The detail investigation of both these phenomena in storage ring are important to ensure the beam stability. In this thesis, comprehensive theoretical estimation and experimental observation of beam–ion interaction have been performed for the Indus-2 storage ring.

The indus-2 storage ring may be filled with maximum 291 bunches, each separated by 2 ns. The stability of ions in the bunched electron beam was estimated using the combination of kicks offered by electron bunch (linear approximation of Bassetti-Erskine formula) and drifts between the consecutive bunches. When all the 291 bunches are filled, the ions of probable gas species (H_2, CO, O_2, and CO_2) present inside the vacuum chamber were found to be trapped in the

beam potential. The effect of bunch gaps on stability of ions were studied and an optimal bunch filling pattern was determined to get rid of the ion trapping. The evidence of ion trapping was ascertained experimentally in Indus-2 by detecting the betatron tune shift and additional bremsstrahlung radiation, when no bunch gap was provided.

The FBII was studied numerically using a simulation code FASTION, assuming the residual gas in the vacuum chamber consists of a single species (CO). In the simulation, multiple beam-ion interaction locations were carefully chosen based on the lattice parameters of Indus-2. The simulation shows that, the FBII in Indus-2 will arise at vacuum pressure of about 50 nTorr, and 200 mA beam current. In an experiment, vacuum pressure of the storage ring could be raised to 6.7 nTorr from the operating pressure of 0.5 nTorr by switching OFF all the sputter ion pumps except at few sensitive locations. The snapshots of the electron bunches are captured by streak camera and the signature of FBII could not be observed at the elevated vacuum pressure which is consistent with the simulation result.

This study was further continued by considering the spread in ion frequency due to multiple ion species present in the storage ring. The inclusion of spread in ion frequency in the study of FBII was modelled by means of the wake function approach. The outcome of this analysis shows a further suppression of the instability growth due to Landau damping mechanism caused by ion frequency spread. As a mitigation strategy of this instability, the ion density in the beam path was reduced by replacing single long bunch train into many short bunch trains. Using this analysis, an optimal multi-train bunch filling pattern was evolved which can suppresses the FBII effectively even at 50 nTorr vacuum pressure in Indus-2.

LIST OF FIGURES

LIST OF TABLES

CHAPTER-1

ACCELERATOR BEAM DYNAMICS AND COLLECTIVE EFFECTS IN ELECTRON STORAGE RINGS

Synchrotron radiation sources based on electron storage rings are being widely used since five decades as an important tool to carry out frontline scientific research in various fields including material science, biology and medicine. In order to cater such applications, the light source is required to operate with stable and reliable beam parameters. Beam-ion instability has been observed as one of the major bottlenecks in achieving stable and high beam current in a 3rd generation light source and it can be overcome by some suitable mechanism. In electron storage ring, positive ions are regularly produced via ionization of residual gas molecules present in the vacuum chamber. These ions get attracted towards the electron bunch and in multi turns they get accumulated near the beam axis and this phenomenon is known as conventional ion trapping (CIT) [1-3]. It can cause various undesirable effects on the electron beam such as shift in betatron tune, emittance blow up and beam instabilities and such phenomena were observed in many operating third generation electron storage rings worldwide including ALS [4], UVSOR [5], NSLS [6], ELETTRA [7], PF [8], PLS [9], APS [10], SPEAR3 [11], and PETRA III [12]. The CIT can be cured by partial bunch filling pattern via introduction of a long bunch gaps comprising of several bunches. Effort has been put to understand this effect in Indus-2 storage ring during its operation and an optimized bunch filling pattern was evolved to mitigate this effect. However within a bunch train in single passage, low emittance beam along with high beam current may exhibit transient ion trapping known as fast beam ion instability (FBII) which degrades the beam quality and is also expected to be a limiting factor in future ultra-low emittance light sources. Considerable amount of theoretical (both analytical and simulation) studies of FBII have been carried out elsewhere and the phenomenon was experimentally observed in many electron storage rings [13-22]. Most of the studies of FBII were performed by solving coupled equations of motion for electrons and ions which takes care of single ion species at a time and same average pressure throughout the ring circumference. These studies estimate higher growth rate of the instability than it was observed experimentally in various storage rings. This is mainly because it doesn't consider frequency variation of ions along the circumference of the ring, which reduces the instability growth rate via Landau damping mechanism. In order to have a more realistic consideration, L Wang et al. modelled the study of FBII in the frame work of coupled bunch instability by estimating the wake field and impedance of ion clouds [23-25].

For better understanding of the beam-ion interaction in the storage ring, comprehensive knowledge of basic accelerator physics is quite essential and therefore selected concepts of beam dynamics relevant to this thesis work has been introduced in chapter-1. Sections 1.1-1.4 describes linear beam dynamics of a storage ring. Beam properties are discussed in section 1.5. Radiation damping is discussed in section 1.6 followed by beam lifetime in section 1.7. The collective effects are described in section 1.8. At the end, we introduce the Indus-2 storage ring in section 1.9.

1.1 Accelerator beam dynamics

Accelerators are machine that increases the energy of charged particle and store them for a longer time in the storage rings. There are many types of accelerators, but here we focus only on electron storage ring, a circular accelerator. The electron beam is guided in a particular circular trajectory and transversely focused with the help of periodic electromagnetic fields provided by dipole and quadrupole magnets respectively in the ring. The beam particles experience a Lorentz force [26] given as

$$\vec{F} = e\left(\vec{E} + v \times \vec{B}\right) \qquad \dots (1.1)$$

where e is the charge of the beam particle, $\vec{E}$ is the electric field and $\vec{B}$ is the magnetic field. The charged particles are accelerated by longitudinal electric field provided by the RF cavities installed at few locations in the ring. Under the influence of magnetic field **B**, the electron with momentum ***p*** follows a circular path with radius of curvature, ρ which can be calculated by balancing the transverse Lorentz force and centrifugal force acting on the electron. This provides the basic principle of synchrotron which is given as

$$\rho = \frac{p}{eB} \qquad \dots (1.2)$$

The motion of the electron beam with respect to a reference orbit is described by the curvilinear coordinate system shown in Fig. 1.1, which is basically a moving frame on a reference orbit that passes through the center of all magnetic elements. This is also known as Frenet-Serret coordinate system [27]. The *x* and *y* are transverse coordinates pointing away from the reference trajectory in horizontal and vertical plane respectively. The ***s*** coordinate describes motion of electron in the longitudinal plane and it also gives the path length advance from any staring location s_0.

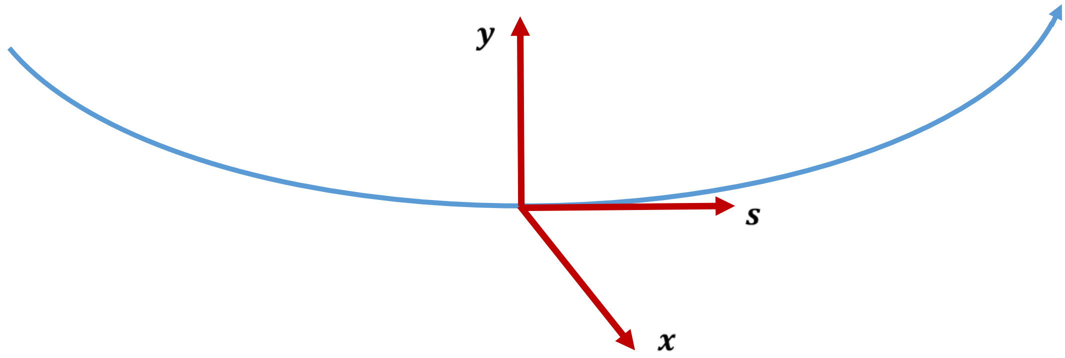

Figure 1.1: Curvilinear coordinate system (x, y, and s) that describes the motion of electron with respect to a reference trajectory. Along the orbit, the coordinate system co-propagates. The direction tangential to the ideal orbit is designated by s.

The equation of motion of electrons for right momentum particle in transverse plane in this new coordinate system is derived from eqn. (1.1) and is given by Hill's equation as [26]

$$\frac{d^2x}{ds^2} + \left[\frac{1}{\rho(s)^2} + k(s)\right]x = 0 \qquad \text{....}(1.3)$$

$$\frac{d^2y}{ds^2} - k(s)y = 0 \qquad \text{....}(1.4)$$

where *k(s)* is the quadrupole strength which is a function of s and given as

$$k(s) = \frac{1}{B\rho}\frac{\partial B_y(s)}{\partial x} \qquad \text{....}(1.5)$$

$k > 0$ represents a focusing quadrupole and $k < 0$ represents defocusing quadrupole. Conventionally, focusing quadrupole means it does the focusing action in horizontal plane and simultaneously defocusing action in vertical plane. Since there is no vertical dipole in a storage ring, the equation (1.4) does not have any focusing term ($1/\rho^2$) generated due to dipole field. Equation (1.3) and (1.4) can be written as

$$\begin{cases} x'' + K_x(s)x = 0 \\ y'' + K_y(s)y = 0 \end{cases} \qquad \text{....}(1.6)$$

in which, $K_x(s) = 1/\rho^2(s) + k(s)$, $K_y(s) = -k(s)$ and $x'' = d^2x/ds^2$. The equation of motion resembles the harmonic oscillator with the restoring force K, which varies with s. However, in storage ring, K remains piecewise constant which means within each accelerator component, K is considered to be constant. The solution of the differential equation 1.6 takes the form [26]

$$x(s) = \begin{cases} a\cos\left(\sqrt{K}s + b\right) & K > 0 \\ as + b & K = 0 \\ a\cosh\left(\sqrt{|K|}s + b\right) & K < 0 \end{cases} \qquad \text{....(1.7)}$$

where a and b are constants that can be determined from the initial condition of beam particle. Considering the initial position and divergence of particle as $x(s_i)$ and $x'(s_i)$ respectively, the solution can be represented via matrix form as

$$\begin{pmatrix} x(s) \\ x'(s) \end{pmatrix}_f = M\left(s_f \middle| s_i\right) \begin{pmatrix} x\,(s) \\ x'(s) \end{pmatrix}_i \qquad \text{....(1.8)}$$

where $M\left(s_f \middle| s_i\right)$ is the transfer matrix connecting between two locations s_f and s_i. Every accelerator component has its own transfer matrix and transport matrix for any accelerator interval consisting of N number of components is described as product of individual transfer matrix as

$$M = M_N\, M_{N-1} \ldots \ldots M_2\, M_1 \qquad \text{....(1.9)}$$

The transfer matrix of elements with length L and constant focusing function K for three different cases such as K= 0 (drift space), K > 0 (focusing quadrupole) and K < 0 (defocusing quadrupole) is given as

$$M_D = \begin{bmatrix} 1 & L \\ 0 & 1 \end{bmatrix} \qquad , K = 0 \qquad \text{....(1.10)}$$

$$M_{QF} = \begin{bmatrix} \cos(\sqrt{K}L) & \dfrac{1}{\sqrt{K}}\sin(\sqrt{K}L) \\ -\sqrt{K}\sin(\sqrt{K}L) & \cos(\sqrt{K}L) \end{bmatrix} \qquad , K > 0 \qquad \text{....(1.11)}$$

$$M_{QD} = \begin{bmatrix} \cosh(\sqrt{|K|}L) & \frac{1}{\sqrt{|K|}}\sinh(\sqrt{|K|}L) \\ \sqrt{|K|}\sinh(\sqrt{|K|}L) & \cosh(\sqrt{|K|}L) \end{bmatrix} \quad , K < 0 \qquad \ldots.(1.12)$$

where D, QF and QD stands for drift space, focusing quadrupole and defocusing quadrupole respectively. In thin lens approximation, i.e. when length of the quadrupole becomes very small keeping KL constant, the transfer matrix of quadrupole becomes

$$M_{QF} = \begin{pmatrix} 1 & 0 \\ -KL & 1 \end{pmatrix}, \qquad M_{QD} = \begin{pmatrix} 1 & 0 \\ |K|L & 1 \end{pmatrix} \qquad \ldots.(1.13)$$

Thin lens approximation becomes very useful for simple and handy calculation. Similarly, the transfer matrix for a sector type dipole magnet with bending angle $\theta = L/\rho$ and $K = 1/\rho^2$ is given as

$$M_{Dipole} = \begin{bmatrix} \cos\theta & \rho\sin\theta \\ -\frac{1}{\rho}\sin\theta & \cos\theta \end{bmatrix} \qquad \ldots.(1.14)$$

1.2 Accelerator beam optics

In a circular accelerator, the focusing strength, K (s) is periodic over the circumference C of the ring.

$$K(s) = K(s + C) \qquad \ldots.(1.15)$$

Under this condition, the solution to the Hill's equation can be described using Floquet's theory [28] and a more general solution using beam optics parameters is given as

$$x_\beta(s) = \sqrt{\varepsilon}\sqrt{\beta(s)}\, cos(\mu(s) - \mu_0) \qquad \ldots.(1.16)$$

where ε is a constant known as beam emittance, μ_0 is the initial phase, $\beta\,(s)$ is the betatron function and $\mu\,(s)$ is the betatron phase function given by the relation

$$\mu(s) = \int_0^s \frac{ds}{\beta(s)} \qquad \ldots.(1.17)$$

The solution can be expressed through transfer matrix as

$$\binom{x}{x'}_f = \begin{pmatrix} \sqrt{\frac{\beta_f}{\beta_i}}\ (\cos\psi + \alpha_i \sin\psi) & \sqrt{\beta_f\beta_i}\ \sin\psi \\ -\frac{1+\alpha_i\alpha_f}{\sqrt{\beta_f\beta_i}}\sin\psi + \frac{\alpha_i - \alpha_f}{\sqrt{\beta_f\beta_i}}\cos\psi & \sqrt{\frac{\beta_i}{\beta_f}}\ (\cos\psi + \alpha_f \sin\psi) \end{pmatrix} \binom{x}{x'}_i \quad \ldots.(1.18)$$

where *i* and *f* refers to initial and final location of the ring. ψ is the phase advance between the initial and final location, $\psi = \psi(s_f) - \psi(s_i)$. α, β and γ are known as Twiss parameters or Courant-Snyder parameters [29] and they are inter related as

$$\alpha = -\frac{1}{2}\frac{d\beta}{ds} \quad , \qquad \gamma = \frac{1+\alpha^2}{\beta} \qquad \ldots.(1.19)$$

If ϕ is the phase advance over one revolution, the phase function satisfy the following relation

$$\mu(s + C) = \mu(s) + \phi \qquad \ldots(1.20)$$

The general form of one turn transfer matrix is represented as

$$M = \begin{pmatrix} cos\,\phi\ + \alpha\, sin\,\phi & \beta\, sin\,\phi \\ -\gamma \sin\phi & cos\,\phi\ - \alpha\, sin\,\phi \end{pmatrix} \qquad \ldots.(1.21)$$

Considering *M* as one turn transfer matrix of a storage ring, the particle motion after *n* revolution is described by M^n. The particle with initial value x_i and x_i' will remain stable if the following product becomes finite for any value of *n*.

$$M^n \begin{pmatrix} x_i \\ x_i' \end{pmatrix}$$

Since the phase advance in one revolution ϕ should essentially be a real quantity, this results into a stability condition [29], as follows

$$|Tr(M)| \leq 2 \qquad \ldots.(1.22)$$

where *Tr (M)* is the trace of transfer matrix M.

1.3 Betatron tune and closed orbit distortion

The beam particles undergoes transverse oscillation due to focusing and defocusing action of quadrupoles distributed all over the circumference of the storage ring and this is known as betatron oscillation. The amplitude of the betatron oscillation of the particle is known as betatron function or beta function. The number of betatron oscillation in one revolution depicts the betatron tune (ν) of the ring and is given as

$$\nu_{x,y} = \frac{1}{2\pi}\int_{s}^{s+C} \frac{ds}{\beta_{x,y}(s)} \qquad \ldots.(1.23)$$

where x and y represents the horizontal and vertical plane respectively. The angular betatron frequency, ω_β is related to betatron tune by the following relation

$$\omega_\beta = 2\pi\nu f_0 \qquad \ldots.(1.24)$$

where f_0 is the revolution frequency of the electron beam. In a storage ring, the closed orbit is the trajectory of electron beam which have the same value of displacement after one revolution and is represented as

$$x_{co}(s) = x_{co}(s+C) \qquad \ldots.(1.25)$$

In an accelerator with ideal optics, the closed orbit passes through center of all magnetic elements, i.e $x_{co} = 0$ and that path is a trivial solution to Hill's equation. However in reality, the particle beam is not exactly at the center due to the field errors of bending magnet and misalignment or tilt error of quadrupole magnet etc. A dipole field error at some location s_0 of the storage ring deflects an electron beam with an additional angular kick, $\Delta\theta(s_0) = \Delta\mathrm{B}(s_0)\, l/\mathrm{B}\rho$, where l is the magnetic length of the dipole magnet. A misaligned quadrupole at s_0 gives an angular kick, $\Delta\theta(s_0) = \mathrm{K}\, l\, \Delta x(s_0)$, where K is the strength of the quadrupole, l is the magnetic length of the quadrupole magnet and Δx is the placement error of the magnet which is also known as misalignment error. These extra kicks in the ring makes the closed orbit of the ring to a new distorted orbit and the difference of this new orbit from the ideal orbit is known as closed orbit distortion (COD). There may be several such errors at different locations of the ring contributing to total COD and at any location, the COD, $\Delta x_{co}(s)$ is given by the linear superposition of the distribution generated by these kicks

$$\Delta x_{co}(s) = \frac{\sqrt{\beta(s)}}{2\sin\pi\nu}\sum_{j=1}^{n}\sqrt{\beta(s_j)}\cos(\pi\nu - |\psi(s) - \psi(s_0)|)\,\Delta\theta(s_j) \qquad \text{....}(1.26)$$

The above COD expression suggests that for stable operation of the storage ring, the integer value of betatron tunes shall be avoided. For an integer value of tune, the particles will receive the kicks in each turn with same phase value which will lead to ever growing oscillation amplitude and eventually particle will hit the chamber wall and get lost. Similarly the errors from higher order multipoles such as quadrupoles and sextupoles does not allow operation of storage ring with half-integer and third-integer value. In other words, the tune of a circular accelerator is usually fixed to a non-integer and irrational number to avoid resonances due to magnetic imperfections. The equation for resonance condition can be written as

$$m\,\nu_x + n\,\nu_y = p \qquad \text{....}(1.27)$$

where *m*, *n*, and *p* are any arbitrary integers. The above condition constitutes several straight lines in ν_y vs. ν_x space known as tune space. The order of those resonance lines is given by $|m| + |n|$. Resonance lines upto 4th order are shown in Fig. 1.2 and it shows that fixing the tune point specified by both ν_x & ν_y is very difficult, as the tune space becomes dense as higher order resonance lines are included. As a thumb rule, higher the order of resonance, lesser will be its impact on the electron beam. The operating tune of Indus-2 is also shown in figure as a solid green circle. The electron beam consists of a large number of particles distributed in amplitude and energy. When they are circulating in the storage ring, different particles will have different tunes and if tune approaches or crosses any dangerous resonance lines, the oscillation amplitude of those particle grows and that may cause loss of particles leading to reduction in beam lifetime. Mostly the tune shifts are caused by quadrupolar field errors [26] and the amount of tune shift ($\Delta\nu$) is given as

$$\Delta\nu = \frac{1}{4\pi}\oint \beta(s)\Delta k(s)ds \qquad \ldots.(1.28)$$

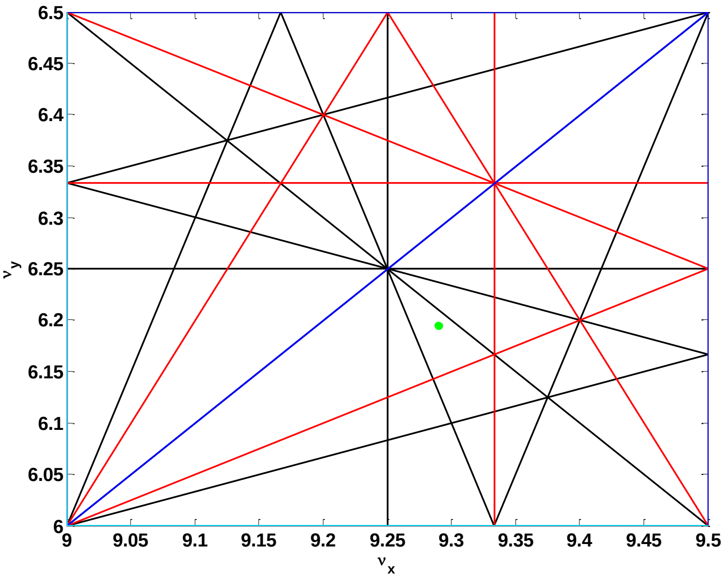

Figure 1.2: Tune diagram showing the resonance lines up to 4th order with different color specified for each order. First order: Cyan, Second order: Blue, Third order: Red, Fourth order: black. The operating point of Indus-2 is shown as solid green circle.

1.4 Off momentum particle motion

So far, only right momentum particle dynamics is discussed. However in reality, particles in the beam have finite energy spread or they have finite momentum offset, $\Delta p=p-p_0$, p_0 is the momentum of right energy particle. Particles with different energy have a different deflection in a magnetic field and will travel on a different trajectory. The Hill's equation for off-momentum particles is written as

$$\frac{d^2x}{ds^2} + \left[\frac{1}{\rho(s)^2} + k(s)\right]x = \frac{1}{\rho(s)}\frac{\Delta p}{p} \qquad \ldots.(1.29)$$

A particular solution to this equation is written as

$$x_\eta(s) = \eta(s)\frac{\Delta p}{p} \qquad \ldots.(1.30)$$

where $\eta(s)$ is the dispersion function. The general solution of the equ. 1.29 is given as

$$x(s) = x_{co}(s) + x_\beta(s) + x_\eta(s) \qquad \ldots.(1.31)$$

with $x_{co}(s)$ as closed orbit which is considered as a static offset, $x_\beta(s)$ representing the betatron oscillations about a closed orbit and $x_\eta(s)$ as the offset of such orbit due to the off-momentum particles.

1.5 Beam emittance and beam size

Beam consists of large number of charged particles distributed in a six dimensional space, $(x, x', y, y', t, \delta p/p)$. However, the linear beam dynamics is normally studied independently in three, two-dimensional space namely transverse horizontal (x, x'), transverse vertical (y, y') and longitudinal $(t, \delta p/p)$ which are referred as phase spaces. The solution of Hill's equation is given in eqn. (1.16) which notify the position coordinate x in horizontal phase space as a function of s. By differentiating it two times with respect to s and plugging it in Hill's equation [26], it gives

$$\gamma(s)x(s)^2 + 2\alpha(s)x(s)x(s)' + \beta(s)x'(s)^2 = \varepsilon \qquad \ldots.(1.32)$$

Here ε is known as beam emittance which remains constant along a particle trajectory and is also known as Courant-Snyder invariant. The above equation represents equation of an ellipse which is followed by the phase space coordinates (x, x') at any location s in the storage ring. The motion of a single particle at a fixed location over several turn, which maps into an ellipse in phase space is shown in Fig. 1.3. The area of the phase space ellipse is known as the emittance of a single particle. The orientation and shape of this ellipse may be different at different locations in the storage ring, but the area of the ellipse remains constant.

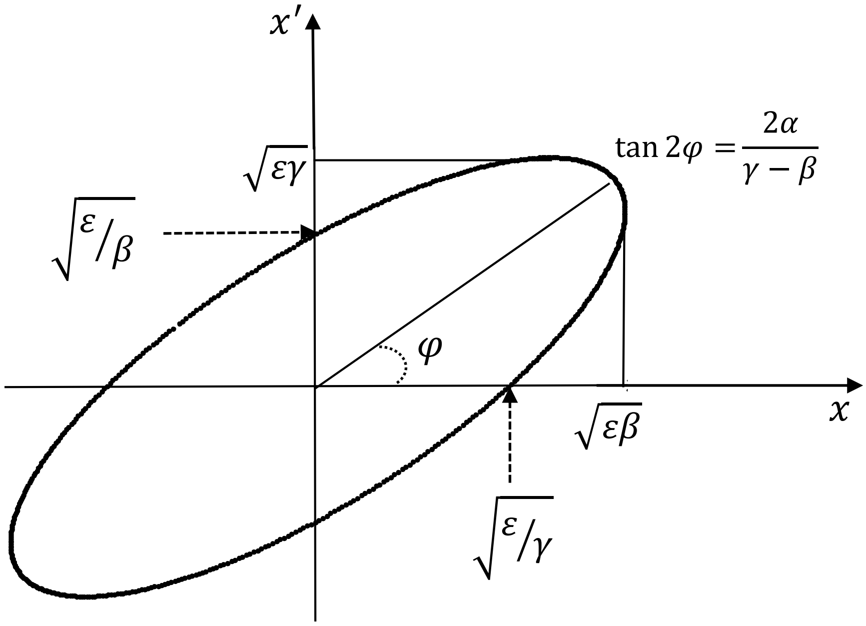

Figure 1.3: Phase space ellipse at one position in the ring where alpha is non-zero. This shows a tilted ellipse and the area of the ellipse represents the beam emittance. For an upright ellipse (alpha=0), the magnitude of semi axis signifies the beam size and beam divergence.

For an ensemble of particles populating the beam, the $(x,\ x')$ of eqnuation 1.32 will represents the centroid of the particles given as

$$\bar{x} = \sqrt{\frac{1}{N}\sum_{i=1}^{N} x_i^2} \qquad \text{....}(1.33)$$

$$\bar{x'} = \sqrt{\frac{1}{N}\sum_{i=1}^{N} x_i'^2} \qquad \text{.... (1.34)}$$

$$\overline{xx'} = \frac{1}{N}\sum_{i=1}^{N} x_i x_i' \qquad \text{.... (1.35)}$$

where N is the number of particles in a beam. Thus for a beam, the invariant equation can be written as following which explains the beam emittance as the area of the phase space ellipse with contour defined by the particles distribution in the phase space.

$$\gamma\bar{x}^2 + 2\alpha\overline{xx'} + \beta\bar{x'}^2 = \varepsilon_{rms} \qquad \text{.... (1.36)}$$

For a beam, the beta function and dispersion function together with emittance defines the beam size, σ [26] and the horizontal and vertical beam size is given as

$$\sigma_x(s) = \sqrt{\varepsilon_x\,\beta_x(s) + \left(\eta_x(s)\frac{\Delta p}{p}\right)^2} \qquad \text{.... (1.37)}$$

$$\sigma_y(s) = \sqrt{\varepsilon_y\,\beta_y(s)} \qquad \text{.... (1.38)}$$

The above equations show that the horizontal beam size depends on the horizontal beam emittance and as well the dispersion, whereas the vertical beam size only depends on vertical beam emittance. Usually the vertical dispersion is zero as there are no vertical bendings in an accelerator where the beam is bent in horizontal plane. Vertical emittance is decided by the amount of betatron coupling occurs between the horizontal and vertical motion of electron beam. The betatron coupling arises due to the vertical beam offset in the sextupole magnets and tilt of the quadrupoles around the beam axis which effectively generates skew quadrupole fields. The betatron coupling coefficient, κ is defined by the emittance ratio and given as

$$\kappa = \frac{\varepsilon_y}{\varepsilon_x} \quad \text{....}(1.39)$$

where ε_y and ε_x are vertical emittance and horizontal emittance respectively. The beam emittance may be influenced by various phenomena such as beam-beam scattering, beam-residual gas scattering, synchrotron radiation emission, wake field and space charge effect. It is challenging and an important task to preserve the beam emittance against above phenomena or even reduce the emittance which has a direct impact on the brightness of the photon beam. The beam emittance or brightness are considered as a figure of merit of any storage ring [27] and they are related as

$$B \propto \frac{I}{\varepsilon_x \varepsilon_y} \quad \text{....}(1.40)$$

where *B* is the brightness and *I* is average beam current in the storage ring.

1.6 Radiation damping

In a storage ring, the ultra-relativistic electrons emit electromagnetic radiation when they are accelerated inside dipole magnet and the radiation emitted is known as synchrotron radiation (SR). In the process of SR emission, the energy lost by the electron is replenished by RF cavities installed in the ring. This phenomenon gives rise to damping of both synchrotron oscillation and as well betatron oscillation, known as radiation damping. However there is another counter phenomena due to random photon emissions in the storage ring known as quantum excitation, which amplifies the oscillation amplitude of the beam particle. The equilibrium of this two competing phenomena “radiation damping” and “quantum excitation” occurs when the excitation and damping rate balances and that determines the equilibrium beam emittance. In case of isomagnetic lattice, the total energy lost by electron beam per turn [27], U_0 is given as

$$U_0 = \frac{e^2}{3\varepsilon_0}\frac{\beta^3\,\gamma^4}{\rho} \qquad \text{.... (1.41)}$$

where β and γ are relativistic factors and ρ is the bending radius of the particle trajectory. When a photon is emitted, the transverse momentum of the beam is reduced but the longitudinal momentum remains unchanged as the RF cavity provides only longitudinal electric field. The energy loss and gain process of the electron beam is shown pictorially in the Fig. 1.4. This explains the damping of betatron oscillation upon SR emission in vertical plane and the damping rate is given by

$$\frac{1}{\tau_y} = \frac{U_0}{2E_0T_0} \qquad \text{.... (1.42)}$$

where E_0 is the nominal beam energy, T_0 is the revolution time of the beam in a storage ring and τ_y is the damping time in the vertical plane. The damping time is the exponential decay time of oscillation amplitude and it is different in both the transverse plane and longitudinal plane and can be written as

$$\tau_i = 2\frac{E_0}{\mathcal{J}_i U_0}T_0 \qquad \text{.... (1.43)}$$

where *i* refers to *x*, *y* and *ε* representing horizontal, vertical and longitudinal plane respectively. $\mathcal{J}_i$'s are the damping partition numbers, satisfying the following relation

$$\mathcal{J}_x + \mathcal{J}_y + \mathcal{J}_\varepsilon = 4 \qquad \text{.... (1.44)}$$

For a synchrotron without having any gradients in bending magnets, $\mathcal{J}_x \simeq 1$, $\mathcal{J}_y = 1$ and $\mathcal{J}_\varepsilon \simeq 2$

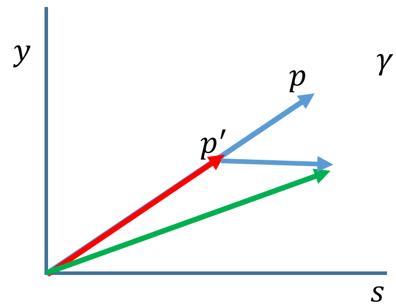

Figure 1.4: The effect of SR emission and energy gain in a RF cavity on electron beam momentum. During radiation process, particle losses a portion of its momentum. RF cavity restores only the longitudinal component of loss momentum.

1.7 Beam lifetime

The stored beam current in a storage ring decays nearly exponentially because of various loss mechanism [28] and decay pattern follows the relation given as

$$I(t) \approx I(0)\exp\left(-\frac{t}{\tau}\right) \qquad \ldots.(1.45)$$

where $I(0)$ is the initial beam current, $I(t)$ is beam current at time t and τ is the instantaneous beam lifetime. The primary loss mechanism of electrons is due to scattering between electrons and gas molecules which are present in vacuum chamber and this contributes to the vacuum lifetime (τ_{vac}). The other dominant loss mechanism is the scattering between electrons within a bunch and that contributes to Touschek lifetime (τ_{tou}). This involves inelastic scattering among electrons in the transverse plane and electrons lost through momentum acceptance. The electron beam has a Gaussian distribution which shows ideally infinite long tail while the storage ring vacuum chamber has a finite aperture. The chance of the beam loss through an aperture restriction is less, since the aperture available to the beam is still much larger than the rms size of the beam. However during quantum excitation, electron may suffer large energy fluctuation which will produce sufficient radial displacement as large as aperture limit. In this process, the probability of loss of electron through collision with vacuum chamber or any restriction in the aperture is governed by quantum lifetime (τ_{qua}). The total beam lifetime is given as

$$\frac{1}{\tau} = \frac{1}{\tau_{vac}} + \frac{1}{\tau_{tou}} + \frac{1}{\tau_{qua}} \qquad \ldots .(1.46)$$

1.8 Collective effects

So far, only single particle beam dynamics is discussed which is most essential at the design phase of any accelerator. However beam is considered as an ensemble of many particles in which its interaction with the surrounding is studied as collective effect to ensure the beam stability issue at the time of operation of accelerator with beam. There are number of collective effects such as interaction of beam with the wake-field generated by beam itself in association with vacuum chamber of accelerator in which beam is travelling, space charge force of beam and the focusing forces from the positive ions generated due to beam-residual gas scattering. These phenomena could limit the performance of accelerator in terms of beam quality and maximum stored beam current. These collective effects generate an additional force on the beam which perturbs the motion of the beam. It is therefore very important to properly diagnose the signature of instability and take preventive measures to restore stable beam operation. The space charge force of a beam varies with $1/\gamma^2$ and hence for electron storage ring having energy of the order of GeV where γ is of the order of several thousands, this effect does not pose any threat to the stability of beam.

1.8.1 Wake field and impedance

The electron beam travelling inside a vacuum chamber induces electromagnetic field and the field distribution solely depends on the geometry for a perfect electrically conducting vacuum chamber. Since the induced field always stays behind the charge moving with an ultra-relativistic speed, the electromagnetic field is known as wake field. Discontinuities in the vacuum beam pipe and finite conductivity of the chamber are the most common sources of wake field generation. The wake field generated by the electron bunch in a resonant structure like RF cavity, remains oscillating with decay in amplitude for longer time. This wake field affect the beam dynamics of subsequent bunch or bunches in the storage ring operating with many bunches leading to single or multi-bunch instability. The effect of wake field on beam dynamics is described by wake function in time domain and by the coupling impedance in frequency domain analysis. The wake function $W(z)$ is a function of *z*, the relative distance between the leading charge which excites the wake field and the trailing charge which experience the field. Consider two charge particles as shown in Fig. 1.5 where the leading charge q_1 is displaced vertically by some amount Δy that excites wake field and trailing charge q at a distance *z* receives a force due to the wake field. The wake function in transverse plane is defined as the change in momentum of charge q per unit charge for both the particle per unit transverse displacement of charge q_1 [30]

$$W_y(z) = \frac{\int_{-\infty}^{\infty} F_{\perp}(s,z)ds}{q\, q_1\, \Delta y} \quad \text{....}(1.47)$$

where $F_{\perp}$ is the transverse component of Lorentz force. The wake function has a dimension of *Volt/Coulomb/meter* [V/C/m] in SI unit and *meter*$^{-2}$ [m^{-2}] in CGS unit.

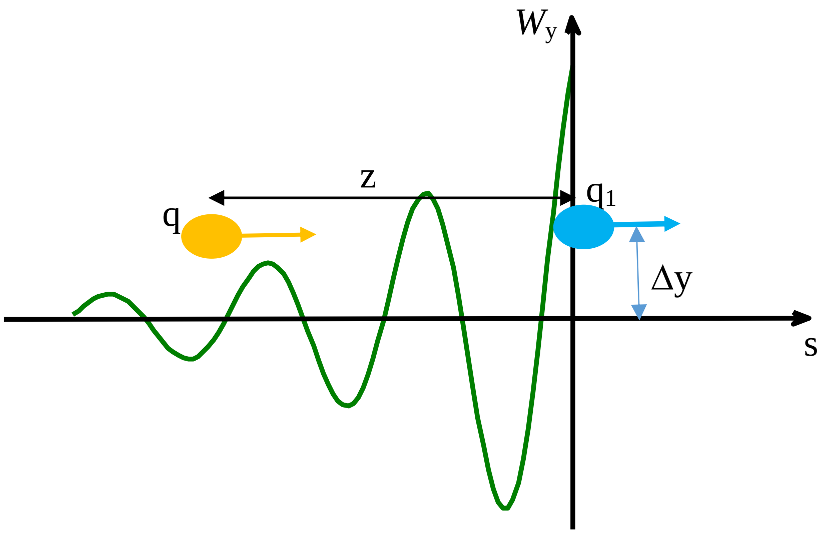

Figure 1.5: Illustration of a transverse wake function excited by an electron of charge q_1 and experienced by a charge q, which is at z distance behind and moving in the same direction.

In a storage ring, the interaction between beam and wake-field repeats in each revolution. As a consequence, investigation of the beam instability becomes more convenient in frequency domain rather than in time domain. The wake functions described in time domain can be transformed into frequency domain using Fourier transforms. The idea of impedance for an accelerator vacuum chamber environment was introduced by A. Sessler and V. Vaccaro for the first time [31]. The impedance is the Fourier transform of the wake function and is defined as

$$Z_{\perp}(\omega) = \frac{i}{c}\int_0^C W_y(z)\, exp\left(\frac{-i\omega z}{c}\right) dz \qquad \text{....}(1.48)$$

From the definition, it can be seen that, the impedance is a complex quantity and it has a dimension of *Ohm/meter* [Ω m^{-1}]. The real part of the impedance describes the growth rate of the instability and imaginary part decides the shift in betatron tune. Impedance of the vacuum chambers are broadly categorized into two families. One is resistive wall impedance that arises from finite resistance of vacuum chamber material and other is resonator type impedance caused by discontinuities in the beam pipe. The resistive wall impedance in the transverse plane varies inversely with the cube of the half height of the beam pipe in respective plane [30]. Therefore in modern synchrotron light sources, and especially in vertical plane the resistive wall impedance plays a major role in beam instability issue due to installation of small aperture insertion devices in the ring. Impedance offered by discontinuities in a beam pipe can be modelled as a resonant cavity with shunt impedance R_s, resonant frequency ω_R and a quality factor Q. The sharpness of the frequency response is described by the quality factor. Resonators with a low quality factor ($Q \approx 1$) are called broadband resonators and with high quality factor ($Q \gg 1$) are called narrowband resonators. For the case of a resonator, equivalent RLC circuit can be used [30] and its impedance is given as

$$Z_{\perp}(\omega) = \frac{c}{\omega} \frac{R_s}{1 + iQ\left(\frac{\omega_R}{\omega} - \frac{\omega}{\omega_R}\right)} \qquad \text{....}(1.49)$$

In a simplified form, the interaction of the beam with the impedance is described as the product of beam spectrum with impedance. The interaction occurs where an impedance overlaps with the beam spectrum or its side bands generated due to betatron oscillations or synchrotron oscillations of the beam.

1.8.2 Beam-Ion instability

Apart from the self-fields, beam experiences another type of collective effects arising from the interaction of electron beam with ionized residual gases inside a vacuum chamber. The ions are generated mainly from the collision between the beam and the residual gases present in a storage ring chamber. These positive ions perturb the motion of electron beam and that leads to many adverse effects like growth of beam emittance, shift in betatron tune and beam lifetime reduction. There are two kind of effects due to ions in storage ring. The generated ions which have mass more than the critical mass decided by the beam dynamics parameter of the ring, gets trapped in the electron beam potential after multiple turn which is known as conventional ion trapping. The other one, in a single turn, the ions may get accumulated along a bunch train causing a transient instability known as fast beam ion instability (FBII). The FBII is more prominent in vertical plane since the beam emittance and thus beam size is very small in vertical plane as compared to the horizontal plane. In FBII, the ion density grows along the bunch train and due to this, bunches towards the end of the bunch train loses more particle than bunches on the front part of the bunch train.

1.8.3 Coupled bunch Instability

When the wake field falls off rapidly with distance and decays on a distance scale equivalent to the length of a single bunch, it is known as short-range wake field and that drives single-bunch instability. In other case, the wake field extends up to many bunches, and such long-range wake fields can drive coupled-bunch instability (CBI). Beam ion interaction also provide long range wake and can be analyzed in the frame work of coupled-bunch instability. CBIs are the most important instabilities encountered in a storage ring operating with multi-bunch operation. The equation of motion for the nth bunch circulating in a storage ring, in the absence of wake fields, is written as

$$\ddot{y_n} + \omega_\beta^2 y_n = 0 \qquad \ldots.(1.50)$$

where ω_β is the betatron frequency. If $W_\perp(z)$ represents the wake function over the entire circumference, then the transverse deflection of the n^{th} bunch is obtained by summing the wake fields generated by all bunches prior to that bunch and over all previous turns. The equation of motion of n^{th} bunch for betatron oscillations in the presence of wake field is written as [30]

$$\ddot{y_n} + \omega_\beta^2 y_n = -\frac{c}{T_0}\frac{r_e}{\gamma} N_0 \sum_k \sum_{m=0}^{M-1} W_\perp\left(-kC - \frac{m-n}{M}C\right) y_m\left(t - kT_0 - \frac{m-n}{M}T_0\right) \quad \text{....(1.51)}$$

where c is velocity of light, r_e is the classical radius of electron, C is the circumference of the ring, γ is the relativistic factor, and T_0 is revolution time of the ring. Here, it is assumed that the storage ring is uniformly filled with M equally-spaced bunches, and each with a total of N_0 particles. The sum over 'm' represents a sum over all bunches in the ring and sum over 'k' represents multiple turns. Normally each bunch oscillate with betatron frequency, but when beam is under the impression of coupled bunch instability, there are different modes of oscillation known as multi bunch modes that depends on how each bunch oscillates with respect to the other bunches. The various modes are indexed using the symbol μ with μ=0, 1,..M-1. The trial solution to the equation 1.51 is written as [30]

$$y_n^\mu(t) \propto exp\left(\frac{2\pi i\mu n}{M}\right) exp\left(-i\Omega_\mu t\right) \quad \text{....(1.52)}$$

where, Ω_μ represents frequency of a mode and the growth rate of the corresponding mode is derived from imaginary part of Ω_μ. The solution to the equation of motion gives the transverse growth rate of the each multi-bunch mode μ [32] and is given as

$$\frac{1}{\tau_\mu} = Im(\Omega_\mu - \omega_\beta) \approx \frac{MN_e e^2 c}{2\omega_\beta E T_0^2} \sum_{p=-\infty}^{\infty} Re\left[Z_\perp\left(pM\omega_0 + \mu\omega_0 + \omega_\beta\right)\right] \quad \text{....(1.53)}$$

where E is the beam energy, T_0 is the revolution time, p is an integer, ω_0 is the revolution frequency and ω_β is the betatron frequency. This formula suggests that CBI grows in strength at a rate proportional to the stored beam current. In practice, the beam is stable at low currents because of natural damping effects caused by synchrotron radiation. However, as more current is injected into a ring, at higher beam current level, a mode or multiple modes become unstable and limits the maximum accumulated beam current in a storage ring. For a given storage ring configuration, there exists a threshold beam current above which the growth rate of instability is more than the natural damping rate and beam shows signature of instability. This single particle model using harmonic oscillator type analysis gives an overall signature of beam instability. However for more realistic estimation, simulation techniques are used where each bunch is treated as large ensemble of macro-particles. To suppress the coupled-bunch instabilities, different mechanisms are adopted depending on the source of instability. Nevertheless for unknown source of instability, bunch-by-bunch feedback (BBF) system is normally preferred. The BBF detects the position of each bunch in the beam by means of signals of beam position monitor and then applies a corrective electromagnetic kick to each one of them. Apart from this, fortunately there is a stabilizing mechanism exit in accelerator known as Landau damping.

1.8.4 Landau damping

Landau damping plays a significant role in plasma physics to damp the collective modes of oscillation in plasma and later this theory is applied in accelerator physics to stabilize the motion of charge particles. The fundamental theories in accelerator physics are mainly described by single particle analysis. Nevertheless, beam contains of a large number of charge particles with finite distributions in their position, energy and oscillation frequencies. The spread in frequencies among the charge particle in a beam leads to Landau damping and acts as a passive damping mechanism against the beam instability. We consider a beam circulating inside an accelerator and assume that for this system, there exists an equilibrium state. One can check whether a small perturbation around the equilibrium state will make the beam unstable. The equation of motion of a beam particle driven by external sinusoidal force is written by

$$\ddot{x} + \omega_\beta^2 x = A\, cos(\Omega\, t) \qquad \text{....}(1.54)$$

where ω_β is the betatron frequency and Ω is frequency of external force. Assume the oscillator is at rest at time $t=0$ when excitation starts and consider the initial condition as

$$x(0) = \dot{x}(0) = 0$$

Solution to the equation 1.54 is given by combination of a homogenous and a particular solution, written as

$$x(t) = \frac{A}{\omega_\beta^2 - \Omega^2}\left(cos\,(\Omega t) - cos\left(\omega_\beta t\right)\right) \qquad \text{....}(1.55)$$

The beam consists of a set of harmonic oscillator having different frequencies ω_β with distribution $\rho(\omega_\beta)$, centered on $\omega_{\beta 0}$ with $\int \rho\left(\omega_\beta\right) d\omega_\beta = 1$. To know the beam response, one can determine the center of mass response of all the oscillators. This can be done by integrating the single oscillator response, over the frequency ω_β weighted with distribution $\rho\,(\omega_\beta)$.

$$\langle x(t)\rangle = \int_{-\infty}^{\infty} x(t)\ \rho\left(\omega_\beta\right) d\omega_\beta \qquad \text{....}(1.56)$$

For a narrow frequency distribution centered on $\omega_{\beta 0}$ and frequency of external force near to this ($\Omega \approx \omega_{\beta 0}$), the solution is given as [33]

$$\langle x(t)\rangle = \frac{A}{2\omega_{\beta 0}} \int_{-\infty}^{\infty} \left\{\frac{1}{\omega_\beta - \Omega}(cos\ \Omega t - \cos\omega_\beta t)\right\} \rho(\omega_\beta)\, d\omega_\beta \qquad \dots.(1.57)$$

After a long time elapsed, ($t \rightarrow \infty$) , and assuming the Ω as complex, the asymptotic response of beam to the excitation is given as

$$\langle x(t)\rangle = \frac{A}{2\omega_{\beta 0}} \left\{\pi\rho(\Omega)\sin\Omega t + \cos\Omega t\ P.V. \int_{-\infty}^{\infty} \frac{1}{\omega_\beta - \Omega}\rho(\omega_\beta)\, d\omega_\beta\right\} \qquad \dots.(1.58)$$

where P. V. represents Cauchy Principal Value. The first part of the solution is a resistive part, i.e. response is in phase with the excitation and resulted into damping. The second part is reactive, i.e. either inductive or capacitive depending on the sign of the driving force. Fig. 1.6 shows the oscillation of all individual particle and the average response, and that shows the average motion is damped.

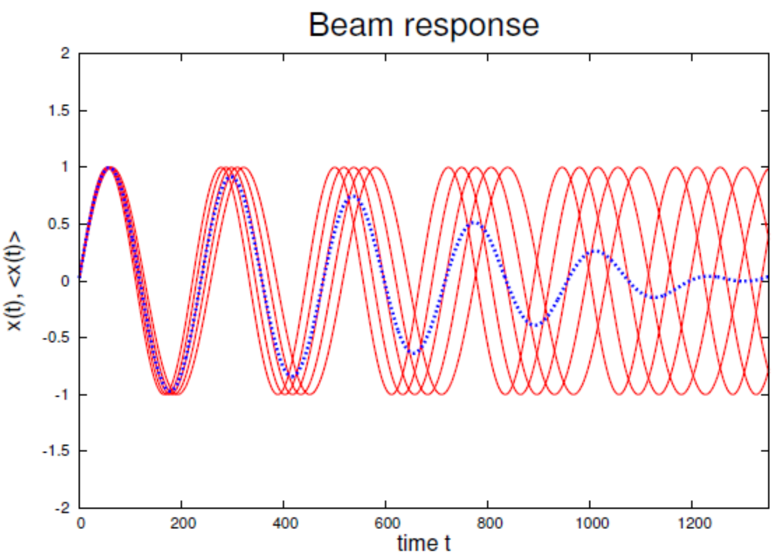

Figure 1.6: Motion of particles with frequency spread and average beam response. Lines with red color shows the beam response at different oscillation frequency and the blue line represents the average beam response. (Courtesy: picture is taken from Ref. 33).

In accelerator, there always exist spread in oscillation frequency among the beam particles because of finite spread in particle momentum and nonlinearities in focusing system. Due to spread in oscillation frequencies of individual bunches in a storage ring, beam stabilizes and this phenomena is called Landau Damping. Additional frequency spread in particle distribution can be realized by increasing nonlinearity in RF cavity (Landau Cavity). Though the frequency (tune) spread helps in stabilization of beam, but more spread can leads to beam emittance growth.

1.9 The Indus accelerator complex

Indus accelerator complex comprises of two storage rings Indus-1 (450 MeV) and Indus-2 (2.5 GeV) along with their injector chain, which are designed, developed, commissioned and made operational at RRCAT, Indore, indigenously [34, 35 and 36]. Both the sources are operated round the clock mode for synchrotron radiation users and they provide congenial environment to the user communities for carrying out research in various scientific domain. Booster synchrotron of circumference ~ 28.5 m serve as a common injector delivering electron beams to both the storage rings. The classical microtron of 20 MeV beam energy serves as a pre-injector to booster synchrotron. Fig. 1.7 shows a schematic layout of the accelerator complex. The electron beam from microtron is guided towards booster through the transport line TL-1. In booster, energy of electron beam is increased to 450 MeV and transferred through transport line TL-2 for injection into Indus-1. For injection into Indus-2, electron beam is accelerated to 550 MeV in booster and then the beam is transported through transfer line TL2 & TL-3. Indus-1 storage ring is of ~19m circumference and is used for the experiments in vacuum ultra violet and soft x-ray region of the electromagnetic radiation spectrum. The maximum beam current of 100 mA is stored in Indus-1 and circulates in the storage ring in the beam decay mode, which has a beam lifetime of 6 hrs at 100 mA. The synchrotron radiation (SR) emitted from its bending magnets is being regularly provided to 7 experimental beamlines.

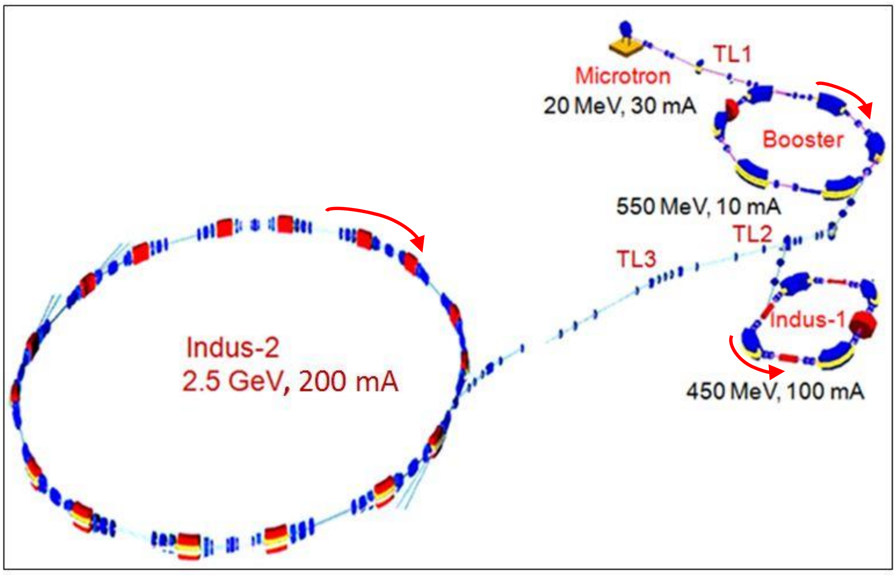

Figure1.7: Schematic diagram of the accelerators in Indus accelerator complex. Beam direction in each accelerators are shown in red curved arrows.

1.9.1 The Indus-2 Storage ring

Indus-2 is a third generation synchrotron radiation source with circumference of ~172 m and being operated routinely at beam energy of 2.5 GeV and stored beam current up to 200 mA. It has adopted a lattice of Double Bend Achromat (DBA) type with 8-fold symmetry. Each unit cell has one long straight sections of length 4.5 m. Among the 8 long straight sections, one is occupied with pulsed magnets for injection, two are for radio frequency (RF) cavities and rest are occupied with various insertion devices (IDs). Each unit cell comprises of two bending magnets, nine quadrupoles and four sextupole magnets. In this way, beam is guided to an orbit by 16 bending magnets, focused by 72 quadrupoles and the chromatic aberration of beam is controlled by 36 sextupoles in Indus-2 storage ring. The basic arrangement of magnetic elements in a unit cell and the lattice function of the storage ring is shown in Fig. 1.8. The summary of Indus-2 storage ring parameters is given in Table 1.1. The circulating electron beam emits SR over a broad spectral range and the critical photon beam energy of the emitted SR spectrum from bending magnets is 6 keV.

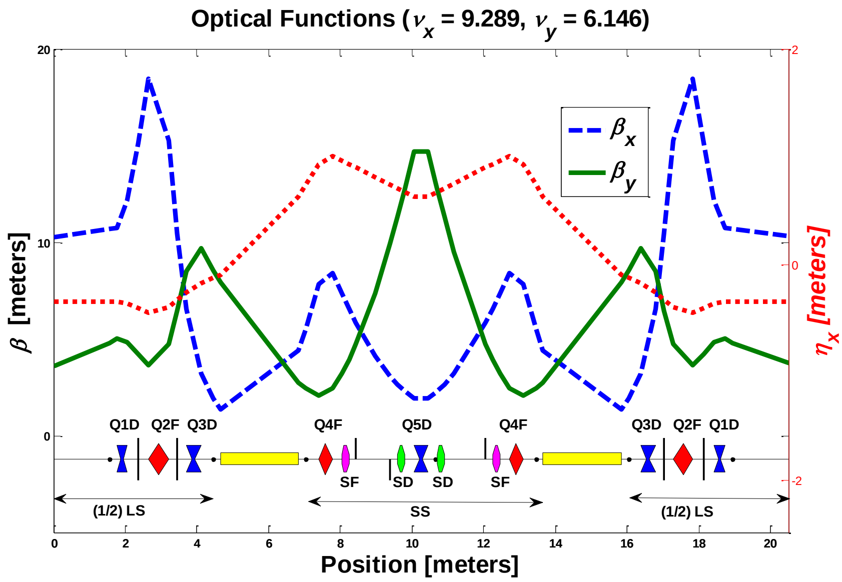

Figure 1.8: Lattice function and schematic of magnet arrangements in one unit cell of Indus-2 storage ring. Q1D, Q2F, Q3D, Q4F & Q5D represent quadrupoles. SF and SD are sextupoles. D signify defocusing magnets & F signify focusing magnets. Long straight section and Short straight section are mentioned with LS and SS respectively.

Table-1.1: Beam parameters of the Indus-2 storage ring.

Parameter	**Value**
Energy E	2.5 GeV
Circumference C	172.47 m
Beam current I	200 mA
Achromatic structure	DBA

Number of unit cell	8
Betatron tune ν_x , ν_z	9.29, 6.14
Synchrotron tune ν_s	0.0143
Natural chromaticity ξ_x , ξ_z	-19, -11
Horizontal emittance ε_x	134 nm rad
Coupling coefficient ε_y / ε_x	1 %
Momentum compaction factor α_c	0.00736
Natural energy spread $\Delta P/P$	9.0e-04
Harmonic Number h	291
RF frequency f_{rf}	505.8 MHz
Radiation damping time τ_x, τ_y, τ_s	4.8 ms , 4.6 ms, 2.2 ms

At present it houses three insertion devices out of which two are planer (named as U1, U2) and one is APPLE-II undulator (U3). The relevant parameters of the installed undulators are provided in Table 1.2. In near future two more devices based on the superconducting technology are planned to enhance the brilliance and other photon beam characteristics of the synchrotron radiation by manifold. One is a multipole wiggler of 2.5 T magnetic field, which will increase the critical energy of the emitted radiation to 10.4 keV. The other one is a 5 T wavelength shifter which will push the critical photon energy to 20.8 keV. The spectral brilliance of the photon beam from the bending magnet and insertion devices in Indus-2 is shown in Fig. 1.9. There are 27 beam lines planned for Indus-2, out of which 22 beam lines are being tapped from its bending magnets and remaining 5 are from the insertion devices. At present sixteen beam lines from bending magnets are in operational mode that includes two diagnostic beam lines.

Beam lines from three installed insertion devices are under different stages of their commissioning phases.

Table 1.2: Relevant parameters of insertion devices installed in Indus-2.

Parameter	U1 Undulator	U2 Undulator	APPLE Undulator
Energy Range of SR	6 eV 250 eV	30 eV to 696 eV	300 eV to 1500 eV
Pole gap range	23 to 109 mm	23 to 61 mm	24 to 70 mm
Period length	126.8 mm	85.2 mm	56.4 mm
Peak magnetic field	1.06 T	0.86 T	0.53 T (V), 0.32 T (H)

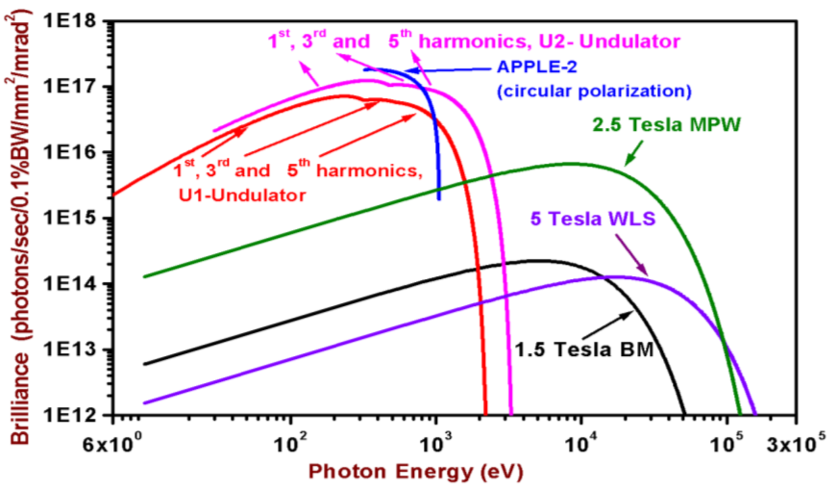

Figure 1.9: The spectral brilliance curve from bending magnet and insertion devices in Indus-2.

1.9.2 Operational status of Indus-2

Looking into the large and diverse user community, efforts are being put to provide near 100 % beam availability with desired beam quality. Among many, implementation of betatron tune feedback plays a crucial role. In reality, a variety of different sources result in drift of actual tune value, that includes gradient errors in quadrupole magnets, closed orbit perturbations, misalignment of sextupole magnets and interaction of electrons and ions of residual gas molecules. The betatron tune in both horizontal and vertical plane were measured using continuous harmonic excitation method. The measurement system employs a spectrum analyzer to analyze the beam signals and a set of strip-line kickers to excite the beam and measure the response of the beam. Fig. 1.10 shows the setup for tune measurement system (left) and beam spectrum captured in spectrum analyzer (right). The strip-line kicker is excited with an excitation frequency (f_{kick}) which is swept from 0 to n $f_0/2$ (with f_0 being the beam revolution frequency and n being an integer). When the frequency crosses the horizontal or vertical betatron frequencies, it generates coherent beam oscillations. Fig. 1.10 (right) shows the betatron sidebands in the beam spectrum in response to the excitation frequency. The fractional part of betatron tune is calculated from the frequency of the betatron peak. The resolution of this tune measurement system amounts to 0.0005 tune units.

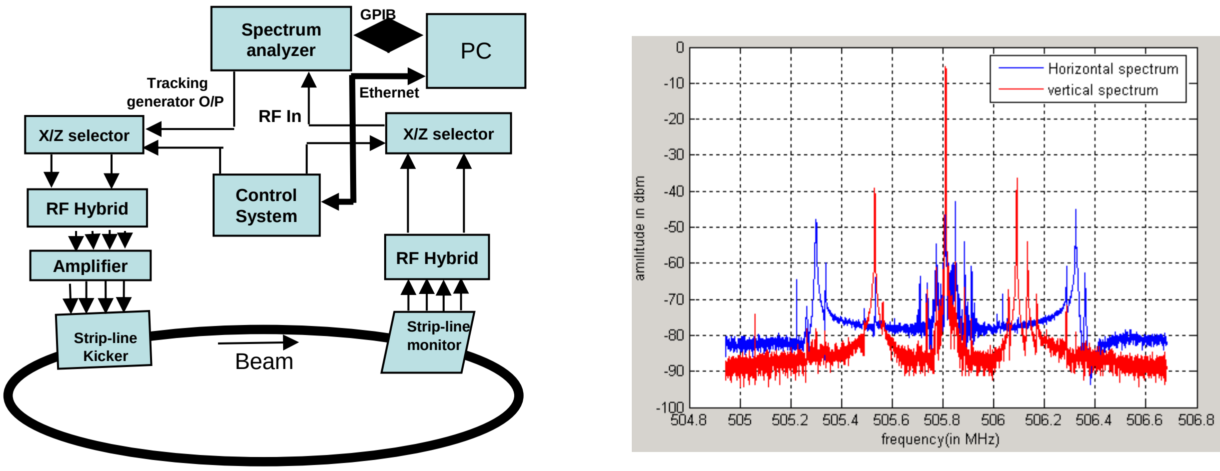

Figure 1.10: (Left) Schematic diagram of tune measurement setup, (right) beam spectrum in both horizontal and vertical planes. The central peak signal shows the RF frequency (revolution harmonics) and the peaks in either side indicates the betatron frequency.

We have observed the random tune variation in Indus-2 during beam current accumulation and it hinders smooth operation. To stabilize the betatron tune during the machine operation, we have deployed a tune feedback system. The feedback system uses two families of quadrupole magnets (one focusing and other defocusing). These two families were chosen out of total five families, based on their sensitivity towards the tune change [37]. Proportional integral (PI) control is used to determine the required changes in quadrupole currents to make the tune feedback system stable and fast converging. The tune feedback provides a real-time correction of tune drifts. Fig. 1.11 shows beam current accumulation in Indus-2 storage ring with and without tune feedback and also shows the measured tune in both horizontal & vertical plane. From the Fig. 1.11, it is clearly observed that the tune variation is large, when tune feedback is kept OFF, and also beam accumulation is not smooth. However, when the tune feedback was put ON, the tune variation in both the plane becomes less and smooth beam accumulation occurs.

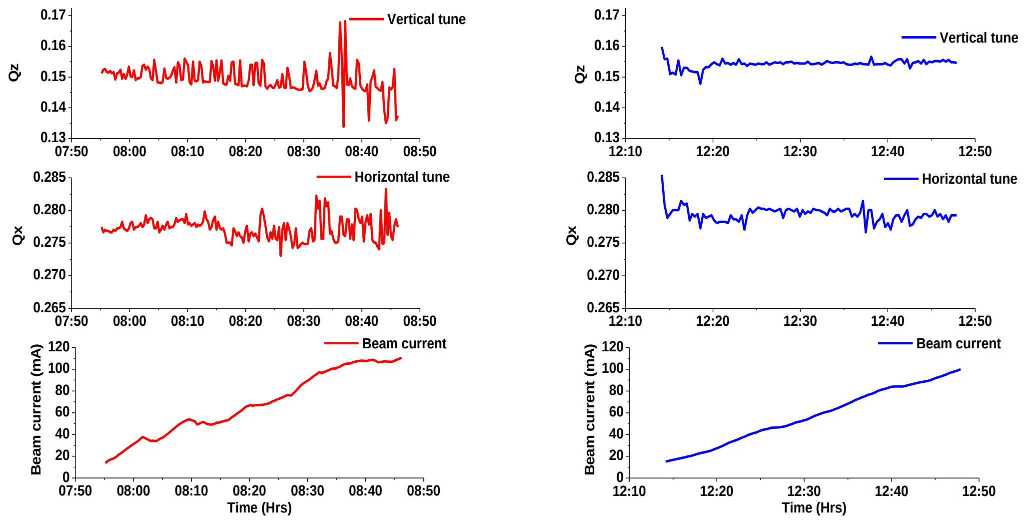

Figure 1.11: Betatron tune variation during beam current accumulation in Indus-2. (Left) Tune feedback ON and (right) Tune feedback OFF. Top graph shows the vertical tune, middle one shows the horizontal tune and bottom one shows the beam current accumulation.

Other major efforts include beam based alignment (BBA), bunch filling pattern optimization, LOCO (linear optics from closed orbit) implementation, slow and fast orbit feedback system, and transverse multi bunch feedback [38]. BBA estimates the relative offset between the center of quadrupole and BPM center with high precision. This helps in reducing the COD to 0.45 mm rms in horizontal plane and 0.2 mm rms in vertical plane [39]. The closed orbit is stabilized globally within ± 30 μm in both horizontal and vertical plane using slow orbit feedback system. These augmentation and continuous operation have resulted in enhancement of Indus-2 performance. It has achieved a measured beam lifetime of 80 hours at 100 mA stored beam current. Usually beam is filled in storage rings once per day and a typical beam current accumulation along with decay curve is shown in Fig.1.12 for Indus-2. To improve the beam quality further in Indus-2, horizontal beam emittance was reduced up to 45 nm rad. Also in order to provide coherent synchrotron radiation in THz frequency range, a trial operation has been executed with the low momentum compaction factor optics that reduces the electron bunch length to sub-picosecond range.

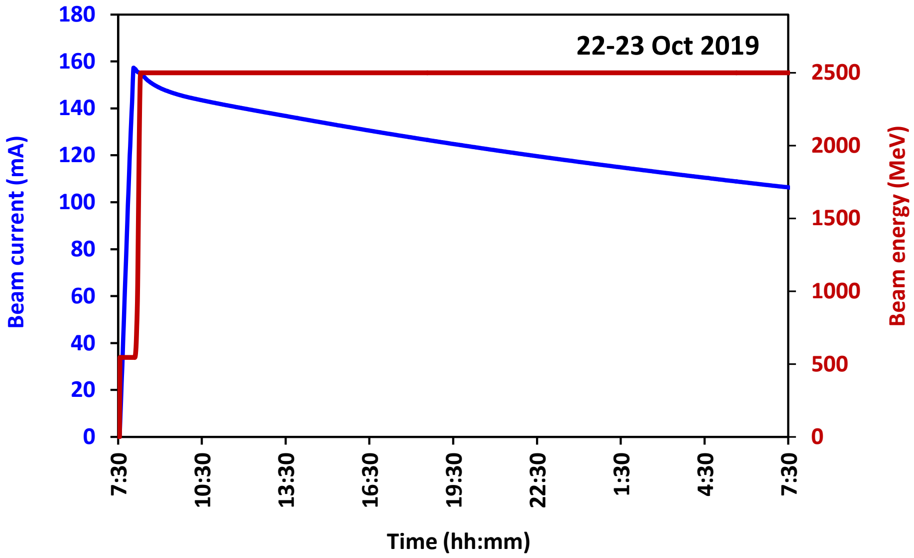

Figure 1.12: Typical beam accumulation, energy ramping and decay pattern in Indus-2.

The thesis is organized into five chapters. The basic accelerator physics and Indus-2 storage ring is discussed in Chapter 1. After the introduction, the criteria for conventional ion trapping in the electron beam potential and techniques to solve the ion trapping problem using partial bunch filling pattern is discussed in Chapter 2. In Chapter 3, the fast beam ion instability caused by the beam ion interaction in a single turn beam circulation in Indus-2 are presented. The simulation study of FBII was described to estimate the growth rate of the instability and the effect of beam emittance, beam current and vacuum pressure of the ring on FBII is also presented. Next, the study of FBII is made using the impedance model similar to conventional instabilities generated due to beam-structure interaction. The effect of multi train bunch filling pattern on FBII is covered in Chapter 4. The conclusions and future perspectives of the thesis are presented in Chapter 5.

CHAPTER-2

ION TRAPPING IN ELECTRON STORAGE RING

The electron beam, while propagating in the storage ring vacuum chamber, ionizes the residual gas molecules present inside. The detached electron from the gas molecules are repelled by the negative potential of electron beam and move away from the beam path and finally lost after hitting the vacuum chamber wall. However the created positive ions of residual gas gets trapped in the negative potential well of the electron beam due to Coulomb force of electron beam. This phenomena is known as ion trapping which can affect the dynamics of electron beam in the storage ring. Initial observation of ion trapping was made in electron-positron storage rings at DORIS [3] (Germany) and ADONE [40] (Italy) during the year 1970-1980. Shortly after its detection, it was realized that it could limit the maximum beam current accumulation in a storage ring. Therefore, to get rid of this problem, several techniques were deployed that includes use of ion clearing electrode inside the vacuum chamber, beam shaking at the specific frequency and creating bunch gaps in bunch train. The ion clearing strategy involves directly removing the trapped ions using an electric field generated by an ion clearing electrode – an instrument similar to a large parallel plate capacitor [41]. The other method of ion clearing involves shaking the beam at betatron sidebands by applying a time varying voltage to a stripline kicker, which drives a beam-ion coupling resonance and knocks the ions out of the center of the beam [42]. There is another method of ion clearing which does not use any external forces, i.e. by providing long bunch gaps (empty RF buckets) in order to give time for ions to drift away from the beam path between bunch trains [6]. Among these three techniques, the last one was studied extensively and an optimized bunch gaps was evolved by analytical means and also verified experimentally in Indus-2. We describe the mechanism of ion production and ionization rate in the section 2.1-2.2. The characteristics of generated ions and electron beam potential are discussed in section 2.3-2.5. Then we analyze the stability of ions in a storage ring filled with electron beam with a homogenous bunch pattern and with a long bunch gaps in section 2.6 - 2.9. The evidence of ion trapping with experimental observation of betatron tune shift, beam lifetime and transverse coupled bunch instability in Indus-2 is discussed in section 2.10.

2.1 Ionization process in electron storage ring

There are several ionization mechanisms in synchrotron light sources namely collision ionization, ionization due to synchrotron radiation and tunneling ionization in beam electric field. Among them, the predominant one is inelastic collision of circulating electron beam with residual gas molecules present inside the vacuum chamber and only this process is considered in the thesis. Synchrotron radiation (SR) ionizes residual gases present between the center of the beam and the vacuum chamber walls. However, the SR generated ions have less density compared to ions generated due to collisional ionization [43]. In addition, the ions generated by SR are also far away from the beam and form a diffuse halo around the beam which has less impact on electron beam dynamics. Therefore ions generated due to photoionization is not considered and beyond the scope of this thesis. The tunneling ionization occurs when the electric fields of the beam is sufficiently large (~ 10 GV/m). This peak electric field suppress the potential barrier which is confining an electron in a gas molecule, and thereby allow the electrons to escape via tunneling effect [44 and 45]. The electron beam size of sub-micrometer produces such extremely high electric field and the gas molecules are ionized by tunneling effect. For a typical beam size and beam current in 3rd generation storage ring, the electric field is few MV/m and hence the chances of ionization by tunneling effect is negligible and ignored in the present thesis.

2.2 Ionization rate

The rate of collision ionization depends on the density of the residual gas, as well as the collision ionization cross section of the gas species. Collision ionization cross section σ_i, for residual gas species is parametrized by following relation [46]

$$\sigma_i = 4\pi\left(\frac{\hbar}{m_e c}\right)^2\left\{C_1\left[\frac{1}{\beta^2}\ ln\left(\frac{\beta^2}{1-\beta^2}\right)-1\right]+\frac{C_2}{\beta^2}\right\} \qquad \text{....(2.1)}$$

where m_e is the mass of the electron, c is the speed of electron, $\hbar = {h}/{2\pi}$, where h is the Planck constant, β is the relativistic factor of the electron beam, and C_1, C_2 are empirically determined constants for different gas molecules which depends on properties of gas. Table 2.1 shows the mass number of gas species found in a storage ring vacuum chamber for an average pressure of 1 nTorr and their value of C_1, C_2. [46]

Table-2.1: Value of C_1 & C_2 to estimate ionization cross section of different gas species.

Gas species	Mass No.	C_1	C_2
H_2	2	0.7	8.1
H_2O	18	3.2	32.3
CO	28	3.7	35.1
O_2	32	4.2	38.8
CO_2	44	5.75	55.9

The ionization cross sections for gas species are weakly depends on beam energy. For example, the ionization cross sections of CO for a beam energy of 550 MeV and 2.5 GeV is 1.55 x 10^{-22} m^2 and 1.76 x 10^{-22} m^2 respectively. The density 'n' of residual gas molecules is expressed by the relation

$$p = n\,k\,T \qquad \text{.... (2.2)}$$

where k is Boltzmann constant, p is the pressure in Pascal and T is the absolute temperature in Kelvin. Thus at 1 nTorr pressure in a vacuum chamber, kept at room temperature of 300 K, the molecular density of the gas is 3.2 x 10^{13} m^{-3}. The time required to create one ion of any molecular species by one electron inside a vacuum chamber is known as the ionization time τ_i, and given as [47]

$$\tau_i = \frac{1}{n\,\sigma_i\,c} \qquad \text{.... (2.3)}$$

The reciprocal of ionization time defines the ionization rate for an electron. The ionization time for various gas species was calculated against pressures using eqn. (2.3) at room temperature of 300 K and shown in Fig. 2.1.

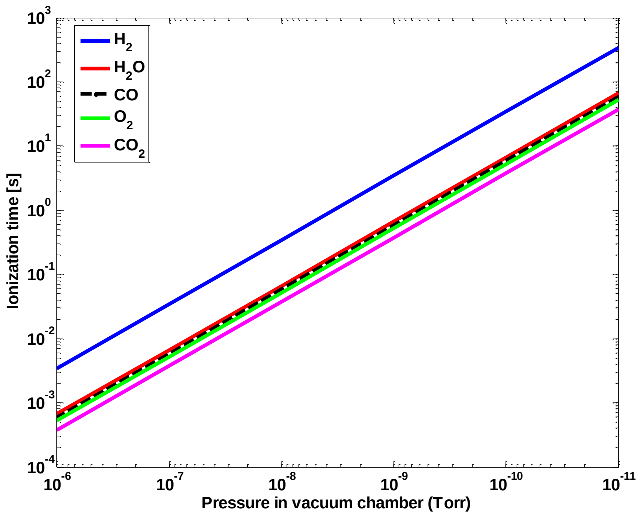

Figure 2.1: The Ionization time of various gas species at different pressure conditions in vacuum chamber of Indus-2 storage ring.

These estimates suggests that the beam will become fully neutralized within seconds, for vacuum pressure as low as 1nTorr. Thus, the ions has to be removed from beam path as early as possible to mitigate its effects on the electron beam. In this analysis, only single ionization state is considered and higher ionization states are ignored as the ionization cross section for higher ionization states is very small. Table 2.2 shows a comparison of single and multiple ionization cross section of H_2 and CO at 500 MeV beam energy [48].

Table 2.2: Ionization cross section of H_2 and CO in single and double ionization state

Process	C_1	C_2	Cross section (Mbarn)
$e^- + H_2 \rightarrow H_2^+ + 2e^-$	0.7	8.1	0.32
$e^- + H_2^+ \rightarrow 2H^+ + 2e^-$	0.046	1.1	0.031
$e^- + CO \rightarrow CO^+ + 2e^-$	3.7	35.1	1.54
$e^- + CO \rightarrow CO^{++} + 3e^-$	0.035	0.30	0.01

The ions are accumulated in the storage ring until their net density approaches the density of the beam. This effect is known as full beam neutralization and that places an upper limit on the maximum ion density that can be achieved. We define the neutralization coefficient as the formula given below and its value lies between 0 and 1.

$$\eta = \frac{Total\ ion\ \ density}{electron\ \ density} \qquad \text{....}(2.4)$$

2.3 Thermal energy and speed of ions

During the ionization process, the energy imparted to the residual gas molecules by the electron beam is negligible and thus the newly formed ions have almost same speed distribution as that of the gas molecules. The speed of gas molecules follows the Maxwell-Boltzmann distribution having the probability distribution function as

$$f(v) = \left(\frac{m}{2\pi kT}\right)^{3/2} 4\pi v^2 \exp\left(-\frac{mv^2}{2kT}\right) \qquad \dots.(2.5)$$

where v is the speed of gas molecules, m is the mass of gas molecule. The rms speed and mean kinetic energy of the gas molecules are calculated as

$$v_{rms} = \sqrt{\frac{3kT}{m}} \qquad \dots.(2.6)$$

$$E = \frac{1}{2}mv_{rms}^2 = \frac{3}{2}kT \qquad \dots.(2.7)$$

These formulation estimates, the generated ions have a speed somewhere between 100 m/s and 2000 m/s and kinetic energy of ~0.04 eV at room temperature (300 K) which is same for all ion species.

2.4 Motion of ions in external magnetic field

The dipole, quadrupole and sextupole magnets in the ring offers magnetic field to the positive ions. The dipole provides magnetic field in vertical direction only, so the vertical motion of the ions is not being affected by the dipole field as $v_{iy} \times B_y = 0$. However the horizontal and longitudinal motion of ions is influenced by dipole field and in those plane, ions perform cyclotron motion with frequency and radius given as [47]

$$\omega_i = \frac{q_i B}{m_i} \qquad \dots.(2.8)$$

$$r_i = \frac{m_i v_i}{q_i B} \qquad \dots.(2.9)$$

where ω_i is the cyclotron frequency of ion, q_i is the charge of ion, m_i is the mass of ion, v_i is the thermal speed of ion and B is the magnetic field of the dipole. For a typical dipole magnetic field of 1.5 Tesla, the radius of gyration of H_2^+ ion is ~ 12 μm which is very small. With the combined effect of electric field of the electron beam and magnetic field of dipole magnet, the ions experiences a cross-field drift velocity (v_{Dc}) with a direction perpendicular to E and B, given as [47]

$$\overrightarrow{v_{Dc}} = \frac{\vec{E} \times \vec{B}}{B^2} \qquad \ldots.(2.10)$$

E_x and B_y will produce drift velocity of ions in longitudinal direction and the ions drift in opposite direction on each side of the central beam axis due to nature of electric field of the beam. This cross drift velocity does not depend on ion mass, which means H_2^+ and CO^+ ion experiences same drift velocity. The drift velocity is zero at beam center as the electric field at center of beam is zero and it rises linearly with distance and becomes maximum at the edge of the beam, which is a small value. Thus in an electron storage ring, ions generated near the center of the beam could not escape with the help of cross field drift velocity. Similarly, the ion experiences a gradient drift velocity, v_{Dg} in longitudinal direction due to the magnetic field of the quadrupole magnet and is given as [48]

$$v_{Dg} = \frac{q_i r_i^2}{2m_i} \frac{\partial B_y}{\partial x} \qquad \ldots.(2.11)$$

where r_i is the radius of gyration defined in eqn. 2.9. For a typical gradient of 15 T/m in a storage ring quadrupole magnet, the gradient drift velocity of H_2^+ ion is 51 mm/s which is rather too small.

2.5 The potential and electric field of the beam

The circulating electron beam produces electric field which acts on the generated ions. This electric field can be estimated using Maxwell's equations for various particle distributions and beam-pipe geometries. The potential is defined from the electric field and the depth of potential well is calculated from the boundary condition with the vacuum chamber at ground potential. The simplest case is to consider a circular beam of uniform density in a circular chamber. The electric field produced by the beam is given as [47]

$$E(r) = \begin{cases} \dfrac{e\lambda}{2\pi\epsilon_0} \dfrac{r}{a^2} & r < a \\ \dfrac{e\lambda}{2\pi\epsilon_0} \dfrac{1}{r} & r \geq a \end{cases} \qquad \text{....(2.12)}$$

where λ is the line charge density defined as the number of electrons per unit length of the beam, *a* is the radius of beam and ϵ_0 is the vacuum permittivity. The electric potential is defined as

$$V(r) = -\int E(r)\ dr \qquad \text{....(2.13)}$$

With the boundary condition, V= 0 at r= r_c (vacuum chamber radius), the potential is given as

$$V(r) = \frac{e\lambda}{2\pi\epsilon_0} \begin{cases} -\dfrac{r^2}{2a^2} + log\dfrac{r_c}{a} + \dfrac{1}{2} & r < a \\ log\left(\dfrac{r_c}{r}\right) & r \geq a \end{cases} \qquad \text{....(2.14)}$$

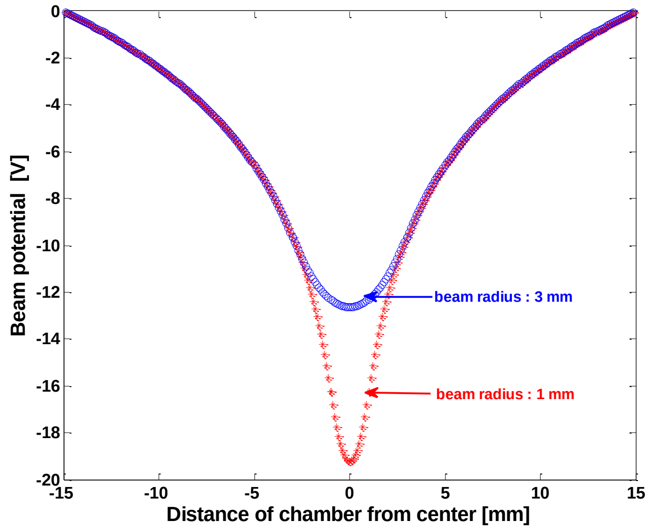

Figure 2.2: Electron beam potential considering circular beam for two different radii, i.e. 3 mm and 1 mm.

Fig. 2.2 shows the beam potential for a circular beam of different size inside a circular chamber of radius 15 mm. The depth of potential well increases as the beam size decreases for a fixed beam current. For typical beam sizes in the storage ring, the depth of potential well is always larger than the thermal energy of created positive ions and it indicates the ion will remain trapped unless any external force is applied. In a storage ring, the potential does not remain constant, rather varies throughout the circumference as the beam size varies due to strong focusing optics of lattice and also due to variation in the beam pipe cross-section. The potential becomes maximum near the minimum beam size, where maximum ion trapping occurs. These trapped ions can be removed by external means using ion clearing electrode (ICE). The ICEs are negatively charged capacitive plates with an applied DC voltage in the range of few kV, fitted into vacuum chamber wall. The ICE divert the positive ions towards them and the ions are neutralized there and return to gas phase [49]. The ICEs shall be placed in the area where the ion concentration is high, which is preferably at minimum beam size location in the ring. In view of this, the best location of ICE is near to focusing quadrupole in vertical plane, however they are normally placed in straight sections because of the availability of space. Thus ion clearing would be relatively ineffective in the magnet region and in electron storage ring the magnets occupies nearly half the ring circumference.

Therefore to remove the ions, it needs to drift them to the longitudinal position of the clearing electrode in a reasonably shorter time than the neutralization time. For a 10 m separation between the electrodes, the time required for CO^+ ion to drift freely up to a clearing electrode will be ~ 20 ms which assumes the thermal speed of CO^+ ion as 500 m/s. The effective neutralization in this scenario will be the drifting time of ions divided by the ion production time and that comes about 0.02 for an average pressure of 1 nTorr. This suggests that the ICE can only reduce the neutralization coefficient to around 2% which means significant number of ions are still there in chamber as electron density exceeds the residual gas density by several order [49]. Also, the ICE impacts significantly on the storage ring impedance which adversely affects the overall beam stability. Thus, this method is not suitable to solve the problem of ion trapping in 3rd generation electron storage ring and as an alternative method, introduction of bunch gaps was evolved afterwards.

2.6 Stability condition of ions

The positive ions gets a kick towards the closed orbit in each passage of electron bunch. The amount of kick is estimated from the electric field of an electron bunch. Most of the ions are created within the beam size, and there the electric field of the bunch is approximately linear. The circulating electron bunch has Gaussian charge distribution and the electric field in a linear approximation is given as [50]

$$E_{x,y} = \frac{\lambda}{2\pi\varepsilon_0\sigma_{x,y}\left(\sigma_y + \sigma_x\right)}\ (x, y) \qquad \text{.... (2.15)}$$

where σ_x, and σ_y are rms transverse electron beam size in horizontal and vertical plane respectively. Since the electron beam size is smaller in vertical plane than that of horizontal plane, the force experienced by ions is more in vertical plane. Thus the ion trapping study is carried out in vertical plane only. The positive ions experience this electric field and the equation of motion for an ion in the influence of electron bunch is given as

$$M_{ion}\ \ddot{y}_i = q_i\ E_y^{elec} \qquad \text{.... (2.16)}$$

$$A\ m_p\ \ddot{y}_i\ = -\frac{e\ \lambda\ y_i}{2\pi\varepsilon_0\sigma_y\left(\sigma_y + \sigma_x\right)}$$

$$\ddot{y}_i = -\frac{N_b}{l_b}\frac{2r_p c^2}{A\sigma_y\left(\sigma_y + \sigma_x\right)}y_i$$

$$\dot{y}_i = -\frac{2N_b r_p c}{A\sigma_y\left(\sigma_y + \sigma_x\right)}y_i + (\dot{y}_i)_0 \qquad \text{.... (2.17)}$$

where standard definition of the classical proton radius (r_p) and line charge density of electron beam is used, which are defined as

$$r_p = \frac{e^2}{4\pi\varepsilon_0 m_p c^2}$$

$$\lambda = \frac{eN_b}{l_b}$$

where q_i is charge of the ion, A is atomic mass of the ion, N_b is the number of particles in an electron bunch, l_b is the bunch length and m_p is the mass of proton. The mechanism of ion trapping in a bunched electron beam can be modelled as the ions experience a focusing force from an electron bunch and drift freely in the bunch gaps. This allows us to study the motion of ions by constructing a transport matrix similar to thin lens quadrupole approximation for the electron bunch and drift space for the bunch gap. The stability of ion motion is studied in the same fashion as described in circular accelerator theory. The vertical displacement of the trapped ions at a time t and a position s in a ring affected by an electron bunch is modelled as [1]

$$Y = MY_0$$

Or

$$\begin{pmatrix} y \\ \dot{y} \end{pmatrix}_{t=t} = \begin{pmatrix} 1 & t_b \\ 0 & 1 \end{pmatrix} \begin{pmatrix} 1 & 0 \\ -k & 1 \end{pmatrix} \begin{pmatrix} y \\ \dot{y} \end{pmatrix}_{t=0} \qquad \text{....} (2.18)$$

where M is transfer matrix for a period (electron bunch + bunch gap), t_b is separation in time between successive bunches and k is the linear kick parameter derived from eqn (2.17) and defined as

$$k = \frac{2\, N_b r_p c}{A\, \sigma_y (\sigma_x + \sigma_y)} \qquad \text{....} (2.19)$$

At each passage of the electron bunch, an ion experiences the transverse kick towards the bunch center. In a homogeneous beam filling where the electron bunches are equally spaced, the ions may execute stable oscillations about the electron bunch centers. The ion motion remains stable when the trace of the transport matrix M satisfy the inequality -2 ≤ Tr (M) ≤ 2. This can be shown to be satisfied only if $A \geq A_c$, where A_c is the critical mass defined as

$$A_c = \frac{r_p\, N\, C}{2\, n^2\, \sigma_y \left(\sigma_x + \sigma_y\right)} \qquad \text{....} (2.20)$$

where N is the total number of electrons in a ring, *C* is the circumference of the storage ring and *n* is the number of bunches in a storage ring. This condition defines a critical mass which describes that, the ions performs stable oscillation and trapped in the potential well of the electron beam when their atomic mass exceeds A_c. In other words, A_c is the minimum atomic mass of ions that can be trapped. In case of the Indus-2 storage ring, if all RF buckets are filled with uniform charge, A_c becomes 0.07 which means all the possible ion species ranging from H_2 to CO_2 will be trapped in beam potential. In a storage ring of the vacuum in the range of 1 nTorr, the gas species likely to be present have atomic mass less than 45. Thus, storage ring with critical mass above 45 solves the problem of ion trapping. A_c becomes large for small transverse beam sizes, high beam current and less number of bunches in a ring. For Indus-2 storage ring, keeping the beam current and beam sizes fixed, if the ring will be filled with only 12 equidistant bunches, critical mass A_c can be raised above 45 and with this configuration, there will be no ions trapped. However, this filling configuration doesn't allow to store high beam current in storage ring as it leads to the various beam instabilities because of high electron density in each electron bunch. The alternate and more practical approach to get rid of ion trapping is to make one bunch train consisting of several bunches followed by a sufficiently long bunch gap.

Each ion species oscillates with certain frequency inside a beam potential. Considering this as a simple harmonic oscillator, the ion oscillation frequency is derived from the equation of motion of ions, and is given as

$$f_{(ion)x,y} = \frac{c}{2\pi}\sqrt{\left[\frac{4N_b r_p}{3L_{sep}\sigma_{x,y}(\sigma_x + \sigma_y)A}\right]} \qquad \ldots.(2.21)$$

where L_{sep} is gap length between two consecutive bunches. Ions remain almost stationary at the place of their generation because of the heavier mass. The circulating electron bunch pulls these ions towards its center and in the bunch gap ions simply drift. This process continues with successive moving electron bunches and thereby the trapped ions sets up an oscillatory motion around the electron beam. In other words, ions get trapped in the electron beam, if ion oscillation frequency is smaller than the bunch arrival frequency. The exact trapping condition of the ions in the beam is given as

$$4f_{ion} \le \frac{c}{L_{sep}} \qquad \text{....}(2.22)$$

In an electron storage ring, the transverse beam sizes varies around its circumference due to strong focusing lattice. Thus every ion has different frequencies along the circumference and hence may become stable in some part of the ring and unstable in other regions of the ring. For the Indus-2 storage ring, the ion frequencies are spread over a frequency range and they are of the order of few MHz.

2.7 Effect of bunch gaps on stability of ions

Leaving several consecutive RF buckets empty in the bunch filling pattern, reduces the ion density and this helps in curbing the ion trapping problem in the storage ring. In this bunch filling mode, ion experiences a periodic attractive force of electron bunches and a drift in the long beam free gap. Such a repetitive process over many turn makes the transverse ion oscillation amplitude to grow and ultimately ions are ejected or lost in the vacuum chamber wall. For a configuration of bunch train consisting of a series of bunches with equally populated electrons followed by a series of empty buckets, the transfer matrix for the passage of the whole bunch train is expressed as [51 and 7]

$$M = \left[\begin{pmatrix} 1 & t_b \\ 0 & 1 \end{pmatrix}\begin{pmatrix} 1 & 0 \\ -k & 1 \end{pmatrix}\right]^n \begin{pmatrix} 1 & t_b \\ 0 & 1 \end{pmatrix}^{h-n} \quad \ldots.(2.23)$$

where n is the number of bunches in a bunch train and h is the harmonic number of the storage ring. Fig. 2.3 shows a sketch of the bunch trains.

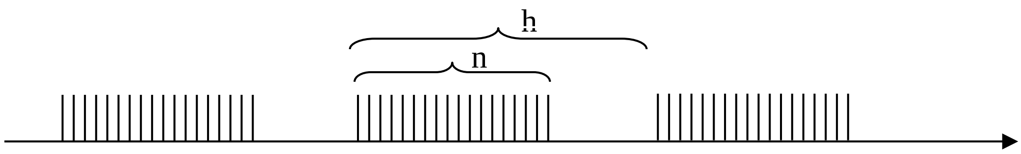

Figure 2.3: An illustraion of bunch train that shows a maximum possible RF buckets 'h' in a train out of which 'n' RF buckets are filled with electron and 'h-n' RF buckets are empty.

The nature of the matrix mentioned in eqn. (2.23) is complicated enough to find out stability conditions in a simple analytical form. However using numerical method, the trace of the matrix can easily be solved that reveals the stable and unstable zone for the ions. Here the condition of stability $-2 \leq Tr(M) \leq 2$ doesn't leads to a critical mass like the case of homogeneous bunch filling. Fig. 2.4 shows the trace of the transfer matrix for a fixed beam current and considering average beam size vs. different ion species in two bunch filling modes of operation in Indus-2 ring. One mode fills all the RF buckets and other mode fills 191 bunches with a gap of 100 successive RF buckets. This indicates that the trace of transfer matrix remains within the range of [-2, 2] in a uniform filling of all 291 bunches and thus all ions perform a stable oscillation. However, the trace of transfer matrix for all ion species was found to be away from the zone of [-2, 2] except few atomic mass number which does not exist in reality, when a long bunch gap is introduced. So for partial bunch filling pattern, it was noticed that ions are not trapped in the electron beam potential as they perform unstable motion around the beam. This draws the conclusion, the asymmetric bunch filling pattern provides considerable alleviation to the ion trapping problem. However, apart from the configuration of the bunch train, the trace of the transfer matrix depends also on beam size which varies along the ring and hence the stability condition differs at different positions in the ring.

The

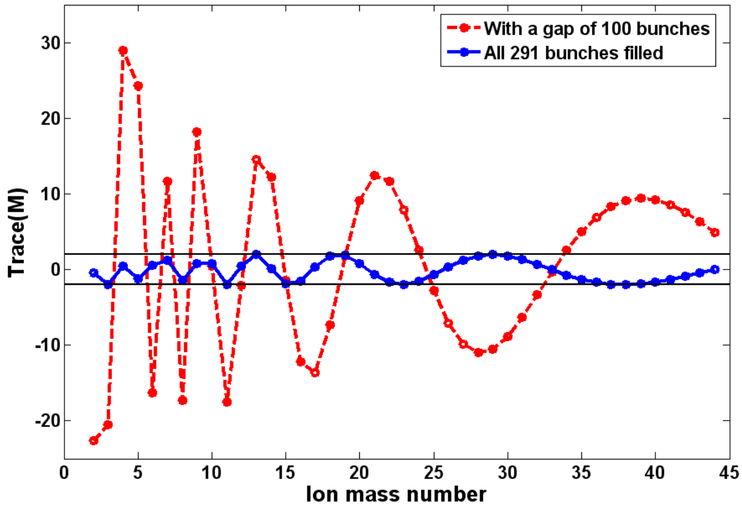

Figure 2.4: Trace of the transfer matrix of ion motion in presence of bunched electron beam as a function of different ion species of atomic mass 2 [H_2] up to 44 [CO_2] for two bunch filling modes. Blue solid curve: all 291 bunches filled. Red dash curve: 191 consecutive bunches filled with a gap size of 100 bunches. Stable zone, $|Trace(M)| \leq 2$ is contained by two horizontal straight lines.

2.8 Stability of ions in the Indus-2 storage ring

We investigate the stability of ions in the Indus-2 storage ring for uniform and partial bunch filling pattern. Fig. 2.5 shows the stability of different ion species versus various bunch gap sizes (0 to 200) for a single bunch train at 20 mA beam current in Indus-2. The graph shows the stable and unstable bands with respect to bunch gaps in the filling pattern for different ion species. It can be noticed that, the extreme left side of the graph ensures all the ions are trapped. This explains that, when all the 291 bunches are filled, all ion species are trapped in electron beam potential. However, as the gaps in filling pattern increases, more and more ion species becomes unstable. The ion trapping is becoming less severe with empty RF buckets and with a gap of 100 bunches (~ corresponds to 2/3rd filling), the ion trapping effects in Indus-2 ring becomes very less. However, as the beam current increases the scenario of the trapping condition verses bunch gap might change [52].

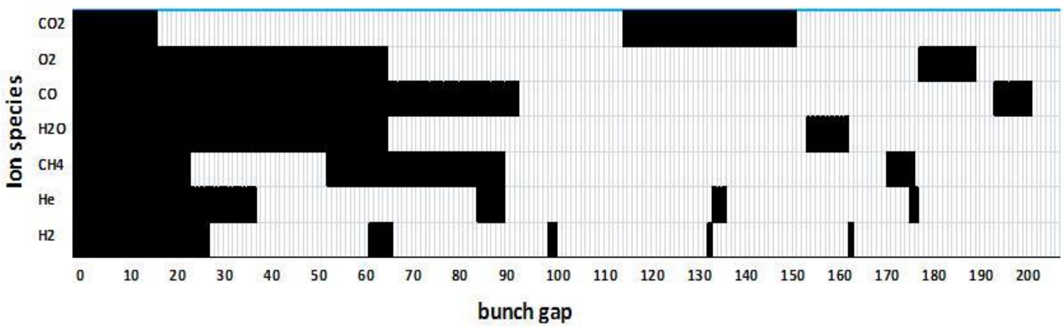

Figure 2.5: Stability of various ion species for different bunch gap size in Indus-2. Dark areas indicate the stability of ions.

The stability conditions for various ion species were also studied for different beam currents at injection energy. Fig. 2.6 shows the percentage of unstable ion as a function of various bunch gap size. This graph explains that, for a gap size of 125 bunches, almost 90 % ions are unstable for the entire beam current range and will not be trapped in the electron beam path. However this analysis was made considering equal population in each bunch but in reality this may not be the situation. Unequal bunch population create spread in ion frequency and to avoid the ion trapping, less bunch gap may be required in bunch train than the above calculated value.

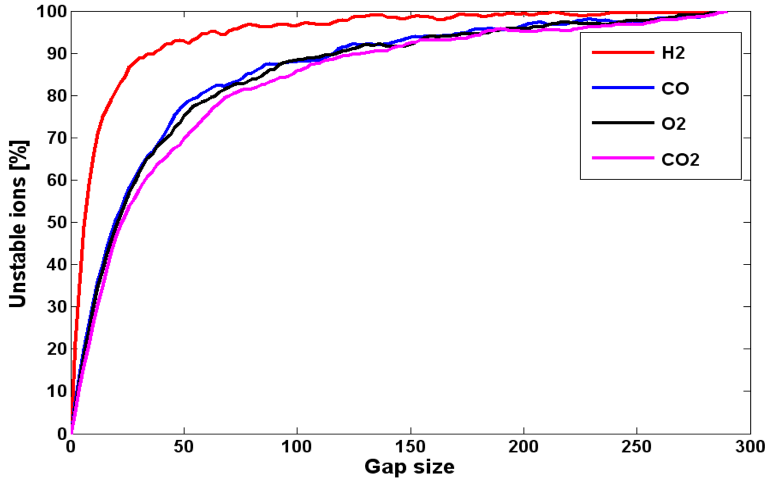

Figure 2.6: Percentage of unstable ions of various gas species for different beam currents as a function of the bunch gap size in Indus-2.

The stability condition of ions varies along the circumference of ring as the electron beam size varies due to strong focusing lattice. Ions may remain stable in some regions of the ring and unstable in the other parts of the ring. The stability of ion species throughout the Indus-2 ring were estimated considering the beam size variation. For this, beam size along the ring circumference is estimated at every 10 cm and in each part, stability condition of CO ion was analyzed. Fig. 2.7 shows the percentage of the region (with color bar representation) where the CO ions are trapped in the ring. It shows that, the ring is surrounded with regions of stable and unstable ion accumulation. This analysis helps us to choose the bunch filling mode of Indus-2 in which effect of ion trapping gets minimized. This ensures that, when the ring is filled with 150 consecutive bunches in a single bunch train, the ion trapping takes place in less than 10% locations.

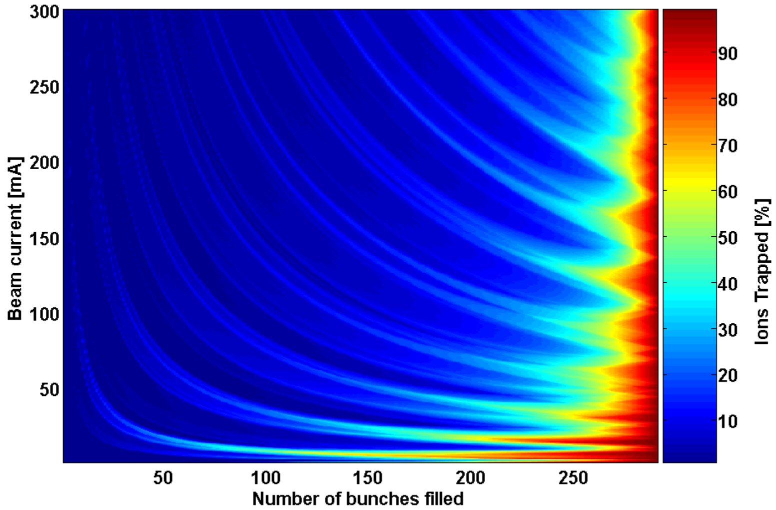

Figure 2.7: Percentage of region of Indus-2 ring circumference where CO ions are trapped for various length of bunch train. The maximum length of bunch train is 291.

2.9 Effects of trapped ions on the betatron tune

In electron storage ring, the trapped ions affect the electron beam quality in various ways. The ions would focus the electron beam that causes incoherent betatron tune shift, and can cause more severe problem like beam instabilities. The trapped ions plays a major role for electron beam current saturation during accumulation. Further, it reduces the beam lifetime and increases the vertical beam size, thereby severely degrading the storage ring performance. The space charge of the accumulated ions provides an electric field and the electron beam experience a focusing force in both horizontal and vertical plane. This causes shift in betatron tune of electron beam and the amount of tune shift is given as [5 and 53]

$$\Delta\nu_{x,y} = \frac{r_e\,\overline{\beta_{x,y}}\,N\,\eta}{4\pi\gamma\sigma_{x,y}(\sigma_x + \sigma_y)} \qquad \ldots.(2.24)$$

where r_e is classical radius of electron, γ is relativistic factor, and $\overline{\beta_{x,y}}$ is average beta function in transverse plane. The ion induced tune shift mainly depends on the density of ions inside the ring vacuum chamber and is independent of ion mass. For a beam current of 100 mA at 2.5 GeV in the Indus-2 ring, the amount of betatron tune shift is $\Delta\nu_x = 0.62\,\eta$, $\Delta\nu_y = 2.76\,\eta$. To limit this tune shift to a tolerable value, neutralization coefficient needs to be minimized. Considering 1% neutralization coefficient, the amount of betatron tune shift is 0.0062 & 0.027 in horizontal and vertical plane respectively. Tune shift in both the plane are positive and it is substantial in vertical plane as σ_y is smaller than σ_x. The operating point of storage ring may approach the resonance line because of large vertical tune shifts and this increases the coupling coefficient. This phenomenon lead to increase of vertical beam size, particularly if the tune is near resonances.

2.10 Evidence of ion trapping in Indus-2 storage ring

2.10.1 Observation of betatron tune shift

We observed the dependence of betatron tune on the bunch filling pattern. The indus-2 storage ring may be filled with maximum 291 bunches, each separated by 2 ns. In a series of experiments, betatron tunes were measured as accumulation proceeds till 100 mA beam current for different bunch filling patterns namely a) all 291 bunches are filled, b) 250 bunches are filled and 41 bunch gaps, c) 180 bunches are filled and 111 bunch gaps, d) 150 bunches are filled and 141 bunch gaps. Fig. 2.8 shows the measured tune on a tune diagram up to 5th order resonance line for these bunch filling patterns. A positive betatron tune shift was observed in both the horizontal and vertical plane and this increases with the beam intensity as more ions accumulate. The tune shift is mainly because of the additional focusing force induced by trapped positively charged ions in the electron beam path. The vertical tune shift is more compared to horizontal tune shift as the focusing force is more in vertical plane due to smaller beam size in the vertical plane. For the bunch filling pattern (a) and (b) in which either do not have any bunch gap or less bunch gap, the observed vertical tune shift is ~ 0.02. However, for the bunch filling pattern (c) and (d) in which the bunch gap is large, shift in vertical tune was found to be less (~ 0.003). All these observation concludes the presence of ions in the storage ring. Nonetheless, the effect of ion trapping on electron beam was reduced while the length of the bunch gap is increased as less number of ions are trapped in the electron beam potential [54].

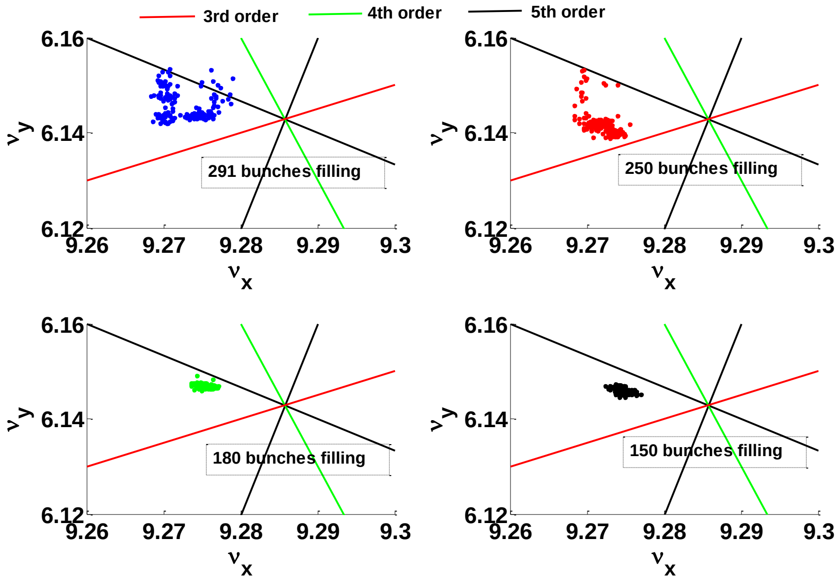

Figure 2.8: Measured betatron tunes in both horizontal and vertical plane for different bunch filling patterns in Indus-2. In 291 and 250 bunches ion trapping is clearly observed as vertical tune drifts with large amount, whereas tune drift is negligible in the optimized bunch filling patterns having 180 bunches and 150 bunches

2.10.2 Observation of Bremsstrahlung radiation

Bremsstrahlung radiation (BR), is generated by collisions of circulated electrons with neutral residual gas molecules and trapped ions. The excess BR yield due to the ion trapping effect was observed in Photon factory [55] and SPring-8 [56] storage ring. This measurement provides a direct method of observing ion trapping instead of measuring the effect of ion trapping on electron beam. The total BR yield (BR_{tot}) is given by a sum of contributions from neutral gas molecules (BR_{gas}) and trapped ions (BR_{ion}) [57] and is written as

$$BR_{tot} = BR_{gas} + BR_{ion} \qquad \dots (2.25)$$

$$BR_{gas,ion} \cong \frac{\sigma_{gas,ion}^{BR} \, L_s \, \zeta \, d_{gas,ion} \, \mathrm{N}}{T_{rev}} \qquad \dots (2.26)$$

where σ_{gas}^{BR} is the bremsstrahlung cross section due to gas, σ_{ion}^{BR} is the bremsstrahlung cross section due to ions, L_s is the length of straight section in which the BR is produced, ζ is the fraction of BR actually hit the detector, d_{gas} is the density of residual gas molecules, d_{ion} is the density of ions, and T_{rev} is the revolution period. The size of the detector plays an important role to correctly measure the absorbed dose. The large ionization chamber misleads the dose counts because it can absorb contribution from other sources too. We use a small ion chamber detector of size 0.6 cc which minimizes background SR. The trapped ions in the electron beam produces additional BR yield due to the electron-ion collision. This can be measured by properly tuning the machine parameters such as in one case there will be maximum ions trapped and in another case trapping of ions in the electron beam is kept minimum. In all bunches filling of Indus-2, maximum ions are trapped, however, in the partial bunch filling (150 bunches), ion trapping is negligible as the gap length is much larger than the ion oscillation period.

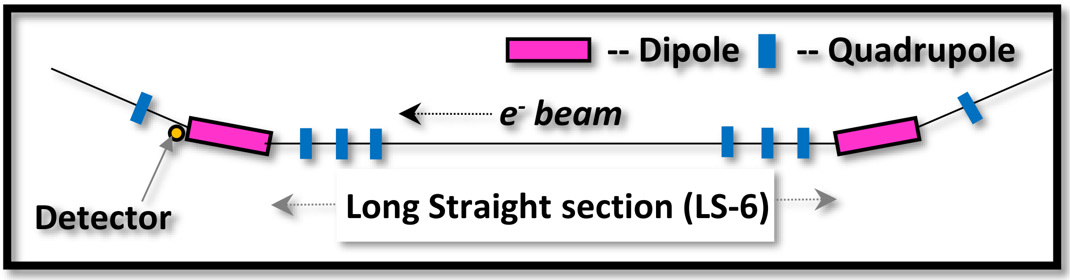

Figure 2.9: The schematic of the arc of Indus-2 storage ring in which the experiment of bremsstrahlung radiation measurement was carried out. Detector is mounted at exit of 2nd dipole in beam direction.

To observe this phenomenon in Indus-2, BR has been measured using a miniature ion chamber detector, installed at the end of a long straight section (LS-6) of length ~ 10 meter. The detector is coupled with a high resolution electrometer. It measures bremsstrahlung intensity in terms of ion current. Fig. 2.9 shows a schematic view of the arc of Indus-2 which was used for this experiment. The detector was installed in front of an end flange of 0^0 port of a bending magnet, inside Indus-2 tunnel. The electrometer was placed in the experimental hall, outside the shielding wall, and connected to the detector through a tri-axial signal cable.

The Indus-2 ring was filled with 125 mA in two different bunch filling patterns, such as 291 bunches and 150 bunches and during the storage condition, the BR yield in terms of ion chamber current was noted, which is shown in Fig. 2.10. In 150 bunches filling, it is believed that no more ions are trapped and hence the BR yield is due to the only electron and residual gas interaction. The figure shows that, in the 291 bunch filling mode, BR yield levels rose vividly due to the increased beam-ion interactions. Bremsstrahlung dose in the filling of 291 bunches is ~5 times higher than that of 150 bunches [58]. This clearly indicates the existence of more trapped ions in the storage ring in the all bunches filling pattern.

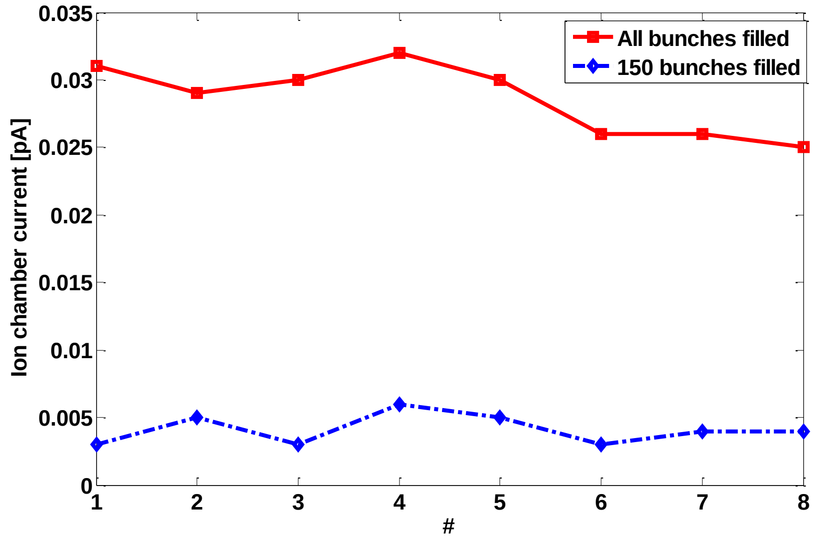

Figure 2.10: Bremsstrahlung count in terms of ion chamber current in different bunch filling pattern at 125 mA in Indus-2 storage ring. The horizontal axis shows the number of measurements.

2.10.3 Observation of transverse coupled bunch instability

The generated positive ions may also develop transverse instability in electron beam and this process increases the electron beam size and even beam loss. [59]. We observed the beam spot on synchrotron light monitor (SLM) in Indus-2. At high beam current it was observed that SR spot was shaking when the ring was filled with a homogeneous bunch filling pattern. In order to understand the phenomena, we measured the transverse coupled bunch mode excitation at beam current more than 100 mA. In vertical plane, large number of modes were seen to be excited but the coupled bunch mode number 290 was detected with greater amplitude. There was no excitation of coupled bunch mode in horizontal plane. Then the same measurement was repeated for partial bunch filling pattern for same beam current. Fig. 2.11 shows the measured amplitude of the 290th coupled bunch mode at the beam current of 150 mA for homogeneous and partial bunch filling patterns.

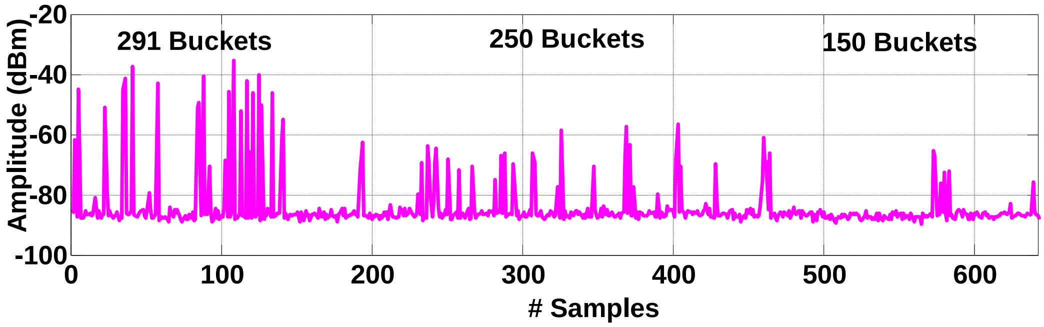

Figure 2.11: Excitation of 290th coupled bunch mode in vertical plane in Indus-2 for different bunch filling patterns at beam current more than 100 mA.

It was observed that the amplitude of 290th mode was suppressed when the ring was filled with 150 consecutive bunches leaving a gap of 141 bunches. This observation indeed seems very interesting, as the excitation of coupled bunch mode 290 normally signify the resistive wall instability type and may not be an ion induced one. Simultaneously it was also observed on SLM that there is no beam shaking phenomena for 150 bunches filling which was earlier noticed for homogeneous filling.

2.10.4 Observation of beam lifetime and beam accumulation rate

The beam accumulation rate and beam lifetime was measured for homogenous and partial bunch filling pattern. Beam accumulation rate increases by ~40%, when the ring is filled with 150 bunches. The beam current saturates at 100 mA in all 291 bunches filling pattern whereas the saturation is observed at 220 mA in 150 bunches. The beam lifetime for both the filling pattern was compared at beam current of 150 mA and we observed that there is an increase of lifetime by two hours in case of partial filling as compared to that of all bunches filling. These observations envisage the occurrence of trapped ions in homogenous filling which are removed in properly selecting a partial bunch filling pattern.

CHAPTER-3

STUDY OF FAST BEAM-ION INSTABILITY IN ELECTRON STORAGE RING

In an electron storage ring operating at higher beam current, apart from the conventional ion trapping, the electron beam exhibits a transient ion trapping within a bunch train in a single passage of the stored beam leading to an instability known as fast beam ion instability (FBII). The bunch gap that alleviates the conventional ion trapping problem is no longer suitable to suppress the FBII. This instability is detrimental to the performance of the storage ring and beam quality as it offers resistance to the accumulation of higher beam current, increases the electron beam size, and also sometime cause partial beam loss [14]. The cascading interaction of electron beam and ions which are formed in the path of the beam is the main reason behind this phenomenon. Even though sometimes the ions are not trapped in the beam potential from turn to turn, the electron beam could interact with ion strongly and cause a beam-ion coherent instability, tune shift, and beam size blow-up. The likelihood of FBII enhances significantly at lower beam emittance with higher beam current and at relatively poor vacuum conditions in the ring. At ALS and PLS, the FBII has been experimentally observed by increasing the residual gas pressure by putting off vacuum pumps and also by purging helium gas locally into the ring vacuum chamber [15, 16]. FBII was also observed at nominal vacuum levels with reduced vertical beam emittance at SOLEIL & SSRF rings [19, 20]. Subsequently, several light sources have studied this phenomenon by using simulation technique and also observe it experimentally by introducing improved diagnostic instruments. With optimized multi-train bunch filling pattern, this instability in storage ring can be suppressed effectively. Section 3.1 provides the theory of FBII and its detrimental effects on beam. Section 3.2 discusses the distribution of ion cloud generated by the ionization of residual gas by the electron beam. Section 3.3 describes the ion cloud build-up and decay in the long bunch gap. Section 3.4 describes the electric field of a Gaussian charge distribution followed by the analytical estimation of instability growth rate in section 3.5. Section 3.6 describes the numerical modeling of FBII and illustrates the simulation code used to analyze the FBII. Section 3.7 gives measured gas composition present in Indus-2 vacuum chambers in the ring. Section 3.8 gives the results of FBII study with its effect on beam current, emittance and vacuum conditions in the storage ring. Section 3.9 gives estimation of the ion trajectory in the presence of electron beam. Section 3.10 provides the experimental trial made to observe the FBII by increasing the vacuum pressure in the Indus-2 storage ring.

3.1 Fast beam ion instability (FBII)

In the storage ring, electron beam moves in the form of bunches and the number of bunches is governed by the ratio of RF frequency and revolution frequency. The FBII occurs in an electron storage ring due to the interaction of an electron bunch and the generated ions by its preceding bunches in the bunch train in a single pass. Existence of a finite displacement between the centroid position of electron bunch and ion cloud, allows the electron bunch and ion cloud to receive a transverse kick mutually from one another. If the coupling between electrons bunches and ion cloud is strong enough to counteract the damping due to synchrotron radiation emission, the instability arises. The motion of the electron bunch becomes similar to a driven harmonic oscillator with a driving force proportional to the transverse displacement between ion and bunch centroid. The amount of kick by the electron bunch to the ion is more in the vertical plane and hence the instability mainly occurs in this plane. Therefore, the study of FBII is carried out in the vertical plane only. The coupled equation of motion for the electron beam and ion is written as [13]

$$\frac{d^2 y_b(s,z)}{ds^2} + \omega_\beta^2 y_b(s,z) = K(s)\,[y_i(s,t) - y_b(s,z)] \int_0^z \rho(z')\,dz' \qquad \ldots(3.1)$$

$$\frac{d^2 y_i(s,t)}{dt^2} + \omega_i^2 y_i(s,t) = \omega_i^2 y_b(s,z) \qquad \ldots(3.2)$$

where ω_β and ω_i are the betatron frequency of electron beam and ion frequency respectively. The ion frequency has a strong dependence on electron beam size as it is inversely proportional to product of beam sizes, $\sigma_y(\sigma_x + \sigma_y)$. $y_b(s,z)$ and $y_i(s,t)$ are the displacement of the electron bunch and ions from the beam axis respectively. The relative longitudinal position of the bunch within the bunch train is specified by *z*. The distance along the ring is denoted by *s*. If the head of the bunch train passes the position *s=0* at time *t*=0, then any bunch position within the train would have *z=ct-s*, since electron bunch moves with a speed of light. Fig. 3.1 shows the coordinates used in the equation of motion.

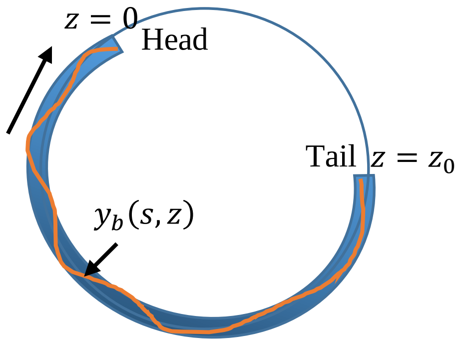

Figure 3.1: Schematic diagram showing the coordinates of bunch train used in the study of FBII in the ring with z=0 representing the head of train and z=z_0 representing the tail.

Here the effect of self space charge force of electrons and ions are ignored. The first equation describes the vertical motion of the electron beam which undergoes betatron oscillation, governed by external magnetic field in the storage ring and a perturbation force proportional to electrostatic potential of ions, represented by the constant *K*, and relative displacement between the centroid of electron and ion. The longitudinal distribution of electron density in a bunch train is denoted as $\rho(z)$. The amplitude of the perturbation force depends only on the number of ions generated upstream the concerned electron bunch at the relative position *z*, which is shown by the extreme right-hand side of eqn. 3.1. The second equation describes the motion of ions in vertical plane at a fixed location *s*, but oscillating in time. Here the ion motion is only perturbed by the number of electrons. Due to heavy mass and non-relativistic velocity of ion, the effect of the external magnetic field on the ion is ignored. The kick parameter, *K* depends on the ion density and electron beam size and given as

$$K = \frac{4\,\lambda_{ion} r_e}{3\,\gamma\,\sigma_y(\sigma_x + \sigma_y)} \qquad \text{... (3.3)}$$

where γ is a relativistic factor for the beam, r_e is the classical electron radius. λ_{ion} is the line density of ions which are created during the passage of electron beam, given as

$$\lambda_{ion} = \frac{\sigma_i N_b n p_i}{kT} \quad \text{....(3.4)}$$

where σ_i : ionization cross section of the gas species, N_b: number of electrons per bunch, n: number of bunches, p_i: partial pressure of gas molecules, k: Boltzmann constant and T: absolute temperature of the gas. It can be noticed that the ion density becomes more, when the number of bunch in a bunch train is large and also number of electron per bunch is large in the storage ring. The ion oscillation frequency, is given as

$$\omega_i = c\left(\frac{4N_b r_p}{3L_{sep}\sigma_y\left(\sigma_x + \sigma_y\right)A}\right)^{1/2} \quad \text{....(3.5)}$$

where A is atomic mass of the ion, L_{sep} is bunch to bunch separation, r_p is classical proton radius and $\sigma_{x,y}$ signifies rms horizontal and vertical electron beam sizes. Also it is necessary to know the distribution of ions, in order to solve the coupled equation of motion for electron beam and ions,

3. 2 Ion distributions

Many studies assume that ions have the same transverse distributions as the electron beam, which are usually Gaussian, as the ions are created from the electron beam [60]. The above assumption is correct only when ions are created. However, under the attractive beam potential, ions redistribute themselves. Since the ions are born via the interaction of residual gas molecules with the electron beam, the initial distribution of ions has the same Gaussian distribution with the same dimension as the electron beam [23], which is given as

$$\rho_0(x_0) = \frac{1}{\sqrt{2\pi}\sigma_x} exp\left(-\frac{x_0^2}{2\sigma_x^2}\right) \quad \text{.... (3.6)}$$

However, since ions are generated randomly in time, it follows a uniform distribution at each position.

$$f(x, x_0) = \frac{2}{\pi\sqrt{x_0^2 - x^2}} \quad \text{.... (3.7)}$$

Therefore the distribution of ions at the equilibrium becomes [8]

$$\rho(x) = \int_x^{\infty} f(x, x_0)\, \rho_0(x_0)\, dx_0$$

$$= \frac{1}{\pi\sqrt{2\pi}\sigma_x} exp\left(-\frac{x^2}{4\sigma_x^2}\right) K_0\left(\frac{x^2}{4\sigma_x^2}\right) \quad \text{.... (3.8)}$$

where K_0 is the modified Bessel function of the second kind. The distribution of electron beam and ion is shown in Fig. 3.2.

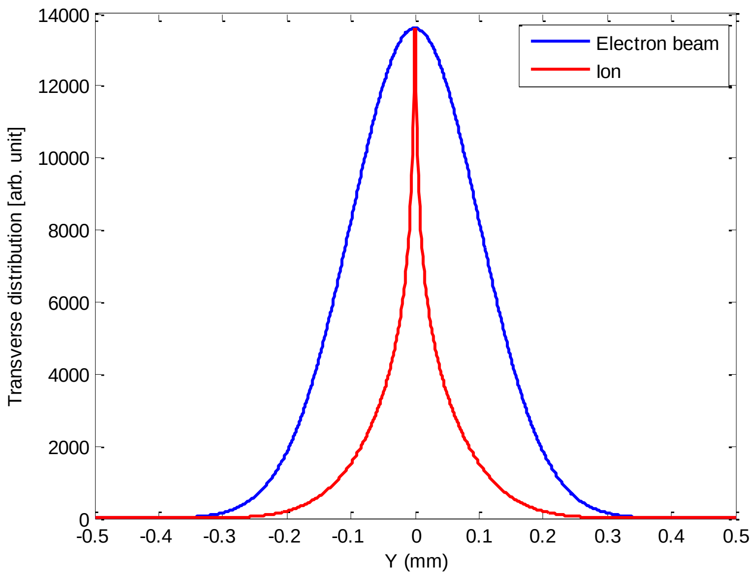

Figure 3.2: The distribution of electron beam and ions generated from electron beam

The figure shows the size of the ion cloud is smaller than that of the electron bunch. This analysis shows that, the distribution of ion is similar to Gaussian distribution as the electron bunch with reduced RMS beam size $\sigma_i = \sigma_e/\sqrt{2}$ [23], where σ_e and σ_I are transverse size of electron bunch and ion cloud respectively.

3.3 Ion cloud build-up

Along the length of the bunch train, the number of ions increases linearly from head of the train to tail of the train and thereafter decreases exponentially in the bunch gap. The ion density in the beam after the clearing gap (L_{gap}) reduces according to the relation [18], which is given as

$$\lambda_i' \approx \frac{\lambda_{ion}}{\sqrt{\left(1 + L_{gap}^2 \omega_{i,x}^2\right)\left(1 + L_{gap}^2 \omega_{i,y}^2\right)}} \qquad \text{....}(3.9)$$

Where λ_{ion} is the density of the ion at the extreme end of a bunch train. The ion cloud build-up along the bunch train and decay during the bunch gap is shown in the Fig. 3.3. This shows the normalized ion density (λ_i'/λ_{ion}) at 1 nTorr pressure for H_2 and CO ions. In Indus-2, the line density of ion is 31 m^{-1} for the CO ions at vacuum level of 1 nTorr and beam current of 200 mA distributed in 200 bunches which corresponds to a per bunch population of 3.6 x 10^9 electrons. The figure also shows that the lighter ions escape quickly as compared to the heavier ones. It also shows that the ion density reduces exponentially to an insignificant level after traversing the 91 bunch gaps. Thus, we can neglect the coupling effect from the tail of the bunch train to the head of the adjacent bunch train. However within a bunch train, the effect of ions on electron beam bunch dynamics is studied.

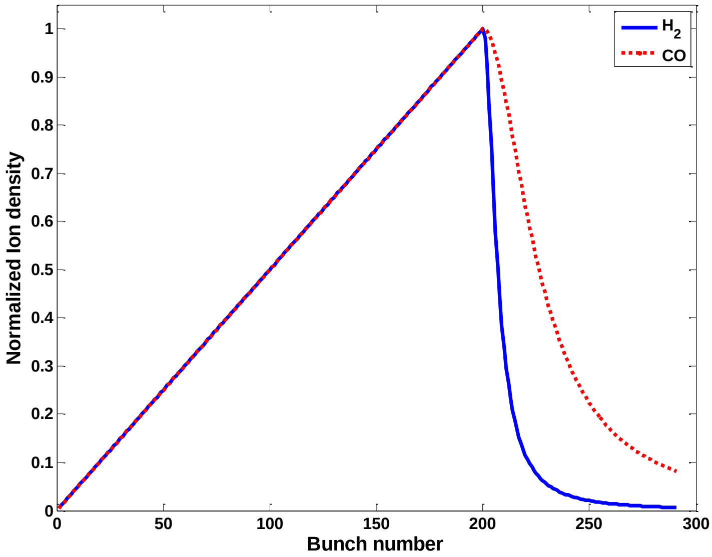

Figure 3.3: The normalized ion density for two ion species (H_2 and CO) along a single long bunch train. Filling pattern: 200 bunches filled + 91 bunch gaps. H_2 ion being a lighter mass diffuse in the bunch gap more rapidly than CO ion.

3.4 Electric field of a Gaussian charge distribution

To study the motion of electron in the presence of ions and vice-versa, one has to estimate the electric field offered by the both the beam. The electric field of a Gaussian charge distribution is described by Bassetti-Erskine formula [50], which is derived by solving Poisson equation given as

$$\nabla^2\phi = -{}^{\rho}/_{\epsilon_0} \qquad \ldots.(3.10)$$

where ϕ is the potential, ϵ_0 is the vacuum permittivity and ρ is the two dimensional charge distribution, written as

$$\rho(x,y) = \frac{Q}{2\pi\sigma_x\sigma_y}\exp\left(-\left(\frac{x^2}{2\sigma_x^2}+\frac{y^2}{2\sigma_y^2}\right)\right) \qquad \ldots.(3.11)$$

The corresponding electric fields are written as

$$E_x = -\frac{\partial \emptyset}{\partial x} E_y = -\frac{\partial \emptyset}{\partial y}$$

$$E_y = \frac{Q}{2\epsilon_0\sqrt{2\pi(\sigma_x^2 - \sigma_y^2)}} Re\left[w\left(\frac{x+iy}{\sqrt{2(\sigma_x^2 - \sigma_y^2)}}\right) - exp\left(-\left(\frac{x^2}{2\sigma_x^2} + \frac{y^2}{2\sigma_y^2}\right)\right) w\left(\frac{x\frac{\sigma_y}{\sigma_x} + iy\frac{\sigma_x}{\sigma_y}}{\sqrt{2(\sigma_x^2 - \sigma_y^2)}}\right)\right] \quad \ldots.(3.12)$$

$$E_x = \frac{Q}{2\epsilon_0\sqrt{2\pi(\sigma_x^2 - \sigma_y^2)}} Im\left[w\left(\frac{x+iy}{\sqrt{2(\sigma_x^2 - \sigma_y^2)}}\right) - exp\left(-\left(\frac{x^2}{2\sigma_x^2} + \frac{y^2}{2\sigma_y^2}\right)\right) w\left(\frac{x\frac{\sigma_y}{\sigma_x} + iy\frac{\sigma_x}{\sigma_y}}{\sqrt{2(\sigma_x^2 - \sigma_y^2)}}\right)\right] \quad \ldots.(3.13)$$

where w(z) is complex error function given as

$$w(z) = \exp(-z^2)\left(1 - erf(-iz)\right)$$

$$\mathrm{erf}(x) = \frac{2}{\sqrt{\pi}}\int_0^{\pi} exp(-x^2)\,\mathrm{dx}$$

The electric field is computed for an electron bunch of Indus-2 using the above expression and its vertical component is plotted against position in terms of beam size at x=0 and is shown in Fig. 3.4. This figure envisages that the attractive force acting on the ion increases linearly up to the beam size with the distance between the transverse position of the center of the electron beam and the position of the ion. However, for the displacement of ion from the beam center above the beam size, the attractive force gradually decreases and becomes nonlinear. Therefore, ions that travel farther from the center of the beam are affected by a small attractive force and these ions can move far away from the beam orbit and never return back [51].

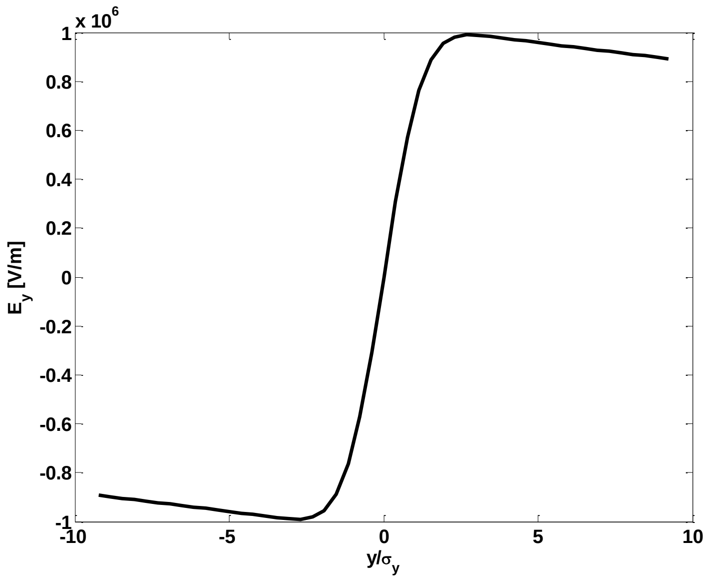

Figure 3.4: Electric field of a Gaussian bunch in vertical plane at x=0 verses displacement in terms of beam size. The field varies linearly up to beam size and thereafter becomes nonlinear.

3.5 Analytical estimation of growth rate

The solution to the coupled equation of motion (Eqn. 3.1 and Eqn. 3.2) are simplified with the following approximations. The force acting on beam from the ions is assumed to be linear, i.e. the force is proportional to distance between beam and ion centroid. Considering the way the ions are generated, the initial condition for ions are written as $y_i(s,t)|t' = y_b(s,z')$ and $dy_i(s,t)/_{dt}\,(t = t') = 0$, as they are assumed to be generated at rest. The ion frequency and the electron density along the bunch train are assumed to be constant. The complementary solution to eqn. 3.2 can be written as

$$y_{ic} = A\cos\omega_i\, t + B\ \sin\omega_i\, t \qquad \text{....(3.5.1)}$$

with A and B as constants, which can be derived from the initial condition mentioned above. After estimating the constants, the solution is given as

$$y_{ic} = y_b \cos(\omega_i\,(t - t')) \qquad \dots.(3.5.2)$$

The particular solution to the eqn. 3.2 can be solved by Greens function technique. For a second order differential equation of the type

$$y''(t) + y\,(t) = f(t) \qquad \dots.(3.5.3)$$

The particular solution is given as

$$y_p = \int_{t'}^{t} G\,(t,t')f(t')dt' \qquad \dots.(3.5.4)$$

With the Green function $G\,(t,t')$ satisfying the relation

$$\frac{d^2G\,(t,t')}{dt^2} + G\,(t,t') = \delta(t - t') \qquad \dots.(3.5.5)$$

The continuity of G and discontinuity of G' at $t = t'$gives rise to

$$G\,(t,t') = \frac{1}{\omega_i} sin(\omega_i(t - t')) \qquad \dots.(3.5.6)$$

With this, the particular solution y_p for the eqn. 3.2 is written as

$$y_{ip} = \omega_i \int_{t'}^{t} sin(\omega_i(t - t''))y_b(s, t'' - s)dt'' \qquad \dots.(3.5.7)$$

$$y_i \;= y_{ic} + y_{ip}$$

$$y_i\,(s,t) = y_b(\mathrm{s}, t' - s)\cos(\omega_i\,(t - t'))$$

$$+\,\omega_i \int_{t'}^{t} sin(\omega_i(t - t''))y_b(s, t'' - s)dt'' \qquad \dots.(3.5.8)$$

By using the integration by parts, i.e. $\int u\,dv = u\,v - \int v\,du$ for the 2nd term of equation 3.5.8, we write the complete solution for ion centroid as

$$y_i\ (s,t) = y_b(\mathrm{s}, t-s) - \int_{t'}^{t} \frac{dy_b(\mathrm{s}, t''-s)}{dt''} \cos(\omega_i(t-t'')) \qquad \ldots.(3.5.9)$$

The above solution shows that, for onset of instability, beam should have non-zero displacement with respect to central axis of the bunch. Now using this solution of ion centroid, we can solve the eqn. 3.1 for estimating the beam centroid, which can again be written as sum of homogeneous part and a particular integral (Green function technique), given as

$$y_b(\mathrm{s},z) = y_b(0,z)\cos\left(\omega_\beta s + \varphi\right)$$
$$-\frac{1}{\omega_\beta}\int_0^s ds'\, K\, sin\left(\omega_\beta(s-s')\right)\int_0^z \rho(z')\,dz' \int_{z'}^{z} dz'' \frac{dy_b(\mathrm{s},z'')}{dz''}\cos(\omega_i(z-z'')) \ldots.(3.5.10)$$

Here, the first term of the solution represents the unperturbed betatron oscillation with a φ phase offset. The second term of the solution represents the beam oscillation at the ion frequency ω_i for each position s of the bunch. The second term of the above equation, which shows triple integration, can be solved by the technique of perturbation series [13] in K/ω_β. The solution can be written as

$$y_b(s,z) = \frac{y_0}{2}\Big\{J_0\left(2\sqrt{\eta(s,z)}\right)\sin(\omega_i z + \omega_\beta s + \varphi)$$
$$+ J_0\left(2i\sqrt{\eta(s,z)}\right)\sin(\omega_i z - \omega_\beta s - \varphi)\Big\} \qquad \ldots.(3.5.11)$$

Where J_0 is the zeroth order Bessel function, and $\eta(s,z)$ is a dimensionless quantity defined as

$$\eta(s,z) = \frac{K\omega_i(z+z_0)^2 s}{16\ \omega_\beta z_0} \qquad \ldots.(3.5.12)$$

In the asymptotic limit, the beam centroid expression can be approximated as

$$y_b(s,z) = \frac{y_0}{4\sqrt{\pi}}\frac{1}{\eta(s,z)^{1/4}}e^{2\sqrt{\eta}}\sin\left(\omega_i z - \omega_\beta s - \varphi\right) \qquad \ldots.(3.5.13)$$

By explicitly writing $\eta(s,z)$, the above solution takes the form

$$y_b(s,z) \cong y_0 \frac{1}{2\sqrt{2\pi}\,({}^{t}/_{\tau_c})^{1/4}} e^{\sqrt{{}^{t}/_{\tau_c}}} \quad \text{....}(3.14)$$

where τ_c is the characteristic growth time of the fast beam ion instability and is given as [13]

$$\frac{1}{\tau_c} = \frac{\sigma_{ion} P\, \beta N_b^{\frac{3}{2}} n^2 r_e r_p^{\frac{1}{2}} L_{sep}^{\frac{1}{2}} c}{k\,T\,\gamma \sigma_y^{\frac{3}{2}} (\sigma_x + \sigma_y)^{\frac{3}{2}} A^{\frac{1}{2}}} \quad \text{....}(3.15)$$

The growth rate depends strongly on the number of bunches ($\propto n^2$), number of electrons per bunch ($\propto N_b^{3/2}$) and transverse beam sizes ($\propto \sigma_y^{-3/2}(\sigma_x + \sigma_y)^{-3/2}$). This analytical formulation estimates the FBII growth rate only in linear regime ($y < \sigma_y$)in which force between electron and ions increases linearly with the displacement. In this regime, the solution predicts that the oscillation amplitude of electron beam increases quasi-exponentially. This does not estimate the growth rate in the nonlinear regime ($y \geq \sigma_y$) where the force between ion and electron beam becomes nonlinear. The non-linear space charge force of electron beam introduces amplitude dependent spread in ion oscillation frequency, which can alleviate the FBII through ion de-coherence [61]. In a strong focusing ring, the beam size varies along the circumference of the ring. This introduces a large spread in ion oscillation frequency and produces decoherence in ion motion. This mechanism generates Landau damping in electron beam and helps in further reducing the FBII growth rate. Fig. 3.5 shows the variation of electron beam size in horizontal and vertical plane in Indus-2 storage ring.

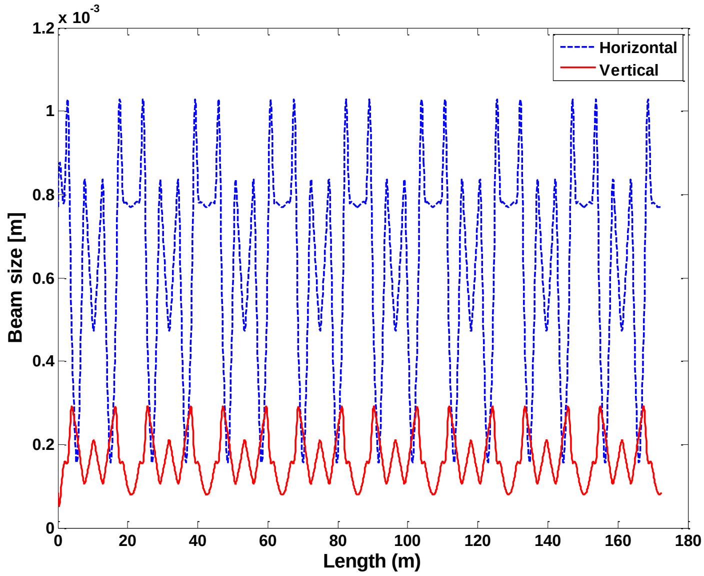

Figure 3.5: The variation of beam size in both horizontal and vertical plane along the circumference of Indus-2 storage ring.

After inclusion of the Landau damping effect caused by the spread in ion oscillation frequency, the electron beam oscillation amplitude increases exponentially [62] and is given by

$$y_b \propto e^{t/\tau_{inst}} \qquad \text{....(3.16)}$$

$$\frac{1}{\tau_{inst}} \approx \frac{1}{\tau_c} \frac{c\sqrt{2\pi}}{4L_{sep} n a_{bt} \omega_i} \qquad \text{....(3.17)}$$

where τ_{inst} is the FBII growth time, and a_{bt} is the relative variation of ion frequency defined by (*standard deviation in ion frequency / average ion frequency*). For a weak focusing lattice, the parameter a_{bt} has small value (~ 0.1), whereas for the strong focusing lattice, it can have maximum value of 1.0 [62]. Considering the space charge force to be linear, the FBII growth time of Indus-2 is estimated to be ~ 16 μs for an average beam current of 200 mA filled in 200 bunches and at vacuum pressure of 1 nTorr. This instability growth time is very small to measure. However considering the spread in ion frequency in Indus-2 storage ring ($a_{bt} \approx 0.25$), FBII growth time is estimated as ~ 0.35 ms. Furthermore, the growth of FBII is suppressed by multi-train bunch filling pattern [12] and in this case the FBII growth time is defined as

$$\tau'_{inst} = \frac{\lambda_{ion-single\ train}}{\lambda_{ion-multi\ train}} \tau_{inst} \qquad \ldots.(3.18)$$

For a two train arrangement that provides proper gap for ion trapping, and keeping the same beam current and total number of bunches as single bunch train, the FBII growth time increases by two fold.

3.6 Numerical modeling of FBII

The FBII in electron storage ring is studied rigorously using numerical modeling which include both the linear and non-linear regime of beam potential [13 and 14]. Under the influence of electric field of ion cloud, the electron bunches oscillates in transverse plane and this leads to beam instability. Solving analytically large number of equations of motion of forced coupled oscillator is quite tedious. However, the complexity was simplified by solving the problem numerically using a simulation code. The beam ion interaction is modeled as two different ways namely strong-strong model and weak-strong model. In strong-strong model, both the ion and electron beam is treated as collection of macro particles [13]. A macro-particle represents the center of mass of a cluster of neighboring particles. Fundamentally, it reduces the number of degrees of freedom and modeling of large number of particle becomes computationally manageable. In weak-strong model, ion beam is considered as a collection of macro-particles and electron bunch is treated as rigid Gaussian distribution which means the distribution of electron bunch does not change during the interaction with ions [14]. This model is a less rigorous compared to earlier one but it helps in reducing the computation time in simulation. To study this instability in Linac, a simulation code named as FASTION was developed at CERN which has features of both the strong-strong and weak-strong model [63]. Later it was configured for a circular accelerator [64]. In our study, we used this simulation code that uses the weak-strong model. The code considers the ionization process of electron beam by using single gas species defined by its ionization cross section and partial pressure in the storage ring. The simulation code describes numerically two beams and calculates the space charge force of each beam and is applied to the other beam.

A fixed number of ionization points were chosen along the circumference of the ring, known as beam- ion interaction points (IPs). The IPs are specified by the twiss parameters (alpha, beta and phase advance) of the storage ring and the simulation code tracks a train of electron bunches through these IPs. At every interaction point, each passing electron bunch generates a number of ions in accordance with the vacuum pressure, composition of residual gas, and beam dynamical parameters. First bunch of a bunch train does not interact with ions, as it just generated the ions. All the subsequent bunches got influenced by the ions formed by the preceding electron bunches and the last bunch of the train perturbed more as it interacts with maximum number of generated ions. Electron bunches and ions experiences mutual kicks estimated from their electric field. In both the horizontal and vertical plane, ion distribution is assumed to be Gaussian as they are born after the interaction of the residual gas and Gaussian shaped electron bunch. However, the net transverse kick between bunch and ions gets nullified, when the ion cloud is produced perfectly symmetric to the center of the electron bunch. In an operating accelerator, bunches are always displaced from each other because of various unavoidable errors in the machine. So in the simulation, the first bunch was displaced slightly with respect to the other bunches in the train. The interaction of ion and electron bunch is envisioned through mutual velocity kicks. Since electron bunch is assumed to be rigid Gaussian during the process of interaction, using Bassetti-Erskine formula, the field of electron bunches are calculated and applied to ions. However, the electric field of the ion cloud is calculated with an FFT based PIC solver. The kick to the rigid electron bunch by an ion and sum together for all of the ions is written as [62 and 65]

$$\Delta y_e' + i\Delta x_e' = \frac{2N_b r_e}{\gamma}\sum_i f(x_{ie}, y_{ie}) \qquad \dots.(3.19)$$

Similarly, the kick on the ion due to the electron bunch is given by

$$\Delta y_i' + i\Delta x_i' = -\frac{2N_b r_p}{A_{ion}}\sum_i f(x_{ie}, y_{ie}) \qquad \dots.(3.20)$$

where x_{ie}, y_{ie} are the transverse distances of the ion from the bunch center. $f(x_{ie}, y_{ie})$ is a factor taken from the Bassetti-Erskine formula and is given as

$$f(x,y) = -\sqrt{\frac{\pi}{2(\sigma_x^2 - \sigma_y^2)}}\left[w\left(\frac{x+iy}{\sqrt{2(\sigma_x^2 - \sigma_y^2)}}\right) - exp\left(-\left(\frac{x^2}{2\sigma_x^2} + \frac{y^2}{2\sigma_y^2}\right)\right) w\left(\frac{x\frac{\sigma_y}{\sigma_x} + iy\frac{\sigma_x}{\sigma_y}}{\sqrt{2(\sigma_x^2 - \sigma_y^2)}}\right)\right] \qquad \dots.(3.21)$$

After the interaction process is over at one IP, the coordinates of electron bunches in the train are transported to the next IP using the transfer matrix of the optics in between the IPs and the process continues. After tracking one bunch train for one revolution period through all IPs, all the generated ions are assumed to be clear due to the ion clearing gap. The transverse offsets of each electron bunch are updated for the next turn estimation with the fresh ions produced. The trajectory of electron bunches and ion clouds are estimated as an output of the simulation. FBII is dominant in vertical plane because of much smaller electron beam size in that plane, and all the simulation results are shown for vertical plane.

3.7 Residual gas species in Indus-2

To measure the composition of residual gases present in Indus-2 and their concentration, residual gas analyzers (RGA) are installed on each dipole magnet vacuum chamber. The spectrum of one of the RGA [66] is shown in Fig. 3.6, which displays the concentration of residual gas species in the ring at 200 mA beam current with the operating vacuum pressure of 1 nTorr. The major species of residual gas in Indus-2 vacuum chamber are H_2 (hydrogen) and CO (carbon monoxide). Gas molecules having larger ionization cross-section and more gas concentration are most effectively influences the instability. Although, the concentration of H_2 is more, CO becomes more effective because of its 6 times higher ionization cross section than that of H_2. Hence, CO^+ ion with ionization cross section, 1.55 x 10^{-22} m^2 is taken as instability source in the simulation study.

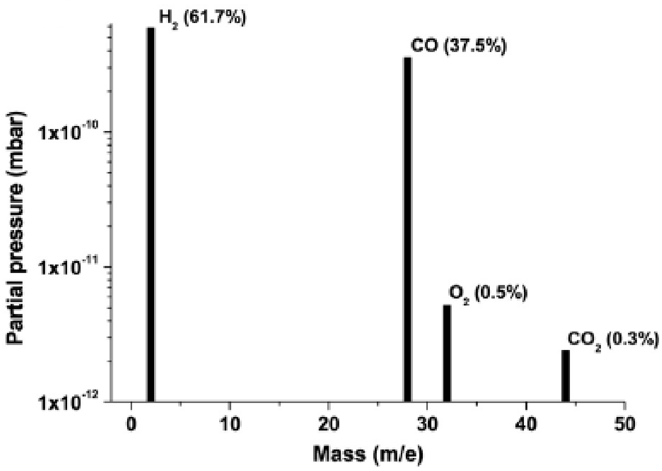

Figure 3.6: Measured RGA spectrum of Indus-2

3.7.1 Pressure profile

The vacuum pressure in Indus-2 was measured using 32 BAGs symmetrically placed along the storage ring [66]. The Fig. 3.7 shows the measured vacuum pressure profile of Indus-2 at 150 mA beam current and also without beam. At the time of this measurement, the storage ring vacuum has reached more than 2500 Ah of beam scrubbing. The dynamic pressure rise is estimated from measured vacuum pressure and it is approximately ~ 2 x 10 $^{-12}$ mbar/mA. At initial stage of beam commissioning, dynamic pressure rise was significant because of high photo induced desorption yield. However, at present, the pressure rise is very much negligible as the accumulated beam dose is too high.

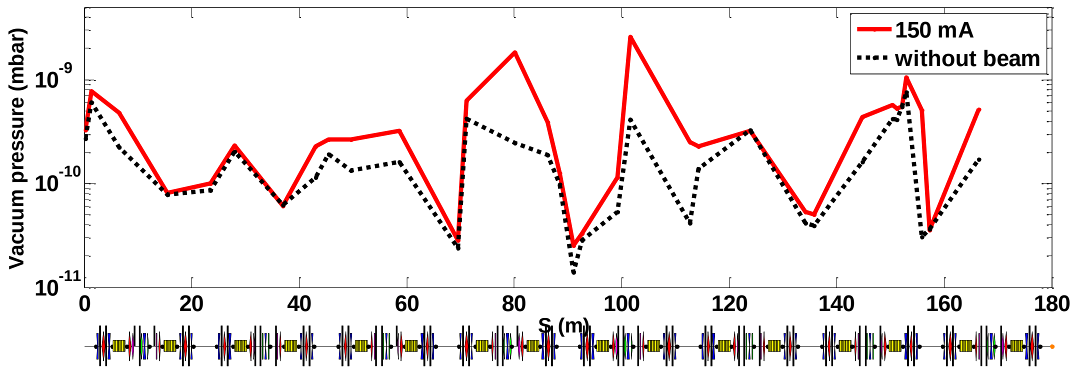

Figure 3.7: The measured vacuum pressure profile of Indus-2 storage ring for 150 mA beam current and without beam. The Indus-2 lattice configuration is embedded below.

3.8 Simulation study of FBII for Indus-2

The number of ionization points in the ring plays a major role for the simulation study of the FBII. Different number of beam-ion interaction points are considered for the FBII simulation, which are distributed all around the storage ring. To start with, only one IP is considered with small vertical beta function, as at that location the electron bunch generates maximum negative beam potential due to the minimum size of the electron beam. Then, the number of IPs were increased to 5, 10, 20 & 40 and distributed among low beta and high beta locations. At last IP of the ring for all the above cases, the centroid of bunches in a bunch train consisting of 200 bunches are determined keeping all other beam parameters and residual gas pressure fixed and the result is shown in Fig. 3.8. It shows that for 20 or more IPs, results are converging for bunches towards the tail of the bunch train [67]. Considering the lattice configuration and to save the computation time, 20 IPs are selected along the circumference of the ring which corresponds to nearly two IPs per betatron oscillation. The ion cloud generated at each interaction point in Indus-2 is represented by 1000 macro-ions and simulation is carried out for a bunch train of 200 bunches. Number of macro-ions is taken as an integer multiple of four to avoid any kind of additional effect generated from asymmetric distribution of macro-ions [68].

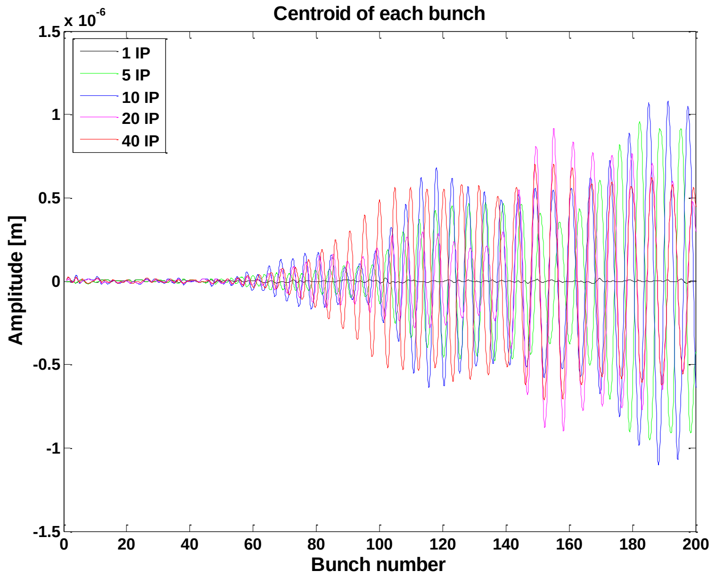

Figure 3.8: Centroid of each bunch of a bunch train consisting of 200 bunches, in vertical plane considering different number of interaction points (IPs) along the circumference of Indus-2.

3.8.1 Effect of vacuum pressure

The ion density increases with the residual gas pressure in the ring. We have studied the onset of the instability by gradually increasing vacuum pressure in the ring. The simulation is carried out considering the lattice of Indus-2 operated at reduced beam emittance of 45 nm rad [69], which is demonstrated at Indus-2. Different partial pressure of 1 nTorr, 10 nTorr and 50 nTorr CO is assumed in the ring during simulation. A bunch train of 200 bunches and holding total 200 mA beam current is tracked in the above machine configuration. Fig. 3.9 shows centroids of each bunch at the location of last interaction point as a function of bunch number. Bunch serial number 1 denotes the head of the bunch train.

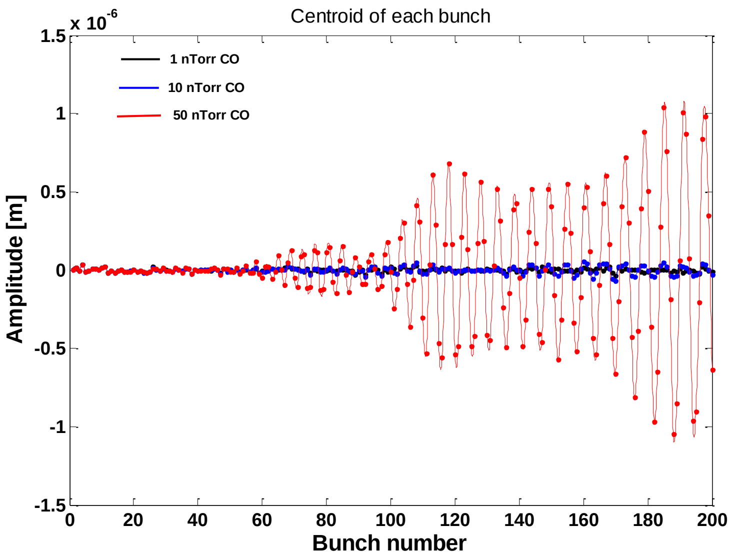

Figure 3.9: The centroid of each bunch in the presence of ion cloud interaction in vertical plane in a bunch train of 200 bunches. Simulation is carried out at three different pressures in the ring: 1 nTorr CO (black), 10 nTorr CO (blue) and 50 nTorr CO (red)

It is noticed that the FBII is not excited in Indus-2 at the nominal operating vacuum (1 nTorr). However, at elevated pressure, bunches towards the tail of the bunch train are seems to oscillates with larger amplitude than that of bunches towards head of train. It can be seen that, in a single turn, oscillation amplitude of bunches at extreme end of the train extents up to 1 μm. This predicts that, FBII can be experimentally observed at elevated residual gas pressure of approximately 50 nTorr in Indus-2 storage ring.

3.8.2 Effect of beam emittance

The reduction in electron beam emittance increases the beam's ion trapping potential. At two different beam emittance, the FBII simulation is performed at the beam current of 200 mA with 50 nTorr CO gas pressure. The bunch train of 200 bunches having beam emittance of 130 nm rad (nominal) and 45 nm rad (reduced) is tracked through the beam-ion interaction points. Fig. 3.10 shows the effect of beam emittance on bunch centroid. As the emittance is decreased, it is observed that beam centroid start to grow at earlier sequence of bunch number.

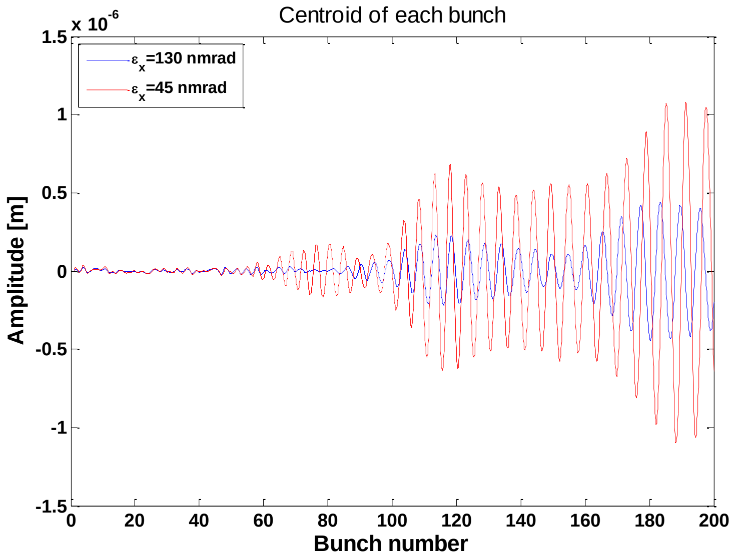

Figure 3.10: The centroid of each bunch of a bunch train in vertical plane at two different beam emittance (150 nm rad and 45 nm rad) values in Indus-2.

3.8.3 Effect of beam current

To observe the effect of beam current, FBII simulation is executed at two beam currents, 100 mA and 200 mA, assuming pressure of 50 nTorr and beam emittance of 45 nm rad. Fig. 3.11 shows the centroid of each bunch at different stored beam current. The instability begins earlier in the bunch train when the current per bunch is larger. The result of simulation indicates that, storage ring having high beam current and low emittance excites FBII with higher growth rate.

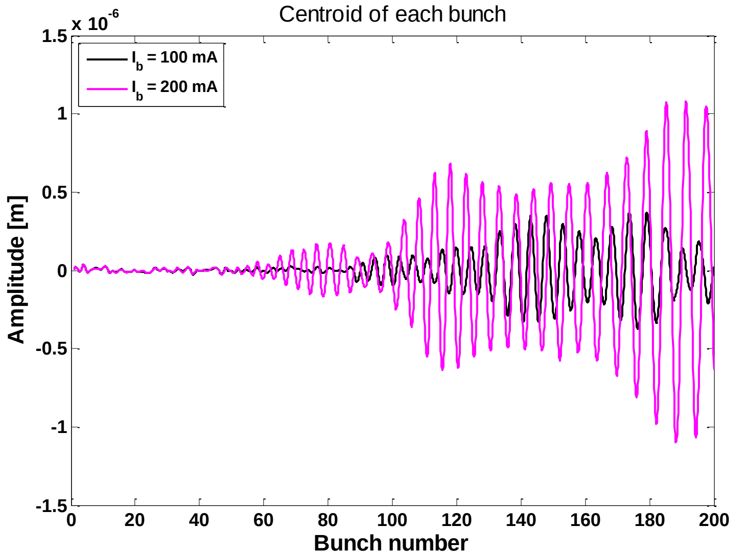

Figure 3.11: The centroid of each bunch of a bunch train in vertical plane when bunches are filled with two different intensities corresponding to beam current values of 100 mA and 200 mA.

3.8.4 Time evolution of oscillation amplitude of electron bunch

Tracking is carried out for large number of turns over the Indus-2 ring. Fig. 3.12 shows the centroid of each electron bunch due to interaction with ions at 10th, 100th, 500th and 1000th turn. It can be observed from the graph, the amplitude of individual bunches are growing over the turn. After a large number of turns, it may so happen the oscillation amplitude of trailing bunch corresponds to the nonlinear regime of electric field offered by ions and at the same time head of the bunch train may be in linear regime.

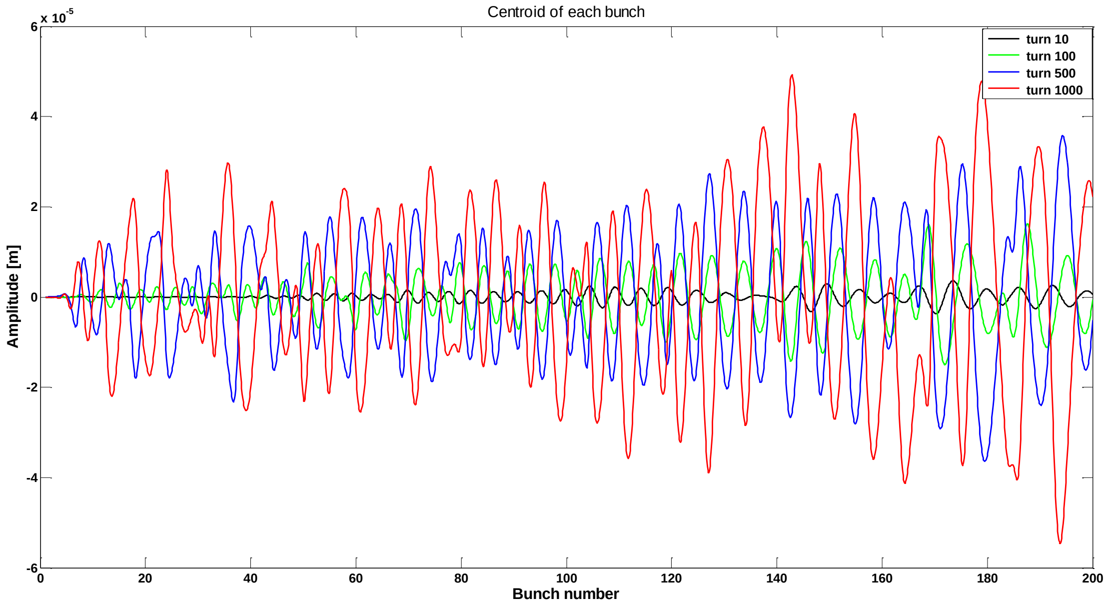

Figure 3.12: The centroid of each bunch of a bunch train at 10th, 100th, 500th and 1000th turn at 50 nTorr pressure and 200 mA beam current in Indus-2.

Two electron bunches (one towards the head of train and other towards the tail) are tracked through the beam-ion interaction points for 2000 turns inside the Indus-2 ring. In the simulation, the oscillation amplitude of theses bunches are calculated at each turn. The oscillation amplitude of bunch centroid is half of the Courant-Snyder invariant [18] and is given by

$$J_y = \frac{1}{2}\left\{\frac{(1+\alpha^2)}{\beta}y^2 + 2\alpha yy' + \beta y'^2\right\} \qquad \text{....(3.22)}$$

where α and β are the machine twiss parameter governed by the lattice of the ring. For the simulation, ring pressure of 50 nTorr CO, stored beam current of 200 mA filled in 200 bunches are assumed. The evolution of vertical oscillation amplitude, $\sqrt{J_y}$ is shown for 50th and 150th bunch of the bunch train in Fig. 3.13 and compared with the vertical beam size.

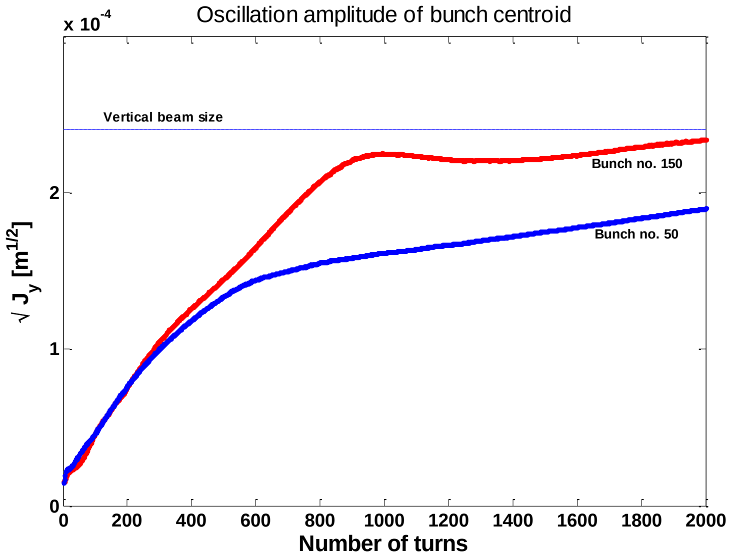

Figure 3.13: Oscillation amplitude of 50th and 150th bunch of a bunch train of 200 bunches over 2000 turns at a pressure of 50 nTorr CO. Bunch 1: Head of the bunch train, Bunch 200: Tail of the bunch train.

It is clearly observed that the oscillation amplitude of bunches does not increases continuously, rather the growth slows down after a specified turn. The oscillation amplitude grows exponentially for short duration and after sometime it grows at a much slower rate. The transition from exponential growth to linear growth is a distinct phenomenon and this peculiar characteristic distinguishes the FBII from other instabilities in the electron storage ring. This happens due to the fact, when the amplitude becomes comparable to the beam size, electric field offered by the ion cloud at its boundary becomes nonlinear and also started decaying. The time duration in which the oscillation amplitude of the bunch centroid grows from $0.1\sigma_y$ to σ_y is defined as the FBII growth time. This graph shows that for the same population in each bunch, the growth time of the FBII are different for different bunch. The estimated growth time for the bunch serial number 50 is more than 2000 turn, whereas for the bunch serial number 150, it is approximately 1000 turn which corresponds to 0.6 ms. This is because of the fact that the 150th bunch in the bunch train interacts with an ion cloud of much higher density than that of 50th bunch.

3.9 Ion trajectory in the presence of bunched electron beam

Simulation is also executed to observe the ion trajectory under the influence of bunched electron beam. Following assumptions are made in the simulation. The longitudinal velocity of ions are considered to be negligible. Ions are produced with some transverse displacement from the beam axis, and the ion’s transverse motion is non-relativistic. The restoring force on the ions in the bunch gap is presumed to be zero. The ion receives a displacement-dependent kick and drifts with constant velocity in between bunches. Thus a deviation in initial position of ion yields change in velocity and due to this, the ion acquires large deviation in position during the long beam free gap and ultimately results in a different trajectory [70]. With this process, as time advances, ions gain amplitude and migrate away from the beam axis until they reach the vacuum chamber walls and are lost. The simulation was carried out in Indus-2 at 50 nTorr pressure having only CO^+ ions and at 200 mA beam current. For two slightly different positions of ion, the trajectories in vertical plane are shown in Fig. 3.14. It is observed that a small deviation in initial position of ion results in a different trajectory. The graph also indicates that as the bunch train passes through the beam-ion interaction points, ions are seems to be focused and defocused. This predicts that, after circulation of large number of turns upon interacting multiple times with the same ion cloud, ions slowly reaches the vacuum chamber wall and get lost.

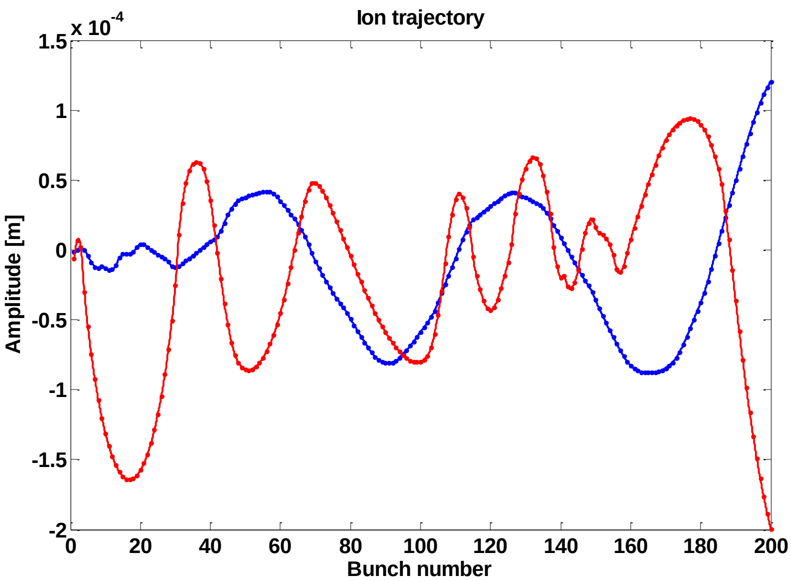

Figure 3.14: The trajectory of CO^+ ion with different initial position in vertical plane in the presence of electron beam. Blue curve represents ions with zero displacement and red curve represents the ions generated due to the displaced bunch.

3.10 Observation of FBII

To observe this instability, many storage rings set up their experiments to measure beam size, betatron tune and snapshots of every bunch using streak camera [17 and 21]. In Indus-2, we measured the betatron tune of each bunch using bunch by bunch feedback system and snapshots of each bunch using a streak camera attached to a diagnostic beamline. In the beginning of experiment, we stored 150 mA beam current in 200 consecutive bunches and then we reduce the beam emittance to 45 nm rad from 130 nm rad (nominal operation) using preplanned quadrupole tuning procedure [69]. Then to elevate the ring average pressure, we switched OFF all the sputter ion pumps

(SIPs) except in the RF and undulator sections. In two RF sections, installed in long straights (LS-7 and LS-8), the vacuum pressure cannot be deteriorated due to the multipactoring problem in RF cavities. In three undulator sections, installed in long straights (LS-2, LS-3 and LS-5), the residual gas pressure cannot be increased due to the presence of NEG coating in their vacuum chamber. Then to generate more residual gas load by internal means, filaments of titanium sublimation pumps (TSPs) were used in bake mode at few locations. With these setting, the ring average pressure could be elevated by ~ 13 times (from the nominal pressure of 0.5 nTorr to 6.7 nTorr). At this raised ring average pressure, we measured the concentration of CO using RGA. This shows that, the partial pressure of CO only increase to 0.5 nTorr.

We have captured the snapshot of bunches using a dual sweep synchro-scan streak camera (Optronis SC-10) and Fig. 3.15 shows the images of bunches at nominal as well as elevated ring pressure. The horizontal axis (fast time axis of 1000 ps) represents the bunch length and vertical axis (slow time axis of 375 ns) represents the longitudinal position of the bunch separated by 2 ns each. The streak camera operates at ~252.4 MHz i.e. half the frequency of Indus-2 RF system. With this, one can monitor two bunches in each sweep. We can get odd and even numbered bunches in separate columns by phase (delay) adjustment of the trigger.

The storage ring was filled with beam current of 150 mA in 200 bunches at the reduced beam emittance of 45 nm rad. The Fig.3.15 (a) shows the snapshot of electron bunches in the bunch train at nominal vacuum pressure of the Indus-2 storage ring. With proper phase adjustment of the trigger unit of streak camera, all bunches are brought in a single column as shown in Fig. 3.15 (a). With this configuration of streak camera, at elevated pressure of 6.7 n Torr, snapshots of bunches are again captured. However, any noticeable change could not be observed between the snapshots taken at nominal and elevated vacuum pressure. Here, our interest was to find out the centroid shift of trailing bunches in a bunch train due to increase in vacuum pressure. Thus to find out any small oscillations (if any) among bunches towards the tail of the bunch train at elevated pressure, we tried to separate odd and even numbered bunches and shown in Fig.3.15 (b). However, we couldn't observe the snake-tail type oscillation of bunches in the bunch train which is a signature of FBII [22]. Although in the Fig.3.15 (b), it appears that there is an increase of the bunch length at the elevated vacuum pressure, practically there is no such elongation, as the odd and even numbered bunches are placed in separate column. Also we measured the bunch by bunch tune at both the pressure level while putting OFF the transverse multi bunch feedback, but increasing trend in tune shift along the bunch train could not be detected.

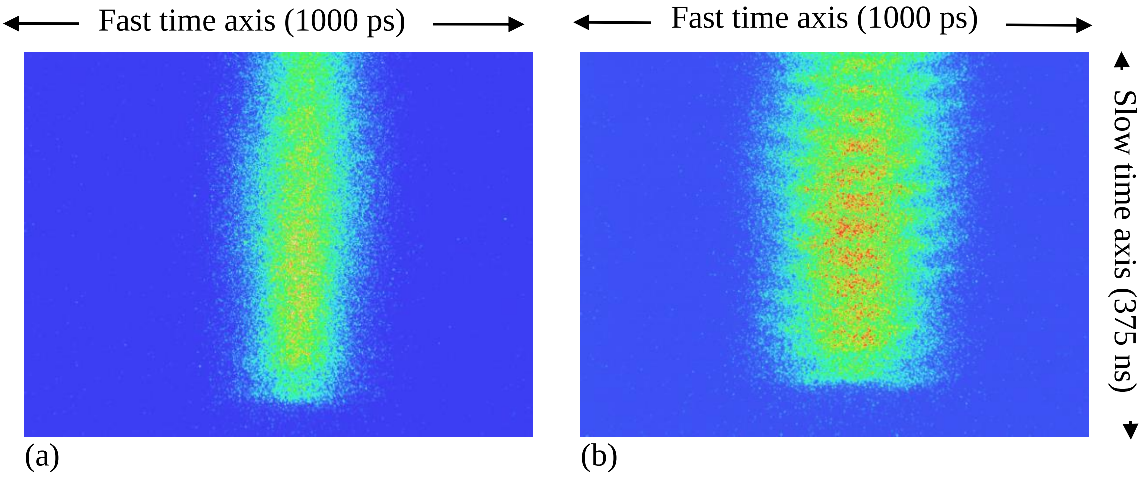

Figure 3.15: The snapshot images of a bunch train as observed by streak camera. The storage ring was filled with 150 mA beam current at 45 nm rad beam emittance. (a) Nominal ring average pressure of 0.5 nTorr and (b) elevated pressure of 6.7 nTorr with separate odd and even numbered bunches.

With the Indus-2 beam parameters and at elevated pressure of 0.5 nTorr CO in the ring, the simulation study predicted that the FBII cannot be observed and the same is concluded after the experimental measurements. The simulation study reveals that, to observe such instability, partial pressure of 50 nTorr CO is required. However, during this experiment, vacuum couldn't be deteriorated upto this level in Indus-2. In order to elevate the pressure in the ring to a desired level in future, we plan to generate extra residual gas load by injecting inert gases like helium (He) [16], and argon (Ar) or krypton (Kr) [21] in controlled manner in a localized segment of the Indus-2 ring. The inert gases are mainly used for this purpose as they are chemically very low reactive. The motivation behind using Ar gas is that the ionization cross-section of Ar and CO are similar. A larger cross section would create a more number of ions, and thereby increases the instability at lower elevated pressure, and in this context Kr can also be used. Many storage rings have chosen helium (He) gas because of its light mass and ease of pumping out from the vacuum chamber.

CHAPTER-4

INVESTIGATION OF FAST BEAM-ION INSTABILITY (FBII) IN WAKE FUNCTION FORMALISM

In the previous chapter, we have studied the fast beam ion instability (FBII) in electron storage ring by solving two coupled equations of motion for electrons and ions. With the analytical formulation and also by the numerical method using strong-weak interactions between electrons and ions, the instability growth rate was estimated. In a storage ring, despite good vacuum conditions, several molecular gas species exists. Ion species generated after ionization of respective molecular gas species have different ion frequencies at different locations along the circumference, due to variation of electron beam size in a strong focusing lattice. This generates a spread in ion frequencies and that helps in damping the instability via Landau damping. In essence, ions of each molecular gas species couple the electron beam with different oscillating frequencies. Solving the FBII in the wake function formalism, automatically takes care the combined contributions of multi-gas species and optics variation in the lattice. Here, the wake field of the ion cloud surrounding the electron beam is estimated. The wake function associated with the ion cloud extends up to many number of bunches and that leads to multi-bunch instability. L Wang et al. estimated the growth rate of the FBII using analytical formulation based on conventional multi-bunch instability [24]. This analysis guides to choose an appropriate bunch filling pattern that suppresses the FBII. The FBII is sensitive to the bunch filling pattern as it decides the ion density near the beam and also the ion species in vacuum chamber due to their different ionization cross-section.

Chapter 3 describes the interaction of electron beam with a single ion species, as the available version of FASTION code has the option of considering only one ion species. For two or more number of ion species interacting with electron beam, three or more number of coupled equations are required to solve. However, the wake-field approach models the effect of composition of multiple ion species simultaneously. Also this method allows to study the FBII using multi-train bunch filling pattern, whereas in the FASTION simulation code, only single train bunch filling pattern can be considered. The wake-field formalism models the beam-ion interaction by estimating the wake field of the ion cloud from the coupling force between the motion of electron beam and ion cloud [23 and 24]. Since the wake-field approach integrate the effect of multi-ion species and multi-train bunch filling pattern concurrently, this approach is applied in this chapter to study the beam-ion interaction.

We investigate the possibility of FBII in the Indus-2 storage ring and a suitable bunch filling pattern is mooted for suppression of the FBII. This chapter systematically resolves the suppression of beam-ion instability by using multi-train bunch filling patterns. In Indus-2, maximum 291 bunches can be filled with a bunch to bunch separation of 2 ns. In our booster, maximum 3 bunches are circulated and only 2 bunches with a separation of 32 ns (equivalent to 16 bunch separation of Indus-2) could be extracted every second and injected into Indus-2. This filling scheme allows to incorporate only few bunch filling patterns in Indus-2, keeping same number of bunches filled. We consider three filling patterns namely, 1) single long bunch train, 2) double bunch trains and 3) triple bunch trains, consisting of 192 total filled bunches. The FBII growth rate for different bunch filling patterns are estimated, and the results are discussed. The chapter is organized as follows. In section 4.1, we describe the wake function of an ion cloud. We estimated the quality factor of ion cloud in Indus-2 storage ring and wake function due to ions for different bunch filling patterns. In section 4.2, we calculated the impedance due to ions in Indus-2. In Section 4.3, estimates for the growth rate of FBII for multi-train bunch filling pattern are obtained and compared them with synchrotron radiation damping.

4.1 Wake function of an ion cloud

In an electron storage ring, the wake function describes the electromagnetic interaction of the beam and its environment, which is mostly depends on the geometry of the vacuum chamber. However, in our case, the environment is ionized residual gas molecules in the ring. The wake function arises due to ion cloud surrounding the electron beam is evaluated in the time domain and its effect on the electron beam dynamics is studied. Consider an ion cloud is generated from an electron bunch which is displaced transversely by Δy_e amount with respect to the other bunches in a bunch train, as shown in Fig. 4.1. A source particle which travels on-axis can't induce a net transverse force on a particle that follows it on the same axis in an axi-symmetric geometric structure [71].

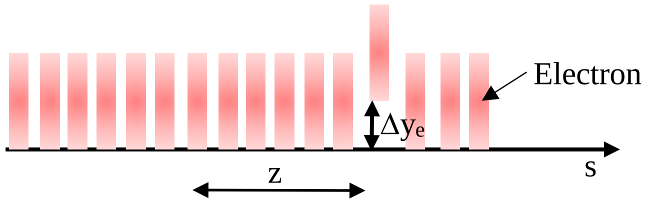

Figure 4.1: Illustration of an electron bunch with its center of mass deviated by Δy_e generates ion cloud. Subsequent electron bunches behind it gets a kick from the ion cloud depending on how far it is from the source of wake.

The wake function of ion cloud seen by the subsequent electron bunch separated at a longitudinal distance 'z' from the ion generated at the displaced electron bunch is defined as the transverse kick of ion cloud normalized by the product of charge of both the source and witness particle. The dipole component of the transverse wake function is dominant for the small transverse displacement between ion cloud and electron bunch. This is defined as the transverse wake per unit displacement of the source charge from the beam axis [71], given by

$$W_y(z) = \frac{\int_{-\infty}^{\infty} q_i \left[\vec{E}(s,z) + \vec{v} \times \vec{B}(s,z)\right]_{ion} ds}{q_i q_e \Delta y_e} \qquad \text{....} (4.1)$$

where q_i: charge of ion, q_e: charge of electron and Δy_e: offset of generated ion cloud from the beam axis. The SI unit of wake function defined above is V C^{-1} m^{-1}. The relative distance between the source of the wake (ions) and the electron bunch that receives the consequence of the wake field, and the range of the wake field plays the important role for this instability. However, the source of the wake function is not at unique location, rather distributed all over the circumference of the ring.

Since the speed of ion is very small, we neglect the contribution from the force generated due to magnetic field of ion while estimating the wake field of ion cloud. The Bassetti- Erskine formula [50] suggests that the electric field of Gaussian charge distribution, varies linearly with the displacement up to the electron beam size and afterward it becomes nonlinear. The electric field of a Gaussian bunch in vertical plane at a certain displacement y from the centroid of the bunch ($y \leq \sigma_y$), is given as

$$E_y = \frac{\lambda}{2\pi\epsilon_0} \frac{y}{\sigma_y(\sigma_x + \sigma_y)} \qquad \text{.... (4.2)}$$

where λ is the line charge density of electron beam, σ_x and σ_y are transverse beam sizes in horizontal and vertical plane respectively, and ϵ_0 is the vacuum permittivity that has a value of 8.85 x 10^{-12} C V^{-1} m^{-1}. The amplitude of the wake in linear regime ($y \leq \sigma_y$) is estimated from the coupling force between electron bunch and ion cloud [23]. The ion cloud receives a linear kick from the electron bunch and it oscillate with certain amplitude. Subsequently, the electron bunch receives a kick from the oscillating ion cloud. The amplitude of the wake is given by the maximum kick received by the electron bunch. The procedure of estimation of wake amplitude is described in APPENDIX-A.

$$\widehat{W_y} = \frac{N_i}{4\pi\epsilon_0} \left[\frac{L_{sep} r_p}{A N_e}\right]^{1/2} \left[\frac{4}{3} \frac{1}{\sigma_y(\sigma_x + \sigma_y)}\right]^{3/2} \qquad \text{... (4.3)}$$

where N_e: Number of electrons per bunch, L_{sep}: Bunch to bunch separation, A: atomic mass of the ion under consideration, r_p: Classical proton radius, N_i: Number of ions. As long as the electric field of ion cloud is linear, the wake amplitude does not depend on the offset of the electron bunch. However, when bunch offset becomes more than the beam size, the wake of the ion cloud turn out to be nonlinear and its amplitude reduces. Including the nonlinear electric field, the wake of the ion cloud was estimated numerically by L. Wang [72] and then the simulated wake was fitted to an analytical form given in equation 4.4 which shows good agreement. At a longitudinal location *s* of the ring, the wake function of an ion cloud is written as [23 and 73]

$$W_y(s,z) = \widehat{W_y} exp\left(\frac{-\omega_i(z)s}{2Qc}\right) sin\left(\frac{\omega_i(z)s}{c}\right) \quad \text{....}(4.4)$$

where $\widehat{W_y}$ is the wake amplitude and ω_i is the ion oscillation frequency given as

$$\omega_i = c\left(\frac{4N_e r_p}{3L_{sep}\sigma_y(\sigma_x+\sigma_y)A}\right)^{1/2} \quad \text{....}(4.5)$$

where c: Speed of light, and Q: Quality factor of the ion cloud. In an electron storage ring, due to strong focusing optics, the electron beam size varies along the circumference and thus ion density also varies over its circumference. Therefore, we integrating the wake over the ring circumference, C to estimate the total wake function due to the ion cloud, [24 and 72], which is given by

$$W_{tot}(s) = \int_0^C \frac{4}{3}\frac{\omega_i(z)}{c}\frac{\lambda_i(z)L_{sep}}{4\pi\epsilon_0 N_e}\frac{1}{\sigma_y(z)\left(\sigma_x(z)+\sigma_y(z)\right)} exp\left(\frac{-\omega_i(z)s}{2Qc}\right) sin\left(\frac{\omega_i(z)s}{c}\right) dz \quad \text{...}(4.6)$$

where $\lambda_{i:}$ Line density of ions that depends on the ionization cross section and the total number of electrons in a bunch train. The ion density increases linearly along the bunch train, becomes maximum at the tail of the bunch train and decays exponentially in the gap between bunch trains. The total wake function over the entire ring circumference due to any ion species can be determined by the above eqn. 4.6.

4.1.1 Frequency spread of ions and quality factor

The variation of beam size over the ring circumference leads to frequency variation of ions. The frequency spread provides effective Landau damping to the beam-ion instability. Fig. 4.2 shows the ion frequencies for various residual gas species.

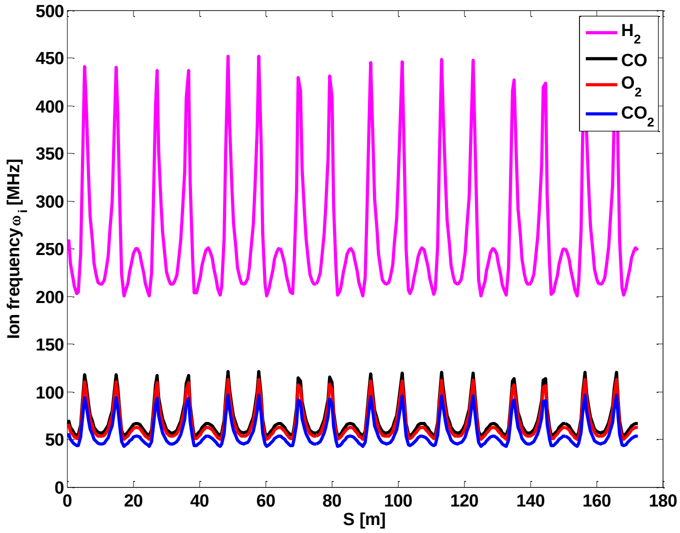

Figure 4.2: The ion frequencies of H_2, CO, O_2, and CO_2 along the circumference of the Indus-2. The ion frequency varies because of the beam size variation in strong focusing lattice.

The resonant behavior of the wake field of ion cloud is characterized by a vital parameter known as Quality factor. Typically Q for any resonant model is defined as

$$Q = \frac{\omega_r}{\Delta\omega_r} \qquad \text{.... (4.7)}$$

where ω_r is the resonant frequency and $\Delta\omega_r$ is the full width at half maximum (FWHM). However, for the frequency distribution of CO ions as shown in Fig. 4.3, FWHM cannot be calculated. Thus Quality factor of an ion cloud due to beam size variation is approximated by the formula [72]

$$Q = \frac{\omega_{i,average}}{\sigma_{\omega i}} \qquad \text{.... (4.8)}$$

where $\omega_{i,average}$ is the average ion frequency along the ring and $\sigma_{\omega i}$ is the standard deviation of the ion frequencies.

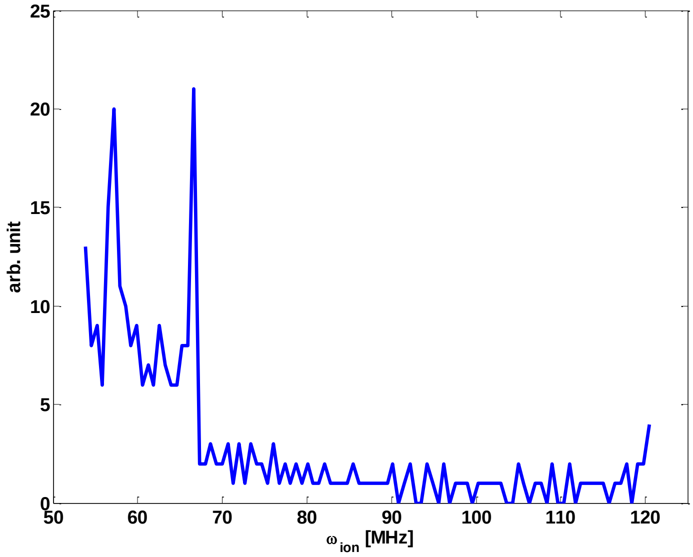

Figure 4.3: The frequency distribution of CO ions in the Indus-2 storage ring.

It can be seen from the eqn. 4.8, the Q of all ion species become same as the atomic mass of ion species is cancelled out in the ratio. The quality factor of the wake generated due to CO ions in Indus-2 comes out to be 3.96 [74]. However for ultra-low emittance storage ring, wake function due to ions may not be represented by single resonance model as beta function variation is quite large along the circumference because of the injection cell optimization. There, the total wake function is characterized by two to three wake functions with different Q in different segments of the ring such as insertion device section, arc section and injection section.

4.1.2 Wake function due to ions in Indus-2

The low emittance beam with small betatron coupling coefficient and high ring average pressure is susceptible to develop the FBII in storage ring. For the estimation of FBII growth rate, beam emittance of 45 nm rad, coupling coefficient of 0.1 %, beam current of 200 mA and total gas pressure of 50 nTorr in Indus-2 storage ring is considered. This low emittance configuration along with beta function at source point of synchrotron radiation produces electron beam size of 150 μm and 13 μm in the horizontal and vertical plane respectively. Filling pattern is assumed as single bunch train consisting of 192 consecutive bunches uniformly filled with a gap of 99 empty bunches. The wake function of different ion species for the above bunch filling configuration in the Indus-2 ring is estimated using eqn. 4.6, and is shown in Fig. 4.4. It is observed that, the range of the wake due to CO and H_2 ions are long enough to cause multi-bunch instability. The amplitude of the wake function along with its range decides the growth rate of the instability. The wake due to ions is mainly dominated by hydrogen (H_2) due to its large concentration followed by the carbon monoxide (CO) due to its second largest concentration and large ionization cross section. Due to the very low concentration of O_2 and CO_2 (as discussed in previous chapter), the wake generated by them are not significant and invisible in this figure.

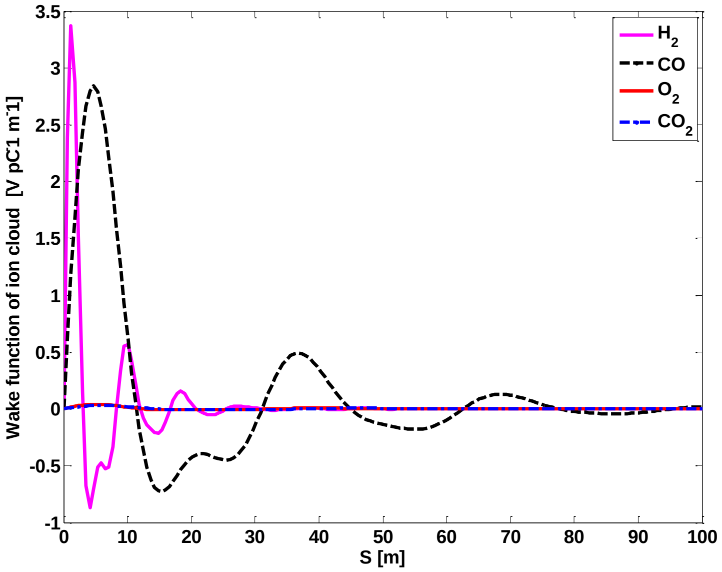

Figure 4.4: Wake function of ion cloud of different residual gas species in Indus-2 storage ring for a single bunch train. Filling pattern: 192 bunches with 99 bunch gaps.

Similarly using the eqn. 4.6, the wake function due to ion cloud for any arbitrary bunch filling pattern can be estimated. We have calculated the wake function for two bunch trains (96 bunch filled +49 empty bunch gap+96 bunch filled +50 empty bunch gap) and three symmetric bunch trains, each comprising of 64 bunches filled and 33 empty bunch gaps. Fig. 4.5 and 4.6 shows the wake function of ion species for two and three train bunch filling pattern respectively as mentioned above. The amplitude of wake function reduces substantially in three bunch train pattern as compared to a single bunch train consisting of same number of filled bunches. This is due to the fact that short bunch train reduces the ion density near the beam compared to long bunch train and that causes a noticeable reduction in wake field in multi bunch train. These observations support the theory that the multi bunch train with short gaps are very effective for suppression of FBII. Further to clear the trapped ion species, required gap between bunch trains should be longer than the ion oscillation period of that gas species. In our two and three bunch train filling patterns, the bunch train gap is more than two oscillation period of CO_2^+ ion. Hence it eliminates the possibility of existence of trapped ions of any gas species over the turn, as the oscillation period of ions of other gas species such as H_2, O_2 and CO are less than that of CO_2^+ ion.

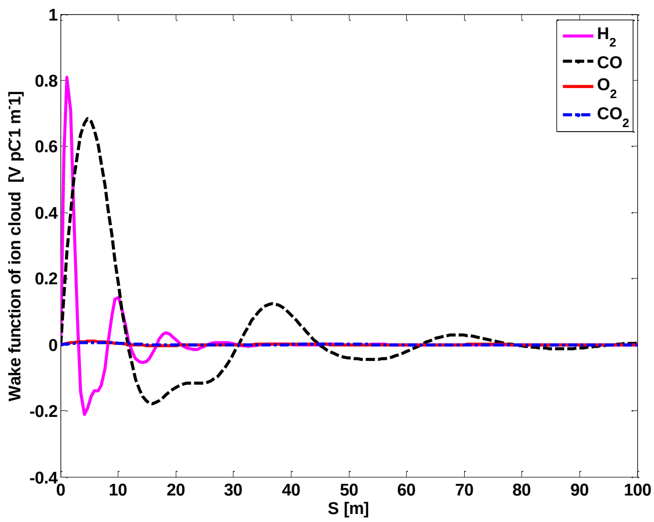

Figure 4.5: Wake function of different ion species in the Indus-2 consisting of 2 bunch trains. Filling pattern: 96 bunch filled +49 bunch gap+96 bunch filled +50 bunch gap.

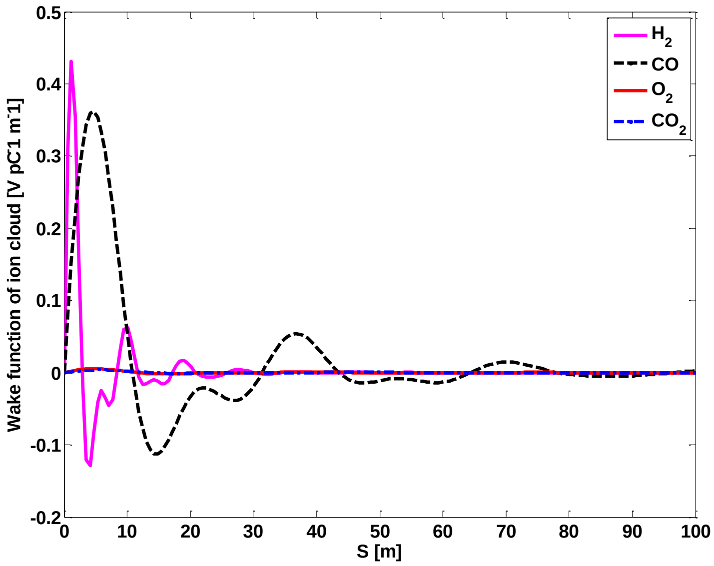

Figure 4.6: Wake function of different ion species in the Indus-2 consisting of 3 bunch trains. Each bunch train comprises of 64 bunches filled and 33 empty bunch gaps.

4. 2 Impedance due to ions in Indus-2

In a circular machine, the multi-bunch instability is very well explained in the frequency domain (impedance). By performing the Fourier transform of wake function, we can estimate the impedance of the ion cloud [23] and is given as

$$Z_{ion}(\omega) = \frac{i}{c}\int_0^C W_{ion}\,(s) exp\left(\frac{-i\omega s}{c}\right) ds \qquad \dots (4.9)$$

The above definition shows that the impedance is a complex quantity. The growth rate of the transverse beam instability is derived from the real part of impedance. Applying the above Fourier transform to the equation 4.3, the impedance of the ion cloud is estimated as

$$Z_{ion}(\omega) \approx \frac{\widehat{W}_{ion}}{\omega}\frac{Q}{1 + iQ\left(\frac{\omega_i}{\omega} - \frac{\omega}{\omega_i}\right)} \qquad \dots (4.10)$$

Comparing this with the impedance of a resonator model, we observed that the shunt impedance of the resonator is equivalent to amplitude of wake and resonant frequency resembles with ion oscillation frequency [32]. Fig. 4.7 shows the real part of transverse impedance for single long bunch train consisting of 192 filled bunches, for different ion species. The total impedance of the ion cloud resulted from the contribution of all the ion species and beam size variation along the ring is also shown in this figure.

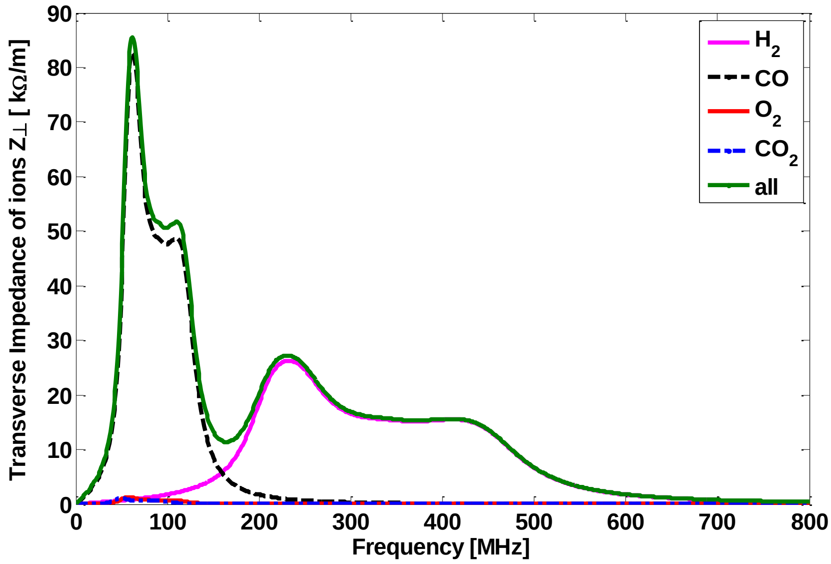

Figure 4.7: Real part of transverse impedance generated due to different ion species and the total impedance in Indus-2 ring. Bunch filling pattern: 192 consecutive filled bunches + 99 bunch gaps. Beam current: 200 mA. Ring average pressure: 50 nTorr.

4.3 Growth rate of the fast beam ion instability

The transverse growth rate of a multi-bunch mode μ for coupled bunch instability is given as [32]

$$\frac{1}{\tau_\mu} = \frac{N_e n\, e^2 c}{2\omega_\beta E T_0^2} \sum_{p=-\infty}^{\infty} Re\left[Z_{ion}\left(pn\omega_0 + \mu\omega_0 + \omega_\beta\right)\right] \quad \ldots.(4.11)$$

where E is the beam energy, n is the number of bunches in a bunch train, T_0 is the revolution time, ω_0 is the revolution frequency, and ω_β is the angular betatron frequency. This formula is directly used here for FBII with wake function generated by ion cloud as the impedance source. The impedance is evaluated at frequencies (pn+μ) ω_0+ ω_β which is sampled by oscillation frequency of ion clouds. At the resonance ($\omega = \omega_i$), the growth rate formula given in eqn. 4.11 can be simplified using eqn. 4.10 as [72]

$$\frac{1}{\tau} \approx \frac{N_e n\, e^2 c}{2\omega_\beta E T_0^2} \frac{\widehat{W}_{ion}}{\omega_i} Q \qquad \dots (4.12)$$

This suggests that, the instability growth rate depends on two important factors, such as the density of ion cloud and quality factor of the wake field produced due to ion cloud. These factors must be reduced to decrease the growth rate of FBII. The Q of the wake can be reduced by generating more spread in ion frequencies. The density of ions can be reduced by redistributing the single bunch train into several mini bunch trains with an optimal bunch gap between the bunch trains.

The growth rate of the FBII driven by different ion species for beam filling with single bunch train is shown in Fig. 4.8. It can be observed that the distribution of growth rates of unstable modes are similar to the distribution of impedance shown in previous figure and this is because of the fact, the growth rate of oscillation mode is proportional to the magnitude of impedance at that frequency. It also shows the damping rate in vertical plane due to synchrotron radiation in the Indus-2. This shows that the few modes have higher growth rate than the radiation damping rate. The minimum growth time of FBII is estimated to be 1.7 ms, which is originated by CO^+ ion at a frequency 85 MHz. As the instability growth time is smaller than the radiation damping time of 4.6 ms in the vertical plane, FBII will occur with the above machine configuration. The occurrence of instability is mainly due to the contribution from CO^+ ion and the growth of instability due to H_2^+ ion is completely suppressed by the synchrotron radiation damping. This confirms that the heavy ions which have large ionization cross-section contribute more to the FBII than the lighter ions.

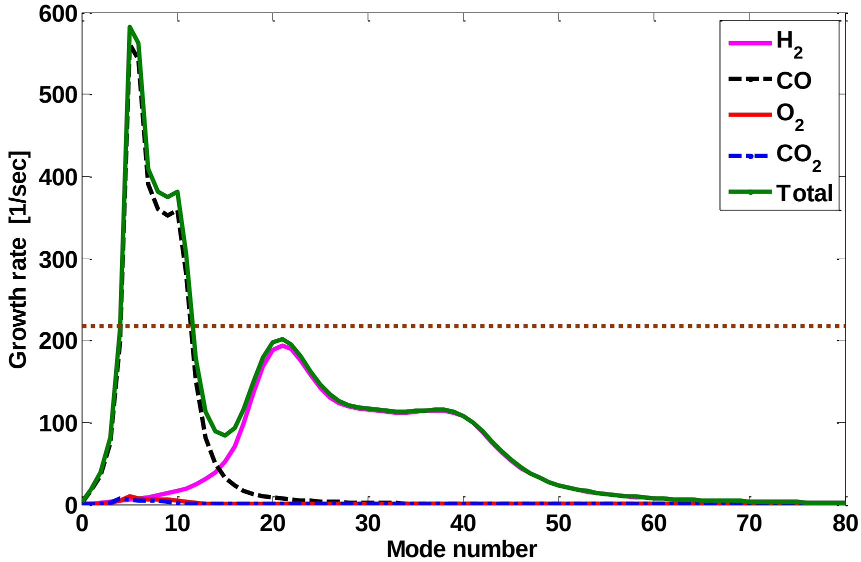

Figure 4.8: The instability growth rate driven by ion clouds of different ion species in Indus-2 for single train bunch filling pattern. The dashed straight line shows the synchrotron radiation damping rate in the vertical plane of Indus-2.

4.4 Effect of multi-train bunch fill pattern on FBII

The maximum ion density accumulated near the beam is proportional to number of bunches in a bunch train and inversely proportional to beam sizes [75], given as

$$\rho_i = \frac{2\sigma_i N_e P\, n}{3kT\, \sigma_y(\sigma_x + \sigma_y)} \qquad ....(4.13)$$

Using the above formula, the ion density is estimated for many storage rings of similar energy to Indus-2 at 1 nTorr average pressure considering CO ion and listed in Table 4.1. It can be noticed from the list, FBII becomes relatively stronger in the storage rings like, SLS, NSLS-II, and SPEAR-3 due to small size of electron beam and higher beam current as compared to Indus-2.

Table-4.1: Comparison of ion density for a single bunch train filling pattern for various storage rings and relevant machine parameters.

Storage ring	**Cir (m)**	**E (GeV)**	**I (mA)**	**n**	**σ_x (μm)**	**σ_y (μm)**	**ρ_i (m^{-3}) ($1x10^{09}$)**
Indus-2	172.4	2.5	200	192	150	13	9.6
ALS	196.8	1.9	400	320	160	23	10.8
PLS	280	2.0	360	180	350	35	4.3
AS	216	3.0	200	300	165	14	10.3
SLS	288	2.4	400	390	111	5.6	104.2
SPEAR3	234	3.0	500	280	200	10	33.5
NSLS-II	792	3.0	500	1040	122	11	162.7

The effect of FBII can be alleviated by reducing the density of ions in a bunch train, as its growth rate is proportional to the ion density. The ion density grows linearly over the bunch train and becomes maximum at the extreme end of the bunch train and after that it decays exponentially in the bunch gap. Fig. 4.9 shows the schematic of different bunch filling patterns in Indus-2 such as single bunch train (192 bunch + 99 gap), double bunch train (96 bunch + 50 gap + 96 bunch + 49 gap) and triple symmetric bunch train (64 bunch +33 gap) *3. Fig. 4.10, shows the ion density accumulation along the bunch train and reduction in the bunch gap for different fill patterns.

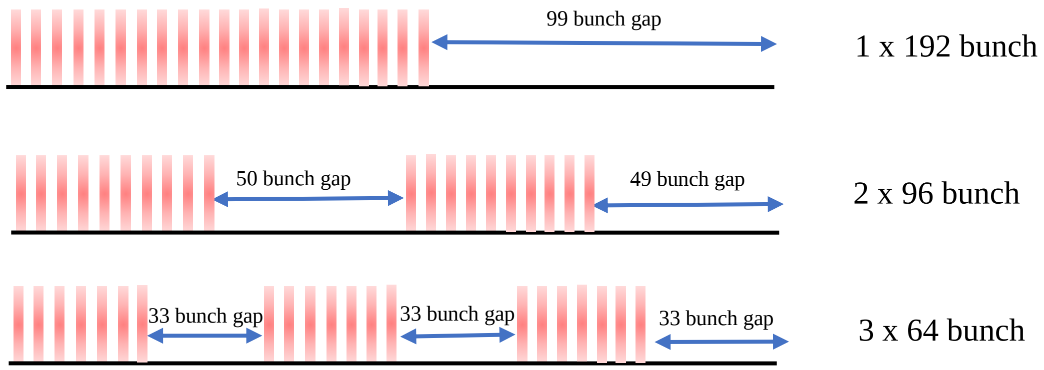

Figure 4.9: Schematic of various bunch filling schemes of Indus-2, each consisting of total 192 bunches. (Top) Single bunch train, (middle) Double bunch trains and (below) Triple bunch trains.

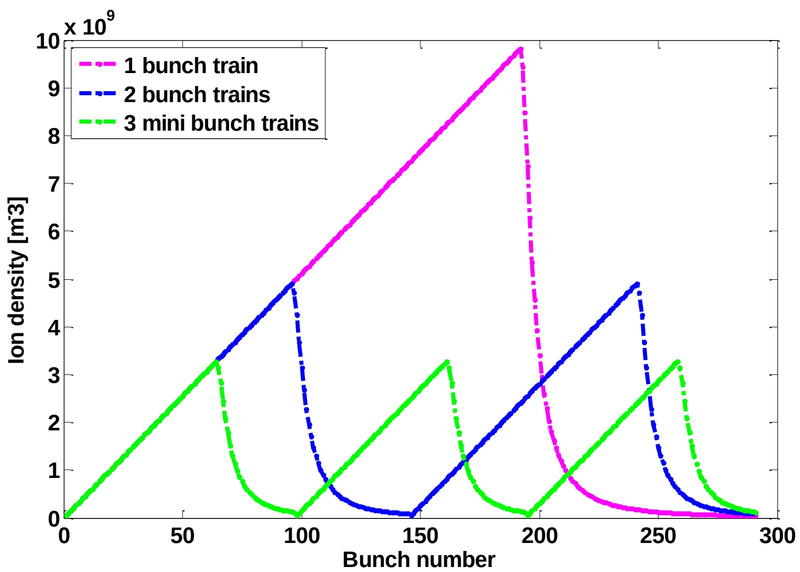

Figure 4.10: Ion density in different bunch filling patterns in Indus-2 storage ring

We estimated the instability growth rate for different multi-train bunch filling pattern by calculating the associated ion cloud impedance for each filling pattern. The FBII growth rate for one, two and three train bunch filling pattern, each consists of total 192 bunches are shown in Fig. 4.11. It can be observed that, for two and three bunch trains, the FBII growth rate is significantly smaller than the synchrotron radiation damping rate. The estimated FBII growth times in Indus-2 are 1.7 ms, 6.7 ms and 16.1

ms for one, two and three train bunch filling patterns respectively at an average residual gas pressure of 50 nTorr. The above analysis shows clearly the effectiveness of the multi-train bunch filling patterns on FBII growth rate. The multi-train bunch filling with suitable gaps in between reduced the ion density and thereby efficiently suppress the FBII.

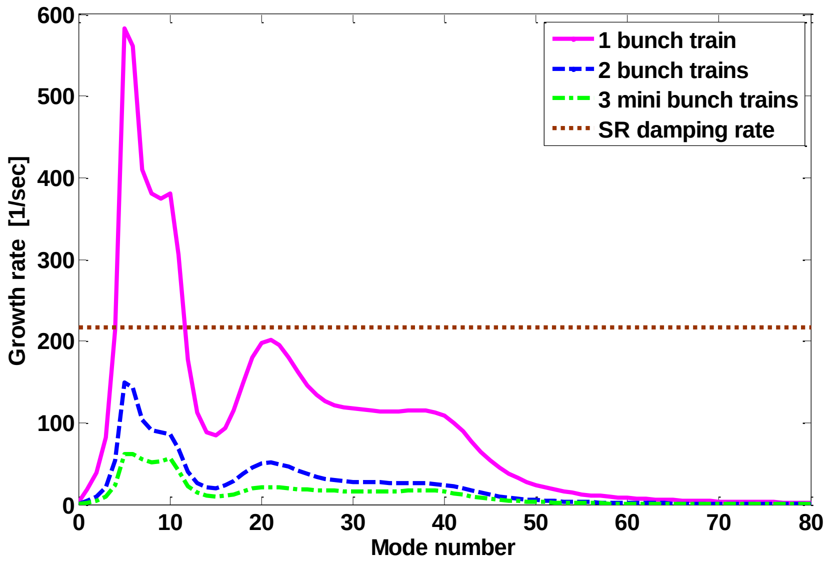

Figure 4.11: The FBII growth rate driven by ion clouds in Indus-2 for different bunch filling patterns. The synchrotron radiation damping rate in the vertical plane is shown by dashed straight line.

4.5 Comparison of the two approaches –FASTION simulation method and wake field analysis method for study of FBII

The phenomenon of fast beam ion instability (FBII) was studied numerically using FASTION simulation code. The vacuum in Indus-2 storage ring has four major composition of residual gas molecules such as H_2, CO, O_2, and CO_2 with the concentration of 61.7 %, 37.5 %, 0.5 % and 0.3% respectively. However, the FBII was simulated with single ion species because of the limitation of simulation code

FASTION. Since the ionization cross section of CO is 6 times higher than the H_2, the simulation was carried out by considering that the residual gas in the storage ring consists of only CO. At elevated vacuum pressure of 50 nTorr CO in Indus-2 storage ring, the simulation study of FBII was carried out and the growth time of the FBII is estimated as 0.6 ms. This instability manifests itself with the growing oscillation amplitude of bunch centroid in vertical plane and this effect is enhanced for bunches towards the tail part of the bunch train.

Multiple gas species in the storage ring vacuum chamber generates large spread in ion oscillation frequency and this weakens the growth rate of beam-ion instability via Landau damping mechanism. The beam-ion interaction was modelled analytically using the wake-field approach, with the inclusion of multiple gas species, analogous to the conventional approach to study beam instability. Results of the wake-field model based approach agrees reasonably well with those obtained using FASTION simulation that includes realistic vacuum pressure for multiple gas species [72], and the same has been benchmarked in SPEAR3 storage ring. Thus, to include the effect of multiple gas species, the impedance of ion cloud generated from the mixture of all gas molecules present in storage ring vacuum chamber was estimated. For this study, a total vacuum pressure of 50 nTorr in Indus-2 storage ring was assumed with the specified concentration of H_2, CO, O_2, and CO_2. In the similar machine condition used in the FASTION simulation, except that the mixture of gas species was considered in the wake-field approach, the FBII growth time is estimated as 1.7 ms. The synchrotron radiation damping time of Indus-2 storage ring in vertical plane is 4.6 ms. The vacuum pressure threshold in the Indus-2 storage ring for FBII was determined by comparing the instability growth time with the radiation damping time. The estimation reveals that the lowest average vacuum pressure of ~17 nTorr can lead to FBII in Indus-2 storage ring. However, for experimental verification in Indus-2 storage ring, where the FBII will appear definitely [15], the simulations of FBII were carried out at elevated vacuum pressure of 50 nTorr.

To compare the result obtained from FASTION simulation, the FBII growth time is estimated by wake-field approach considering the residual gas molecules consists of only CO gas species in the Indus-2 storage ring vacuum chamber. For the vacuum pressure of 50 nTorr CO and beam current filled with single bunch train, the growth rate of FBII is shown in Fig. 1 and the corresponding growth time is calculated as 0.58 ms. The result of wake-field approach agrees well with that of FASTION simulation described in chapter-3.

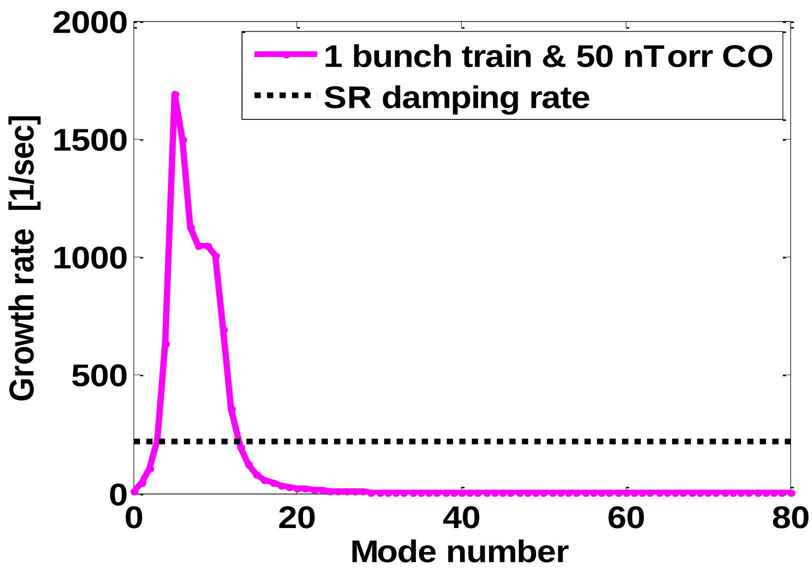

Figure 4.12: The FBII growth rate driven by only CO ion species in Indus-2 storage ring for beam current filled with single bunch train. The synchrotron radiation damping rate is shown as a dashed line.

The wake-field approach is straightforward and does not require time consuming computer simulation, and may therefore be followed for a quicker estimation of FBII growth time for a storage ring consisting of large number of bunches to obtain a-first-hand information. The wake-field approach is considered to be more appropriate for the study of FBII in an electron storage ring, as the residual gas with different composition of gas species is modelled accurately and also it estimates the effect of the multi-train bunch filling pattern [72]. However, the FASTION simulation provides better insight in which every individual bunch centroid motion can be visualized at any desired location of the storage ring.

CHAPTER-5

CONCLUSIONS AND FUTURE PERSPECTIVE

5.1 Summary and conclusions

We conclude the thesis with a brief summary and a few possibilities underlining the future perspectives of the work. The effect of ion trapping and fast beam ion instability (FBII) on electron beam in the Indus-2 storage ring have been addressed with theoretical estimation, numerical simulation and experimental investigations. Though the FBII is not detected for Indus-2 storage ring, the effect of ion trapping on electron beam was observed unambiguously. As a future perspective, in upcoming high brilliance light source (ultra-low emittance electron storage ring), the ion effects would be a major concern, since FBII growth rates to be significantly high.

In the conventional ion trapping, the positive ions are trapped by the negative beam potential and undergo stable oscillations around electron beam. In Indus-2 ring, it was estimated that at a residual gas pressure of 1 nTorr inside the vacuum chamber, full neutralization of beam occurs within about few seconds. The trapped ions adversely affect the electron beam due to the additional electric field of the trapped ion clouds that create non-linear focusing forces leading to changes in beam optics. This yields a coherent tune shifts of $\Delta\nu_y = 2.76\,\eta$ in the vertical plane, where η is the neutralization coefficient. This implies that in order to have stable machine operation, the neutralization coefficient is required to be kept below 1 % level. The first and foremost possibility to reduce the neutralization is by substantial improvement in the vacuum conditions inside the ring. However, because of large volume of the vacuum chambers coupled with low conductance, improvement in vacuum better than 1 nTorr is not feasible. Considering this as a best possible vacuum, the effect of the beam-free time gap on ion trapping phenomena was studied. It reveals that ions are trapped in the electron beam when all bunches equal to harmonic number of the storage ring are filled and those ions become unstable when ring is filled partially. An optimal bunch filling pattern was evolved that leads to unstable ions and thereby significant reduction in trapped ion density. In parallel with this theoretical work, an experimental investigation was carried out to observe the ion trapping in Indus-2. Finally, the required diagnostic tools and measurement of trapped ion effects are discussed. We have conducted several experiments to compare the changes in beam properties like betatron tune, beam current saturation, and beam lifetime in different bunch filling patterns to comprehend the ion trapping phenomenon. We have also provided a direct method of observing ion trapping instead of measuring the effect of ion trapping on electron beam by measuring bremsstrahlung radiation dose using a small size radiation detector. Both the theoretical and experimental investigations confirms that with the filling of 150 bunches leaving a gap of 141 bunches, effect of ion trapping gets suppressed effectively. Moreover, the partial bunch filling facilitates higher beam current accumulation, which otherwise saturates at ~ 100 mA.

It is clear that ions can have a significant and sometimes detrimental effect on the electron beam, but to know the in-depth impacts of ions, we have studied the FBII using simulations code “FASTION”. It has given a detailed insight of the behavior of electron beam and ion species during their interaction process. In FBII, the process of interaction between the ions and electron beam is repeated from its beginning, at every turn, but the perturbation upon the electron beam remains in its memory and this eventually make the electron beam unstable. The simulation result predicts that the bunches towards the tail portion of the bunch train oscillates with larger amplitude and becomes unstable. Amplitude of oscillations initially grows exponentially until the amplitude of a bunch centroid is of the order of the transverse rms size of a bunch. After that, the nonlinear effects slows down the fast growth of the instability and the simulation also confirms the theoretical estimation. We have carried out the simulation based on weak-strong interaction approach using a single gas species which seems perfect when one major species is dominated among all the species present in the residual gas. However, to have a more realistic estimation, we can consider the composition and concentration of several residual gases and the vacuum level along the circumference of the ring. In the present operating condition of Indus-2 (1 nTorr pressure & 130 nm rad beam emittance), the signature of FBII could not be observed. However, in near future, the Indus-2 will be operated in reduced beam emittance of 45 nm rad, which has already been tested experimentally. The simulation shows that at reduced beam emittance and at 50 nTorr residual gas pressure the instability growth time to be ~ 0.6 milliseconds which is much less than the synchrotron radiation damping time. Using a fast bunch by bunch feedback system, this instability can be suppressed before it grows. However, this instability can also be overcome by beam filling with multi-bunch train with a fixed bunch gap between the trains. The gaps between bunch trains reduces the number of ions significantly, which reduces the growth of FBII as well. In addition to this, a good vacuum is required to suppress the effect of FBII, as the simulation shows the oscillation amplitude increases with the vacuum pressure.

We describe the effect of trapped ions in terms of the impedance in chapter-4. This enables us to study the FBII in the frame work of conventional beam instability driven by the impedance governed by strength of the interaction of beam with vacuum chamber components. Here we estimate the impedance offered by the ion cloud generated from the electron beam, and that provides a straight forward method to estimate the FBII growth rate. The FBII was investigated for various bunch filling patterns such as one long bunch train, two bunch trains, and three bunch trains. Total filled bunches in each filling pattern are kept same and is equal to 192. The bunch gaps provided in each bunch filling pattern is sufficient to avoid the conventional ion trapping phenomena for the Indus-2 ring. The study reveals that the multi-train bunch filling pattern suppresses the FBII in effective manner in the storage ring. The reduction of ion density with the help of the multi-train bunch filling pattern plays a decisive role in minimizing the instability growth rate. The frequency spread $\Delta\omega_i$ among ions was prominent in synchrotron radiation sources based on storage ring consisting of an achromatic lattice, and that also contributes significantly in reducing the instability growth rate. To suppress the FBII, a multi train bunch filling pattern was evolved. Three bunch trains, each having 64 bunches and 33 bunch gaps supress the FBII quite effectively. Likewise, the study can be extended to four or five bunch train in which we can store more number of bunches in total, which can curb the conventional ion trapping as well the FBII. The results of FBII using the impedance estimation model are encouraging and this method can be applied for a quick estimation of instability growth rate for future low emittance storage ring in which large number of bunches are present. The time domain simulation took long time for the study of FBII. For example, simulating FBII in a bunch train consisting of 200 bunches over one turn in Indus-2 with 20 interaction points, the FASTION code takes ~ 4 minutes, yielding a run time of 5 days for 2000 turns.

5.2 Future perspectives

The field of ion trapping and fast beam ion instability are very robust and there remains sufficient room for further study in the future. In this thesis work, we have studied the beam-ion interaction in transverse plane. However, it is also necessary to understand the ion dynamics in longitudinal plane [76], in order to design effective mitigation strategies. The magnitude of longitudinal kicks to the ion cloud from electron beam and vice versa is much less compared to the transverse part, but not negligible. As a result, after several thousand beam-ion interaction, ions may drift longitudinally and accumulate at different position of the ring.

The theory of ion trapping has been described in chapter-2 by considering linear approximation of the focusing force of the electron bunch. However, the actual electric field of a Gaussian electron bunch is non-linear in nature as described by Bassetti-Erskine formula. As a future work, the bunch gap will be optimized for suppression of ion trapping effect by including the non-linear beam potential. This would then lead to a realistic optimization of bunch filling pattern.

The ion trapping phenomena was observed in Indus-2 by measuring additional bremsstrahlung radiation (BR) yield as a result of beam-ion interaction. However, quantitative analysis of the BR yield occurred due to the electron-neutral gas molecule interaction and electron-ion interaction was not estimated. These estimations can be made with the help of simulation code which will help in proper modelling of the beam-ion interaction.

The simulation of fast beam ion instability was carried out by assuming average vacuum pressure in the storage ring. As a future work, the simulation will be conducted by incorporating realistic vacuum pressure profile of the storage ring. By this analysis the locations of higher probability of ion trapping in the storage ring can be identified and accordingly efficient vacuum system can be designed [77].

In suppression of FBII growth, the contribution of spread in ion frequency is duly considered. However, there remains another possibility to suppress further the growth of FBII via Landau damping by introducing additional non-linearity in the beam optics by operating the storage ring with higher positive chromaticity [24]. Also, the electron storage rings are sometimes operated with low momentum compaction (alpha) in order to compress the bunch length of the electron beam. During a trial operation, the momentum compaction factor of Indus-2 ring was reduced by a factor of 25. In this operating mode, nonzero chromaticity produces more chromatic frequency shift.

The FBII couldn't be observed experimentally in Indus-2, as the residual gas pressure couldn't be increased to a desired level with existing setup. However in future, this can be realized by generating extra residual gas load by purging of Argon (Ar) gas in controlled manner in a localized segment of the Indus-2 ring. The storage rings such as ALS, PLS & CESR-TA [21] have observed the FBII in a similar way.

In upcoming ultra-low emittance storage rings, the ion effect is considered as one of the very important phenomenon because of the very small beam emittance and high beam intensity [77]. The beam-ion interaction becomes enhanced and may jeopardize the performance of the storage ring. In such storage ring, the beam lifetime of stored electron beam sometimes become extremely short and in that case, round beam mode operation satisfy the operational requirements. To achieve a round beam, coupling coefficient ($\kappa = {}^{\varepsilon_y}/_{\varepsilon_x}$) is made close to unity by introducing strong skew quadrupoles in the lattice or operating the machine at difference resonance (equal fractional tune in both horizontal and vertical plane). RRCAT, has worked out a baseline lattice design of a 6 GeV ultra-low emittance storage ring of emittance ~ 150 pm rad for a future high brilliance light source. Preliminary estimation for this lattice shows that the instability growth rate is much high as compared to flat beam [78]. Also, in the round beam mode, the FBII needs to consider in both the horizontal and vertical plane, notwithstanding the way it was studied only in vertical plane in 3rd generation storage ring.

APPENDIX-A

ESTIMATION OF WAKE FIELD AMPLITUDE OF ION CLOUD

The wake force of ion cloud generated from a displaced electron bunch by Δy is given by

$$W_y = \frac{\int F\,ds}{q_i q_e \Delta y} = \frac{c\,\Delta P}{q_i q_e \Delta y} = \frac{\Delta \upsilon}{c\;4\pi\epsilon_0 r_e N_e \Delta y} \qquad \dots.(1)$$

where q_i: charge of ion, q_e: charge of electron and Δy: offset of generated ion cloud from the beam axis. N_e is the number of electrons in an electron bunch, r_e is the classical electron radius, given as

$$r_e = \frac{e^2}{4\pi\varepsilon_0 m_e c^2}$$

$\Delta\upsilon$ is the velocity kick receives by the electron bunch from the oscillating ion cloud. This can be calculated from following equation of motion for electron

$$m_e\,\ddot{y}_e = e\,E_y^{ion} \qquad \dots.(2)$$

Using linear approximation of Bassetti-Erskine formula for electric field of a Gaussian beam, Eqn. 2 is written as

$$\ddot{y}_e = \frac{e\,\lambda_i\,y_i}{m_e 2\pi\varepsilon_0 \sigma_y\left(\sigma_y + \sigma_x\right)} \qquad \dots.(3)$$

$$\sigma_y = \sqrt{\sigma_{yi}^2 + \sigma_{ye}^2} \quad , \sigma_{yi} = \frac{\sigma_{ye}}{\sqrt{2}}$$

By integrating the Eqn. 3 with respect to time, we get

$$\dot{y}_e = \Delta v = \frac{2r_e c N_i y_i}{\left(\frac{3}{2}\right)\sigma_y\left(\sigma_y + \sigma_x\right)} \qquad \dots.(4)$$

where λ_i is the line charge density of ion cloud, N_i is the number of ions, σ_{yi} is the transverse size of ion cloud, σ_{ye} is the transverse size of electron bunch and σ_y is the cross-sectional area in which the beam-ion interaction took place. y_i is the ion oscillation amplitude and can be calculated as velocity kick received by the ion cloud from the electron bunch divided by ion oscillation frequency, ω_i. The velocity kick can be calculated from the following equation of motion for ion

$$M_{ion}\,\ddot{y}_i = q_i\,E_y^{elec}$$

$$\dot{y}_i = \Delta v_{yi} = \frac{2r_p c N_e\,\Delta y}{A\,\left(\frac{3}{2}\right)\sigma_y\left(\sigma_y + \sigma_x\right)} \qquad \dots.(5)$$

$$y_i = \frac{\Delta v_{yi}}{\omega_i} \qquad \dots.(6)$$

$$\omega_i = c\left(\frac{4N_e r_p}{3L_{sep}\sigma_y\left(\sigma_x + \sigma_y\right)A}\right)^{1/2} \qquad \dots.(7)$$

where, A is atomic mass of the ion, r_p is the classical proton radius. Plugging the Eqn. 4, 5, 6 and 7 into Eqn. 1, the amplitude of wake function is estimated as

$$\widehat{W_y} = \frac{N_i}{4\pi\epsilon_0}\left[\frac{L_{sep} r_p}{A N_e}\right]^{1/2}\left[\frac{4}{3}\frac{1}{\sigma_y\left(\sigma_x + \sigma_y\right)}\right]^{3/2} \qquad \dots.(8)$$

REFERENCES

1. Y. Baconnier and G. Brianti, The stability of ions in bunched beam machines, CERN/ SPS/ 80-2 (1980).
2. Y. Baconnier, Neutralization of accelerator beams by ionization of the residual gas, CERN/PS/PSR 84-24 (1984).
3. R.D. Kohaupt, Ion clearing mechanism in the electron-positron storage ring DORIS, DESY Ml-71/2 (1971).
4. J. M. Byrd, et al., Ion instability experiments on the ALS, SLAC-PUB-7389 (1996).
5. Toshio Kasuga et al., Ion trapping effect in UVSOR storage ring, Japanese Journal of Applied Physics, 24, (9) pp.1212-1217 (1985).
6. Mark Q Barton, Ion trapping with asymmetric bunch filling of the NSLS VUV ring, Nucl. Instrum. Methods in Phys. Res. A 243, pp. 278-280 (1986).
7. C. J. Bocchetta and A. Wrulich, The trapping and clearing of ions in ELETTRA, Nucl. Instrum. Methods in Phys. Res. A 278, pp. 807-817 (1989).
8. S. Sakanaka et al., Observation of ion trapping in single bunch operation at the photon factory storage ring, Japanese Journal of Applied Physics, 27 (6), pp. 1031-1037, (1988).
9. M. Known, Instability studies of the Pohang light source, in Proceedings of European Particle Accelerator Conference, Barcelona, 1096-1098 (1996).
10. CY Yao, et al., Investigation of APS PAR vertical beam instability, in Proceedings of Particle Accelerator Conference, Knoxville, Tennessee, 2393-2395 (2005).

11. Jack G.E. Harris, The Trapping of Ions at SPEAR: A Computational and Experimental Study, SLAC-PUB 6474, (1994).
12. M. Ivanyan et al., The Study of Ion Trapping and Fast Ion Beam Instability in PETRA III Storage Ring, Internal Report, DESY M 09-01 (2009).
13. T.O. Raubenheimer and F. Zimmermann, Fast beam-ion instability, Linear theory and simulations, Phys. Rev. E, 52, 5 (1995).
14. K. Ohmi, Numerical study for the two-beam instability due to ions in electron-storage rings, Phys. Rev. E, 55, 6 (1997).
15. J. Byrd et al., First Observations of a Fast Beam-Ion Instability, Phys. Rev. Lett. 79, 1 (1997).
16. M. Kwon et al., Experimental results on the fast beam-ion instability, Phys. Rev. E, 57, 5 (1998).
17. J. Y. Huang et al., Direct Observation of the Fast Beam-Ion Instability, Phys. Rev. Lett. 81, 20 (1998).
18. Guoxing Xia and Eckhard Elsen, Simulation study of ion effect in the ILC electron damping Ring, Nucl. Instrum. Methods in Phys. Res. A 593 (2008).
19. R. Nagaoka et al., Fast beam ion instability observation at SOLEIL, in Proceedings of the International Particle Accelerator Conference, Kyoto, Japan, TUPD028 (2010).
20. Bocheng Jiang et al., Investigation of fast ion instability in SSRF, Nucl. Instrum. Methods in Phys. Res. A 614 (2010).
21. A. Chatterjee et al., Fast ion instability at the Cornell Electron Storage Ring Test Accelerator, Phys. Rev. ST Accel. Beams 18, 064402 (2015).

22. Weixing Cheng et al., Experimental evidence of ion-induced instabilities in the NSLS-II storage Ring, Nucl. Instrum. Methods in Phys. Res. A 861 (2017).
23. L. Wang, Y. Cai, and T. O. Raubenheimer, Suppression of beam-ion instability in electron rings with multibunch train beam fillings, Phys. Rev. ST Accel. Beams 14, 084401 (2011).
24. L. Wang, et al., Beam ion instability: Measurement, analysis, and simulation, Phys. Rev. ST Accel. Beams 16, 104402 (2013).
25. Lanfa Wang, Beam ion instability in the ultimate storage ring Nucl. Instrum. Methods Phys. Res. A 764 (2014).
26. H. Wiedemann, Particle Accelerator Physics, Third edition, Springer-Verlag, Berlin, (2007).
27. Herman Winick, Synchrotron radiation sources, A primer, World Scientic Publishing Co., Singapore (1995).
28. Matthew Sands, The physics of electron storage ring, an introduction, SLAC-R-121 (1979).
29. E. D. Courant and H. S. Snyder, Theory of the Alternating-Gradient Synchrotron, Annals of Physics 3, 1-48 (1958).
30. Alexander Wu Chao, Physics of collective beam instabilities in high energy accelerators, John Wiley & Sons (1993).
31. A. Sessler and V. Vaccaro, Longitudinal instabilities of azimuthally uniform beams in circular vacuum chambers with wall of arbitrary electrical properties, CERN Report 67/2 (1967).
32. S. Khan, Collective phenomena in synchrotron radiation sources Springer-Verlag Berlin Heidelberg (2006).

33. W. Herr, Introduction to Landau damping, in Proceedings of the CAS-CERN Accelerator School, Norway, (2013).
34. G. Singh, et al., Synchrotron radiation source Indus-2, Indian J. Pure Applied Physics, 35 (3) 183-192 (1997).
35. D. Angel-Kalinin et al., Synchrotron radiation source Indus-1, Current Science, Indian Academy of Science, 82(3) 283-290 (2002).
36. A D Ghodke et al, ICFA, Beam Dynamics Newsletter, 41, 77 (2006).
37. Saroj Kumar Jena, et al., Stabilization of betatron tune in Indus-2 storage ring, Chinese Physics C 38 (6) 067002 (2014).
38. Saroj Kumar Jena, and A.D. Ghodke, Improvements in stable beam operation of Indus-2 storage ring, 6th Accelerator Reliability Workshop (ARW-2017), Paris, Oct. 15-20, (2017).
39. Saroj Kumar Jena, et al., Beam based alignment and its relevance in Indus-2, Rev. Scientific Instrum., 86, 093303 (2015).
40. M. E. Biagini, et al., Observation of ion trapping at ADONE, in Proceedings of 11th International Conference on High-Energy Accelerators pp 687-692, Geneva, (1980).
41. Toshio Kasuga, Ion clearing system of UVSOR storage ring, Japanese Journal of Applied Physics, 25 (11), 1711-1716 (1986).
42. Eva Bozoki and David Sagan, On the shaking of ions in electron storage rings, Nucl. Instrum. Methods in Phys. Res. A 340, 259-271 (1994).
43. D. Villevald, S. Heifets, Ion trapping in the SLAC B-factory high energy ring, PEP-I AP note 18-93, (1993).

44. D. L. Bruhwiler et al., Particle-in-cell simulations of tunnelling ionization effects in plasma-based accelerators, Phys. Plasmas 10, 2022 (2003).
45. A. Oeftiger and G. Rumolo, Fast beam-ion instabilities in CLIC mail Linac vacuum specifications, CERN-OPEN -2011-050.
46. F.F.Rieke and W. Prepejchal, Ionization Cross Sections of Gaseous Atoms and Molecules for High-Energy Electrons and Positrons Phys. Rev. A 6 (4) (1972).
47. A. Poncet, Ion trapping and clearing, CERN /MT/93-01 (1993).
48. Frank Hinterberger, Ion Trapping in the High-Energy Storage Ring HESR.
49. Georg H. Hoffstaetter and Matthias Liepe, Ion clearing in an ERL, Nucl. Instrum. Methods in Phys. Res. A 557 205–212, (2006).
50. M. Bassetti and G.A. Erskine, Closed expression for the electric field of a two-dimensional Gaussian charge, CERN-ISR-TH/80-06.
51. R. A. Bosch and C. S. Hsue, Ion trapping with empty buckets in an electron storage ring, Chinese Journal of Physics , 31 (2) (1993).
52. S. Sakanaka, Difference in the ion trapping between uniform and partial bunch fillings, Nucl. Instrum. Methods in Phys. Res. A 256, 184-188 (1987).
53. Akira Mochihashi, et al., Ion Trapping Phenomenon in UVSOR Electron Storage Ring, Japanese Journal of Applied Physics, 44 (1A), (2005).
54. Saroj Kumar Jena and A. D. Ghodke, Observation and mitigation of ion trapping in Indus-2, Pramana – Journal of Physics, 85 (6) 1193-1205 (2015).
55. H. Kobayakawa, et al., Observation of the ion trapping phenomenon with Bremsstrahlung, Nucl. Instrum. Methods in Phys. Res. A 248, (1986).
56. M. Takao, et al., Observation of Ion Effects at the Spring-8 Storage Ring, in Proceedings of European Particle Accelerator Conference, France, (2002).

57. Pedro F. Tavares, Bremsstrahlung detection of ions trapped in the EPA electron beam, Particle Accelerators, 43(1- 2), pp. 107-131 (1993).

58. Saroj Kumar Jena, et al., Detection of trapped ions by measuring bremsstrahlung photons in Indus-2, in Proceedings of 22nd National Symposium on Radiation Physics, New Delhi, (2019).

59. A. Mochihashi et al., Vertical instability with transient characteristics in KEK-Photon Factory electron storage ring, Phys. Rev. ST Accel. Beams, 4, 22802 (2001).

60. P.F. Tavares, Transverse distribution of ions trapped in an electron beam, CERN-PS/92-55 (LP) (1992).

61. G. V. Stupakov, T.O. Raubenheimer and F. Zimmermann, Fast beam-ion instability: Effect of ion decoherence, Phys. Rev. E, 52 5 (1995).

62. S. K. Tian and N. Wang, Ion instability in the HEPS storage ring, in Proceedings of 60th ICFA Advanced Beam Dynamics Workshop on Future Light Sources, (2018).

63. G. Rumolo and D. Schulte, Fast ion instability in the CLIC transfer line and main Linac, in Proceedings of European Particle Accelerator Conference, Genoa, Italy, 655-657 (2008)

64. L. Mether, G. Iadarola, and G. Rumolo, Numerical modelling of fast beam ion instabilities, in Proceedings of HB2016, Sweden, 368-372 (2016).

65. R. Wanzenberg, Nonlinear motion of a point charge in the 3D space charge field of a Gaussian bunch, DESY M 10-01 (2010).

66. Pradeep Kumar, et al., Dependence of loss rate of electrons due to elastic gas scattering on the shape of the vacuum chamber, Vacuum, 120, 67-72 (2015).

67. Saroj Kumar Jena, A. D. Ghodke, and V. K. Senecha, Simulation of fast beam ion instability (FBII) in Indus-2 and its experimental observation, Journal of Instrumentation, 12 ,P11004 (2017).

68. T.O Raubenheimer, The Fast Beam-Ion Instability and Measurements at the ALS, in Proceedings of the 8th ICFA beam dynamics workshop, (2000).

69. Ali Akbar Fakhri et al., Beam emittance reduction during operation of Indus-2, Rev. Scientific Instrum., 86, 113305 (2015).

70. Pauli Kehayias, Fast Ion Instability Simulations for CesrTA, (2017).

71. L. Palumbo, V.G. Vaccaro and M. Zobov, Wake Fields and Impedance, LNF-94/041.

72. L. Wang, et al., An accurate model of beam ion instability with nonlinear space charge, realistic beam optics and multiple gas species vacuum, SLAC-PUB-15353, (2013).

73. R. Nagaoka, in Proceedings of CAS-CERN Accelerator School, Geneva, (2015).

74. Saroj Kumar Jena, et al., Investigation of fast beam-ion instability (FBII) in wake function formalism for Indus-2 ring, Nucl. Instrum. Methods in Phys. Res. A 919 (2019).

75. N. Wang, et al., Analytical estimation of the beam ion instability in HEPS, in Proceedings of the International Particle Accelerator Conference, Canada (2018).

76. A. Gamelin, et al., Longitudinal and transverse dynamics of ions from residual gas in an electron accelerator, Phys. Rev. ST Accel. Beams, 21, 054401 (2018).

77. Advanced Photon Source Upgrade Project, Preliminary Design Report, Document No. APSU-2.01-RPT-002, (2017).
78. Saroj Kumar Jena, et al., Ion-beam interaction in electron storage ring of high brightness synchrotron radiation source, in Proceedings of Indian Particle accelerator conference, New Delhi, (2019).